ANL-6923

ANL-6923

Argonne National Laboratory

REACTOR DEVELOPMENT PROGRAM

PROGRESS REPORT

July 1964

Price $2.25 . *Available from the Office of Technical Services, Department of Commerce, Washington 25, D.C.*

ANL-6923
Reactor Technology
(TID-4500, 32nd Ed.)
AEC Research and
Development Report

ARGONNE NATIONAL LABORATORY
9700 South Cass Avenue
Argonne, Illinois 60440

REACTOR DEVELOPMENT PROGRAM PROGRESS REPORT

July 1964

Albert V. Crewe, Laboratory Director
Stephen Lawroski, Associate Laboratory Director

Division	Director
Chemical Engineering	R. C. Vogel
Idaho	M. Novick
Metallurgy	F. G. Foote
Reactor Engineering	L. J. Koch
Reactor Physics	R. Avery
Remote Control	R. C. Goertz

Report Coordinated by
R. M. Adams and A. Glassner

Issued August 20, 1964

Operated by The University of Chicago
under
Contract W-31-109-eng-38
with the
U. S. Atomic Energy Commission

FOREWORD

The Reactor Development Program Progress Report, issued monthly, is intended to be a means of reporting those items of significant technical progress which have occurred in both the specific reactor projects and the general engineering research and development programs. The report is organized in a way which, it is hoped, gives the clearest, most logical over-all view of progress. The budget classification is followed only in broad outline, and no attempt is made to report separately on each sub-activity number. Further, since the intent is to report only items of significant progress, not all activities are reported each month. In order to issue this report as soon as possible after the end of the month editorial work must necessarily be limited. Also, since this is an informal progress report, the results and data presented should be understood to be preliminary and subject to change unless otherwise stated.

The issuance of these reports is not intended to constitute publication in any sense of the word. Final results either will be submitted for publication in regular professional journals or will be published in the form of ANL topical reports.

The last six reports issued in this series are:

January 1964	ANL-6840
February 1964	ANL-6860
March 1964	ANL-6880
April 1964	ANL-6885
May 1964	ANL-6904
June 1964	ANL-6912

TABLE OF CONTENTS

		Page
I.	Boiling Water Reactors	1
	A. BORAX-V	1
	1. Operations	1
	2. Experiments	2
	3. Water Chemistry	12
	4. Maintenance and Modification	12
	5. Training	13
II.	Liquid-metal-cooled Reactors	14
	A. General Fast Reactor Physics	14
	1. ZPR-III	15
	2. ZPR-VI	15
	3. ZPR-IX	15
	4. AFSR	18
	B. General Fast Reactor Fuel Development	18
	1. Metallic Fuels	18
	2. Development of Jacket Materials	22
	3. Irradiation of Fast Reactor Fuels	25
	4. Development of Fuels for Zero-power Reactors	26
	5. Development of Carbide Fuels	28
	C. General Fast Reactor Fuel Reprocessing Development	29
	1. Materials and Equipment Evaluation	29
	2. Advanced Processes	30
	3. Head-end Treatments for Refractory Fuels	30
	4. Removal of Nitrogen from Argon	31
	D. Sodium Coolant Chemistry	31
	1. Analysis for Oxygen	31
	2. Solubility of Carbon in Liquid Sodium	32
	E. EBR-II	32
	1. Reactor Plant	32
	2. Sodium Boiler Plant	34

TABLE OF CONTENTS

	Page
3. Power Plant	34
4. Fuel Cycle Facility	35
F. FARET	42
1. General	42
2. Reactor Vessel	43
3. Design of Reactor Vessel Cavity	43
4. In-core Instrumentation	44
5. Fuel Assembly Sodium Flow Test Facility	44
III. General Reactor Technology	46
A. Experimental Reactor and Nuclear Physics	46
1. High-conversion Critical Experiment	46
2. In-core Fast Neutron Spectroscopy	46
B. Theoretical Reactor Physics	48
1. Numerical Analysis	48
2. Use of Very Large Fast Breeder Reactors for Desalinization of Water	49
C. High-temperature Materials Development	49
1. Ceramics	49
2. Corrosion by Liquid Metals	55
3. Thorium and Thorium-base Fuels	57
D. Other Reactor Fuels and Materials Development	59
1. Nondestructive Testing	59
E. Remote Control Engineering Development	62
1. Viewing Systems	62
2. Electric Master-Slave Manipulator Mark E4	62
3. Special Motors for Master-Slave Manipulators	62
4. Higher-sensitivity Force-feedback Systems for Master-Slave Manipulators	64

TABLE OF CONTENTS

		Page
F.	Heat Engineering	64
1.	Two-phase Flow Studies	64
2.	Boiling Liquid Metal Technology	65
3.	ANL-AMU Program	66
G.	Chemical Separations	68
1.	Fluidization and Volatility Separation Processes	68
2.	General Chemistry and Chemical Engineering	72
3.	Chemical-Metallurgical Process Studies	73
4.	Calorimetry	73
H.	Plutonium Recycle Reactor	74
1.	Plutonium Recycle Fuel	74
2.	Plutonium Recycle Control Rods	74
3.	Physics Calculations	75
IV.	Advanced Systems Research and Development	79
A.	Argonne Advanced Research Reactor (AARR)	79
1.	Core Physics	79
2.	Fuel and Core Design	80
3.	Beam Tubes for the Experimental Facility	81
4.	Critical Experiment	83
B.	Magnetohydrodynamics (MHD)	83
1.	MHD Studies with Liquid Metals	83
C.	Regenerative EMF Cells	84
1.	Bimetallic Cells	84
V.	Nuclear Safety	86
A.	Thermal Reactor Safety Studies	86
1.	Metal-Water Reactors	86
2.	Metal Oxidation-ignition Studies	87

TABLE OF CONTENTS

		Page
B.	Fast Reactor Safety Studies	87
1.	Meltdown in Flowing Sodium	87
2.	Photographic Meltdown Experiments with Previously Irradiated Samples	88
3.	Pressure-pulse Calculations	89
4.	Reactor Tests with Meltdown Scanning Device	91
C.	TREAT	92
1.	Large TREAT Loop	92
VI.	Publications	93

I. BOILING WATER REACTORS

A. BORAX-V

1. Operations

Power operation with the PSH-1 core has continued for a total integrated power of 186 MWd. One week of operation was conducted with a single prepared defective boiling fuel rod and one week with ten prepared defective boiling fuel rods.

Radiation levels increased very slightly throughout most of the plant as a result of the installation of defective boiling fuel rods, except for the charcoal filter in the air ejector exhaust system, as can be seen in Table I.

Table I. Plant Radiation Levels with Prepared Defective Boiling Fuel Rods

	Number of Defective Fuel Rods		
	0	1	10
Power Level, MWt	11.3	11-12	11-12
Main Steam Line Reactor Bldg, mR/hr*	65	80-85	90-100
Main Steam Line Turbine Bldg, mR/hr**	40	30-40	45-52
Condenser Hotwell, mR/hr	26	13-33	60-80
Air Ejector Exhaust Charcoal Filters, mR/hr	45	45-70	2000-2900
Reactor Water Line to Bypass Demineralizer (DM-1), mR/hr	47	28-45	33-85
Condensate Return Line, mR/hr†	8	3-8	30-40

*Monitor located on the main steam pipe line. The pipe line distance from the reactor is about 42 ft.

**Monitor located on the main steam pipe line. The pipe line distance from the reactor is 300 ft.

†Monitor located on the condensate pipe line. The pipe line distance from the condenser hotwell is about 300 ft.

Additional flux wire irradiations and miniature ion chamber traverses were made to find the changes in flux distribution under various operating conditions. Other experiments determined the effect of changing

demineralizer flow on changes in power level and on power split between boiling and superheating regions. Routine water chemistry and in-core instrumentation measurements continued.

Following completion of operation with defective boiling fuel elements, an experiment was initiated using defective superheater fuel. The ten defective boiling fuel rods were replaced with good elements and one fresh outlet superheater fuel assembly, containing a sample of defective superheater fuel, was installed. Adjustments in the number and location of boron-stainless steel poison rods were made to maximize reactivity without violating the single-control-rod shutdown criterion.

2. Experiments

a. Defective Boiler Fuel Experiments. The defective boiler fuel rod experiments in core PSH-1 were run in two stages. First, a single boiling fuel rod prepared with a single 1/8-in.-dia hole drilled through the cladding at the vertical core center was placed in the boiler. After a week of operation, the fission product levels in the steam system were barely detectable, so an additional nine prepared defective fuel rods were installed in the boiler. These nine rods contained two 1/8-in.-dia cladding holes, 180° apart, located 1 in. above the bottom of the fuel, and two 1/8-in.-dia holes located in the gas space above the fuel. The fuel rod changes were made through the central reactor-vessel-head nozzle.

The gross specific gamma activity of reactor water and steam was determined throughout these tests. In Table II the results of these measurements, as well as activities for some periods prior to the tests, are given. Each value was obtained by counting at 20 min after sampling, but no decay correction was applied.

Before the tests with defective fuel, the reactor water activity averaged 37 times higher than the activity of the saturated steam and 20 times higher than that of the superheated steam. The superheated steam had (on the average) about 1.8 times as much activity as the saturated steam.

The test with the single defective rod demonstrated that one defect hardly changes the activities or species of activity noticed before. Again using average values, the reactor water activity was (omitting value obtained at 1105 July 7) 31 times higher than the activity of the saturated steam and 26 times higher than that of the superheated steam. The activity of the superheated steam was only 1.2 times higher than that of the saturated steam.

With 10 defective rods (making a total of thirty-seven 1/8-in. holes), the intensity of activities changed by two orders of magnitude in the steam, but rose only slightly higher in the reactor water. The same isotopic

species were found as before. Each examination of the reactor water showed primarily Na^{24}, which gave such an intense gamma spectrum that all other species were masked out. Radio-iodine was also found, but in very low concentrations. In the saturated and superheated steam, Xe^{133}, Xe^{135}, Kr^{87}, and Kr^{88} with their daughters and some radio-iodine were responsible for most of the activity.

Table II. Gross Specific Gamma Activity Comparisons, Defective Boiling Fuel Rod Tests, Core PSH-1

Date	Approx Time	Power (MWt)	cpm/ml Reactor Water	Saturated Steam	Superheated Steam	Condensate	Remarks
			No Defective Boiling Fuel Rods				
5/20	1530	10	178,000	6,200	9,100	3,650	DM-1 off*
6/8	1520	19	147,000	7,600	4,700	-	DM-1 at 30 gpm
6/9	1717	5	91,000	3,300	6,900	-	DM-1 off at 1443
6/17	1319	12	383,000	4,900	24,000	-	DM-1 off at 1055
6/23	1250	10	85,000	2,400	3,500	-	DM-1 off at 1352
6/23	1535	10	145,000	3,600	4,000	-	Aluminum nitrate injected
			Single Defective Boiling Fuel Rod				
7/7	1105	0	6,000	730	640	-	DM-1 off
7/7	1330	5	53,000	2,400	3,000	-	DM-1 at 13.5 gpm
7/7	1445	11.8	89,000	2,800	3,400	1,700	DM-1 at 24.5 gpm
7/8	0910	11-12	98,000	3,600	3,600	2,000	DM-1 at 36 gpm
7/9	1433	10	134,000	3,200	4,600	-	DM-1 at 25 gpm
7/10	1145	5	113,000	3,800	4,100	-	DM-1 at 17 gpm
			Ten Defective Boiling Fuel Rods				
7/14	1050	4.5	79,000	146,000	71,000	-	DM-1 off
7/14	1253	20	144,000	283,000	78,000	-	DM-1 at 39 gpm
7/14	1409	20	162,000	248,000	146,000	-	DM-1 at 39 gpm
7/14	1545	18	174,000	309,000	112,000	-	DM-1 at 39 gpm
7/15	0915	10-11	109,000	296,000	159,000	8,600	DM-1 at 35 gpm
7/15	1117	10-11	111,000	284,000	71,000	5,500	DM-1 at 35 gpm
7/15	1345	9.8	219,000	307,000	70,000	8,700	DM-1 off
7/15	1600	9.5	428,000	261,000	60,000	-	DM-1 off
7/16	0915	9.5	201,000	297,000	76,000	6,900	DM-1 off
7/16	1115	9.5	412,000	256,000	64,000	11,000	DM-1 off
7/16	1335	9.5	581,000	310,000	150,000	9,500	DM-1 off
7/16	1555	9.5	732,000	301,000	157,000	9,200	DM-1 off
7/17	0912	11.6	131,000	371,000	187,000	7,700	DM-1 at 35 gpm
7/20	1600	18.8	142,000	182,000	123,000	-	DM-1 at 35 gpm

*DM-1 is Reactor Water Bypass Demineralizer.

Power level, and especially the flow rate through the reactor water bypass demineralizer (DM-1), strongly affected the activity of the reactor water, but had a much smaller proportional effect on the steam. The first day of the test with 10 defective rods (see Table II, July 14), the saturated steam activity had increased by a factor of 78, making it

1.7 times higher than the activity of the reactor water, which showed only a moderate increase. The superheated steam showed less activity than the saturated steam by a factor of 2.4. On July 15, the average activity of the reactor water had increased, possibly by an increase of iodine concentration (see Table III) and nonvolatile daughters (Ba^{140} and La^{140}, for example). On this day, the averages show the saturated steam activity to be only 1.3 times higher than the activity of the reactor water, but the superheated steam activity became 3.2 times smaller than that of the saturated steam. On July 16, the reactor water demineralizer was turned off; the reactor water activity increased by a factor of 2.2, and the saturated and superheated steam activities went up by factors of 1.01 and 1.23, respectively.

Table III. I^{131} Concentrations and Comparisons, Defective Boiling Fuel Rod Tests, Core PSH-1

Date	Time	Power Level (MWt)	Values in d/m/ml			Remarks
			Reactor Water	Saturated Steam	Superheated Steam	
			Single Defective Rod			
7/7	1016	0	16	4	4	DM-1 off
7/7	1258	5	8	4	4	DM-1 flow - 13.5 gpm
7/7	1421	11.8	5	4	4	DM-1 flow - 24.5 gpm
7/8	0850	11-12	13	5	6	DM-1 flow - 36 gpm
7/9	1415	10	36	5	5	DM-1 flow - 25 gpm
7/10	1125	5	13	5	5	DM-1 flow - 17 gpm
			Ten Defective Rods			
7/14	1030	4.5	180	20	10	DM-1 off
7/14	1230	20	925	22	9	DM-1 flow - 39 gpm
7/14	1343	20	550	13	6	DM-1 flow - 39 gpm
7/14	1525	18	188	6	6	DM-1 flow - 39 gpm
7/15	0843	10-11	136	10	5	DM-1 flow - 35 gpm
7/15	1045	10-11	115	8	6	DM-1 flow - 35 gpm
7/15	1330	9.8	240	10	4	DM-1 off
7/15	1540	9.5	515	16	4	DM-1 off
7/16	0855	9.5	371	26	5	DM-1 off
7/16	1052	9.5	742	24	5	DM-1 off
7/16	1318	9.5	1110	52	18	DM-1 off
7/16	1534	9.5	1590	70	27	DM-1 off
7/17	0854	11.6	438	26	5	DM-1 flow - 35 gpm
7/20	1518	18.8	1920	122	98	DM-1 flow - 35 gpm

The fission product monitor gave fairly steady readings of 120,000 to 140,000 c/m for saturated steam and of 23,000 to 25,000 c/m for superheated steam during the test with 10 defective rods. During the test with the single defective rod, the readings were about the same as for normal operation for the superheated steam (i.e., 1200-2000 c/m), but went up about $2\frac{1}{2}$ times for the saturated steam (i.e., from 400 to 1000 c/m).

To gain some indication of the fission product release, I^{131} in reactor water, saturated steam, and superheated steam was determined, with the results in Table III, all corrected for sampling time. Prior to the defect tests, I^{131} was not detected. It may be seen that (1) the fission product iodine remained mostly in the reactor water; (2) it was at fairly low levels in the steam; (3) the superheater removed up to 92% of the iodine coming in with the saturated steam when the inlet concentration was high; and (4) the iodine concentration in the reactor water was mainly dependent on demineralizer flow.

Decontamination factors for iodine, determined from the data of Table III, are tabulated with power level in Table IV.

Table IV. Iodine Decontamination Factors Defective Boiling Fuel Rod Tests, Core PSH-1

Date	Time	Power Level (MWt)	Reactor Water	
			Saturated Steam	Superheated Steam
		Single Defective Rod		
7/7	1016	0	4	4
7/7	1258	5	2	2
7/7	1421	11.8	1.2	1.2
7/8	0850	11-12	2.6	2
7/9	1415	10	7	7
7/10	1125	5	2.6	2.6
		Ten Defective Rods		
7/14	1030	10-11	9	18
7/14	1230	10-11	42	103
7/14	1343	9.8	42	91
7/14	1525	9.5	31	31
7/15	0843	10-11	13	27
7/15	1045	10-11	14	19
7/15	1330	9.8	24	60
7/15	1540	9.5	32	128
7/16	0855	9.5	14	72
7/16	1052	9.5	31	148
7/16	1318	9.5	32	62
7/16	1534	9.5	23	59
7/17	0854	11.6	17	87
7/20	1518	18.8	16	20

It would seem probable that, at a given power level in a series of measurements, the same decontamination factor should be observed for

a given radioisotope; however, the values of the decontamination factors varied. It should be emphasized that the decontamination factors based on gross activities are not meaningful, because the major part of the steam activity is due to fission product gases or their daughters.

The reactor water was sampled after the extended run without DM-1 flow (July 16) and examined for Mo^{99} and uranium. Mo^{99} was present in detectable concentration, but no uranium (i.e., < 0.014 $\mu g/ml$) could be detected. Cesium isotope determinations were also made on samples of reactor water, saturated steam, and superheated steam, but by the time the analysis was completed (~16 hr) none could be detected.

Decay data were taken on samples from the reactor system during the tests with 10 defective rods. In Table V the data obtained are given in terms of percent decay in the time noted rather than by tabulating half-lives, because each point sampled showed complex decay curves caused by three or more isotopes.

Table V. Decay Data from Water and Gas Samples

Sample Point	% Decay	Elapsed Time, hr
Reactor Water	92.6	~ 54.5
Saturated Steam	98.5	~ 30.0
Superheated Steam	98.3	~ 30.0
Condensate	98.3	~ 28.0
Air Ejector Exhaust Gas	98.1	~ 28.0

Deposition samples placed in the steam line showed that Ba^{140} and La^{140} were the predominant isotopes deposited as determined by gamma-ray spectrometry. Deposition activity attenuated along the length of the steam line, as expected. The data are being analyzed.

b. Power Split Experiments. The last column of Table II, p. 2, in Progress Report for June 1964, ANL-6912, is incorrect. Table VI gives the correct values. The effect of increased demineralizer loop flow is to increase reactor inlet water subcooling and reactor power level. It does not seem to change the percent of power production in the superheater.

Table VI. Change in Superheater-boiler Power Split by Control Rod Manipulation, Core PSH-1

Power Level (MWt)	Superheater Exit Steam Temp (°F)	Control Rod Positions (in.)			Power Produced in Superheater (%)
		Central	Intermediate Gang	Outside Gang	
8.1	820	19.80	19.80	19.80	16.6
7.6	830	17.50	19.80	25.00	17.0
7.4	790	25.00	19.80	16.00	15.7
7.3	765	25.00	25.00	12.00	14.9

Table VII shows the data obtained from new power split experiments. Control rods remained in the full "out" position, and the flow to the reactor water demineralizer loop was varied.

Table VII. Change in Reactor Power with Change in Demineralizer Loop Flow

Demineralizer Loop Flow (gpm)	Reactor Power (MWt)	Power to Steam (MWt)	Power Produced in Superheater (%)
0	8.7	8.7	16.9
10	9.0	8.4	16.6
20	9.7	8.5	16.6
30	10.3	8.5	16.7
31.5	10.5	8.7	16.6
36.0	10.5	8.4	16.5

c. In-core Instrumentation Measurements. During the operation with core PSH-1, the in-vessel instrumentation performed satisfactorily. All data taken to date are being analyzed.

Thermocouples throughout the vessel and core continued to give useful information, and those in the superheater proved to have better life than originally anticipated. After 186 MWd of core burnup, 14 of the 40 superheater fuel thermocouples and one of the eight steam thermocouples in the two instrumented superheater fuel assemblies showed failures at room temperature due to open-circuiting. Of these failures, ten fuel thermocouples were in the second-pass superheater fuel assembly, half of these being located on the vertical center of the assembly. Failure is attributed to the high thermal stress applied to these thermocouples and not to those in the first-pass fuel assembly.

Only one of 12 W-W/26% Re thermocouples in boiling fuel rods has failed.

d. Center Temperatures of Boiling Fuel Rods. Data on fuel temperature as a function of reactor power and burnup have been obtained from 11 instrumented boiling fuel rods throughout the core. Figure 1 shows data from the W-W/26% Re thermocouple in fuel rod 49 (core position 56) at an elevation 8 in. above the fuel bottom. The increase of fuel temperatures with increasing burnup was typical for all 11 thermocouples, with this thermocouple indicating the highest temperatures. The data are accurate to about ±2% of reported values based on accuracies of the system. Irradiation damage to the thermocouple is believed negligible, and any thermal "aging" effects, if present, would presumably cause the indicated temperatures to be slightly lower than true value (see Progress Report for

November 1963, ANL-6808, p. 2, for test results indicating this trend at higher temperatures.) Further analysis of the fuel rod temperature data is in progress.

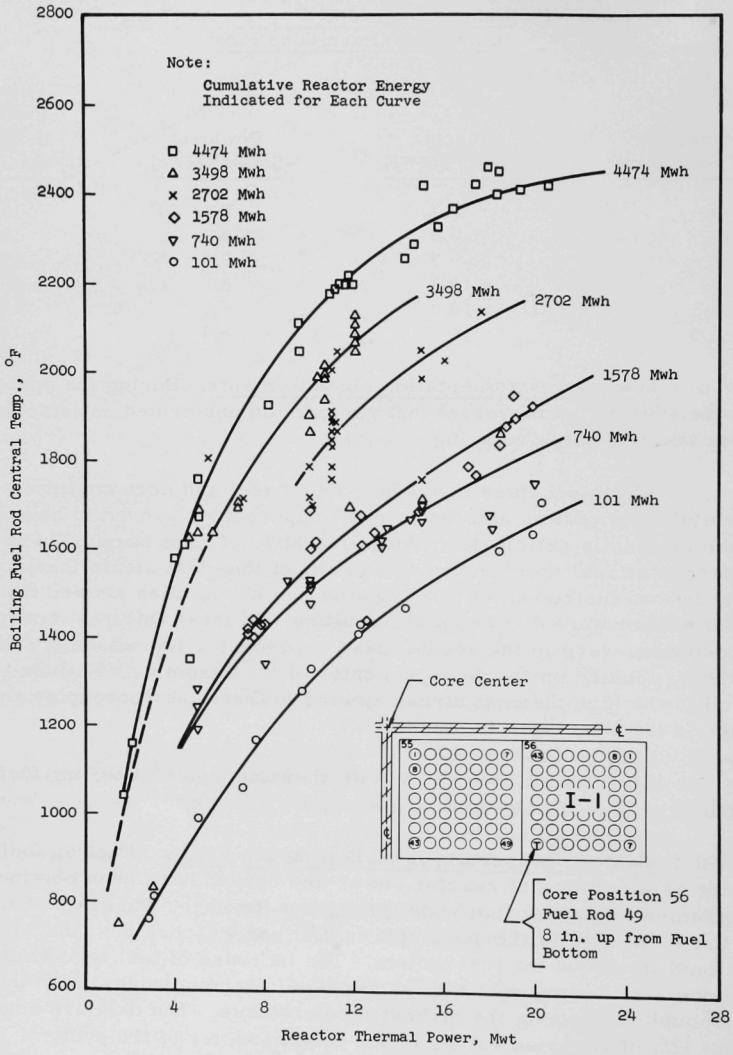

Figure 1. Boiling Fuel Rod Central Temperature vs. Reactor Thermal Power and Burnup, Core PSH-1 of BORAX-V

e. Conductance of Boiling Fuel Rods. Values of the thermal conductance for the boiling fuel rods have been calculated from fuel rod thermocouple readings and power distribution measurements. The overall fuel rod conductance decreased with increased burnup and with decreased power, as shown in Table VIII.

Table VIII. Overall Boiling Fuel Rod Thermal Conductance (Btu/hr-ft-°F)

Power (MWt)	Integrated Reactor Power (MWh)					
	101	740	1578	2702	3498	4474
20	2.20	1.92	1.78	1.50	-	1.30
15	1.87	1.60	1.49	1.23	1.11	1.02
10	1.59	1.24	1.17	0.97	0.85	0.76
5	1.38	0.86	0.86	-	0.58	0.47

The values of the boiling fuel rod conductance were obtained for the UO_2 plus helium and fission gases within the fuel rod jacket by considering the volumetric heat generation within the fuel at the point where the thermocouple was located and the temperature drop between the thermocouple in the center of the fuel and the calculated temperature at the inside of the stainless steel cladding. The thermocouple temperatures used in calculating the conductances were taken from the curves shown in Figure 1 rather than from specific thermocouple readings. The decreased conductance with increased burnup may be due to cracking or disintegration of the fuel, whereas the increase of conductance with increasing power may be due to elimination of the clearance gap between fuel pellets and the cladding tube.

f. Neutron Flux Distributions. Analysis of previously obtained flux wire data revealed that radioactive contamination of the flux wires had resulted in large errors of measurement. This contamination was picked up in the pressure thimbles; even though the wires were wiped with a clean, dry cloth, a great deal of the contamination was not removed. Therefore, irradiations were repeated at power levels of 5, 10, 15, and 20 MWt. Great care was exercised to remove all surface contamination by washing the irradiated wires in acetone before counting. Analysis of the data is in progress.

Neutron flux measurements were also made with a dual miniature fission chamber assembly at powers of 4.8, 10, and 18.4 MWt. The assembly consisted of two ionization chambers, 0.421 in. long and 0.090 in. in diameter; one chamber was bare and the other cadmium-covered. Axial flux distributions were obtained by completely inserting the chambers in pressure thimbles at various core locations and reading the current output as the chambers were withdrawn in 2-in. increments.

Figure 2 shows a comparison of data obtained from the bare ion chamber at 4.8 MWt with data obtained from a flux wire irradiation at 5 MWt. The two sets of data were normalized at a point 10 in. above the bottom of the fuel on flux wire W-5. The values of B_z^2 were obtained from a least-squares cosine curve fit of the data from 5 in. through 13 in. above the bottom of the core.

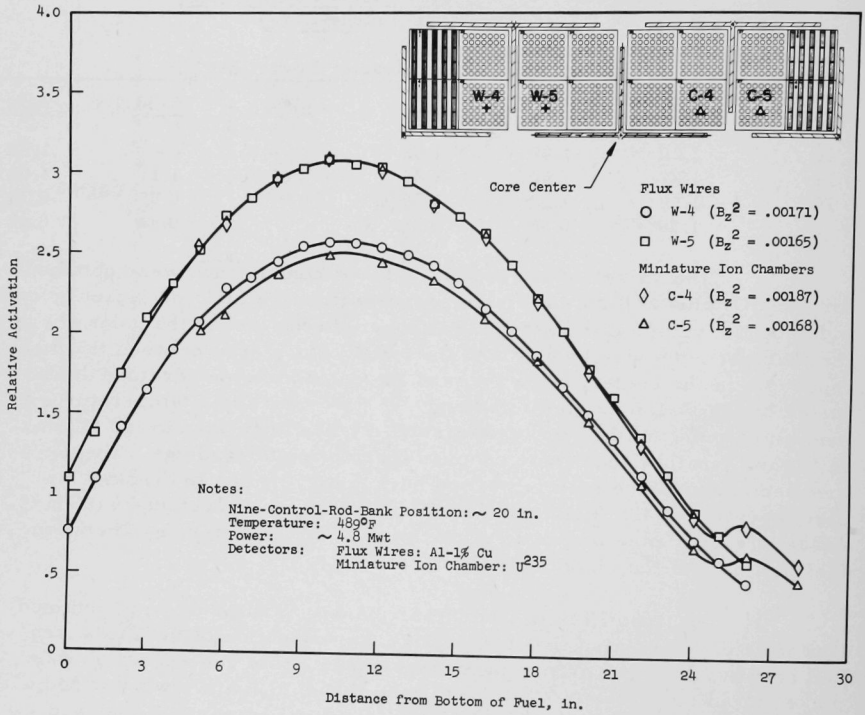

Figure 2. Axial Neutron Flux Distributions, Core PSH-1 of BORAX-V

Figure 3 shows cadmium ratios (ratio of bare to epicadmium activation) from the ion chambers and flux wire activation. The magnitude of the cadmium ratio, through an axial traverse of the core, remains about constant for 4.8-MWt. It had been predicted that the cadmium ratio would be smaller in the upper portion of the core than in the lower portion, because of voids. However, such a trend has not been observed in the data analyzed to date.

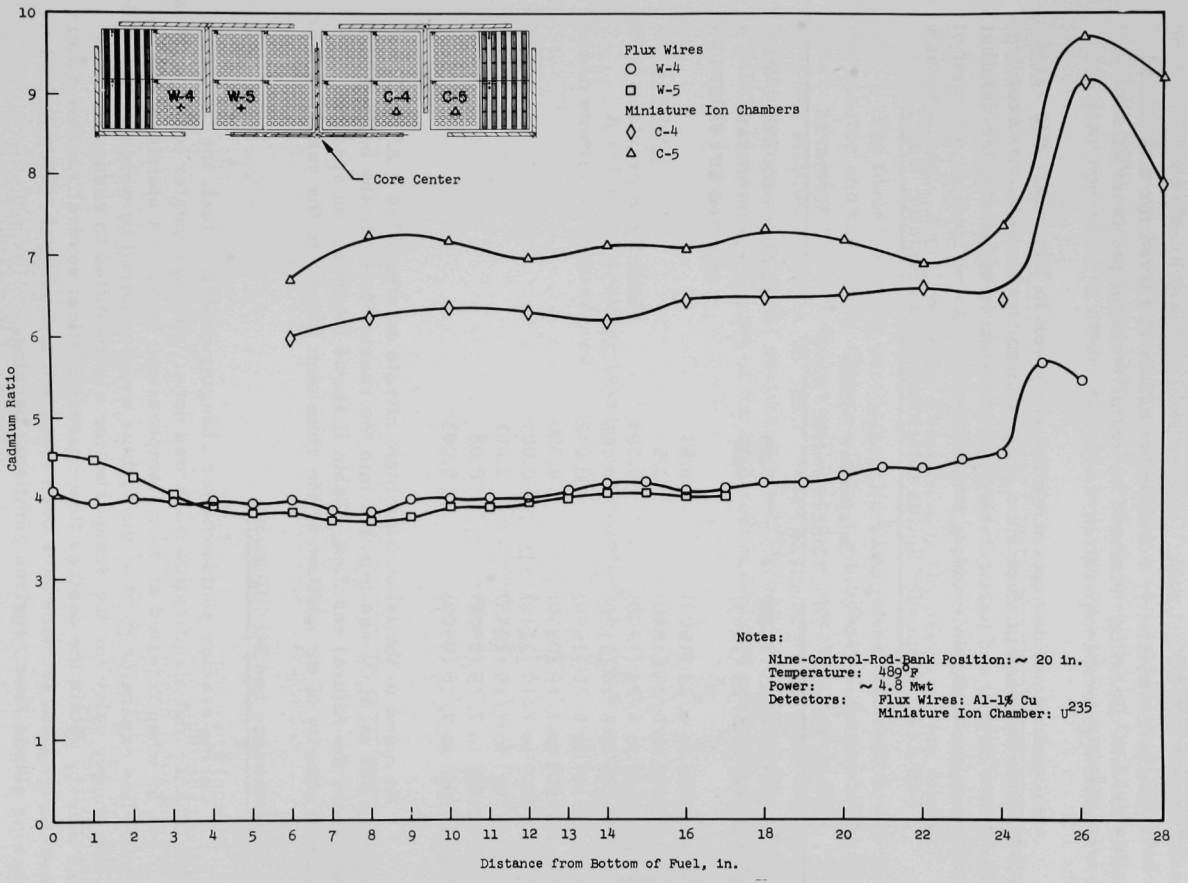

Figure 3. Cadmium Ratio Distributions, Core PSH-1 of BORAX-V

3. Water Chemistry

The pH, resistivity, and chloride values observed for this period during normal operation remained essentially unchanged from values observed during previous operation.

Suspended solids concentrations are given in Table IX. The values demonstrate the good performance of the reactor water demineralizer, DM-1, and filters, and particularly show the results of leaving the demineralizer system off while adding impurities.

Table IX. Suspended Solids Concentration in Reactor Water

Sample Period	Average Suspended Solids Concentration (ppm)	Remarks
6/22 (1000) to 6/23 (0830)	0.09	Running with DM-1 off.
6/23 (0850) to 6/23 (1303)	0.03	Aluminum nitrate injected at 1410.
6/23 (1355) to 6/23 (1500)	0.83	
6/23 (1510) to 6/23 (1840)	2.5	
6/24 (0850) to 6/24 (1500)	0.009	DM-1 ran previous 16 hr.
6/24 (1509) to 6/24 (1100)	0.008	
6/26 (1115) to 6/26 (1600)	0.002	
7/6 (1600) to 7/10 (0930)	0.006	
7/10 (1020) to 7/10 (1240)	0.001	
7/10 (1245) to 7/10 (1545)	0.001	
7/13 (1400) to 7/15 (0900)	0.08	
7/15 (0900) to 7/16 (0900)	0.003	

As noted in the table, aluminum nitrate solution [350 g $Al(NO_3)_3 \cdot 9\,H_2O$ in 500 ml H_2O] was injected into the reactor to study the buildup of Na^{24} from the $Al(n,\alpha)$ reaction. Table II shows the effect on specific gamma activity of the addition of the aluminum nitrate to the reactor water.

4. Maintenance and Modification

During reactor shutdowns for changing defective fuel, the following maintenance and modification work was done: the superheater leak rate was 1.1 gal/hr when retested at room temperature; leaks in a stainless steel steam-line expansion joint at the turbine were repaired by welding; the feedwater supply valve for the desuperheater was modified to change the port and thereby obtain the desired flow characteristics; several reactor water-level gauge glass sections have been replaced; and several valves and other packing glands have required additional packing.

Seventeen superheater fuel-temperature measuring points have been bypassed due to thermocouple failure. Stepping switches on the superheater fuel-temperature scanning system have required considerable adjustment. The steam probe drive failed due to stripping of the teeth of a small gear operating in steam atmosphere; this has been repaired.

The alignment of a control rod latch was adjusted to eliminate intermittent maloperation on relatching. No difficulty has been experienced in releasing. A range resistor was replaced on the linear flux instrument to improve calibration characteristics. One area radiation-monitor channel was repaired. A coil had been overheated in the check source circuit.

The fueled rotating oscillator which had failed was removed from the reactor and examined. The oscillator housing was disassembled under water, revealing that the drive shaft-to-rotor connection was broken. The 17-4 PH stainless steel $\frac{1}{2}$-in. male thread of the screwed connection was broken across the weakest section at a locking roll pin, apparently due to a brittle fracture. Because of the high radioactivity of the rotor (~400 R/hr), no repair is planned.

5. Training

A refresher training session was conducted for all operating personnel in emergency procedures.

II. LIQUID-METAL-COOLED REACTORS

A. General Fast Reactor Physics

1. ZPR-III

Assembly 45 (see Progress Report for June 1964, ANL-6912, p. 16), a multi-zoned reactor in which the composition of the central zone simulates a plutonium carbide-fueled fast power breeder reactor, is primarily intended to investigate Doppler effects in proposed power reactors. The composition of the central zone simulates a carbon-rich PuC-UC-fueled reactor with reduced sodium content, so that the neutron flux is in an energy range of importance in Doppler effects. The compositions of the various zones are listed in Table X. A cross section of the assembly is shown in Figure 4, along with the locations in which the Doppler elements will be placed for the measurements.

Table X. Zone Compositions of Assembly 45 (Atoms/cm^3 x 10^{-24})

Isotope	Central Zone	Low-density Axial Blanket	Buffer	Driver	Radial Reflector	Blanket
Pu^{239}	0.001065	-	-	-	-	-
Pu^{240}	0.000051	-	-	-	-	-
Pu^{241}	0.000005	-	-	-	-	-
U^{235}	0.000015	0.000020	-	0.00448	-	0.000091
U^{234}	-	-	-	0.000046	-	-
U^{236}	-	-	-	0.000019	-	-
U^{238}	0.00723	0.00968	-	0.000256	-	0.03998
Na	0.00635	0.00643	0.00422	-	0.00211	-
C	0.0250	0.0250	0.0166	0.0416	0.0382	-
Ni	-	-	0.0372	0.0186	0.0186	0
SS (304)	0.0130	0.0117	0.01041	0.00775	0.00908	0.00624

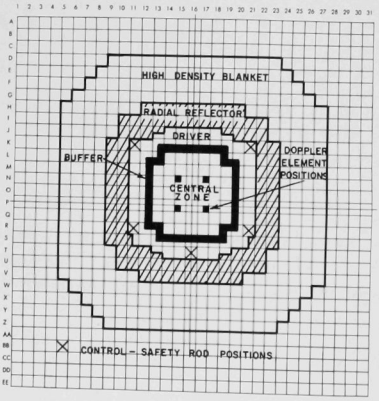

Figure 4

Cross Section of Assembly 45

Assembly 45 went critical with 56.18 kg of plutonium and 0.75 kg of U^{235} in the central zone and with 245 kg U^{235} in the driver. Preliminary measurements of power level versus the degree subcritical indicate that the assembly is approximately 0.5 Ih subcritical at a power level of 40 W due to the spontaneous fission of the Pu^{240} in the central zone. The control rods have been calibrated for shape but not for absolute worth in reactivity. This will be done as soon as a computer code is completed which will calculate the reactivity from a reactor period with a source present.

Three experiments pertaining to the neutron spectrum were performed. Data were obtained by use of a solid-state spectrometer based on the $Li^6(n,\alpha)$ reaction; a combined BF_3/U^{235} counter to measure the ratio of their respective reaction rates; and a combined U^{238} foil/U^{235} fission counter to measure the U^{238} (n,γ) to U^{235} fission ratio. The data are being analyzed.

A fine control rod has been loaded and calibrated (again in shape only) for the Doppler measurements. Initial plans are to limit to two the number of Doppler elements containing only depleted uranium oxide to reduce interactions between the elements. Two elements have been assembled, and all electrical connections are completed. Preliminary interchange of the cold and dummy Doppler elements indicate that the reactivity variation as the Doppler rod is driven into the core can be maintained within satisfactory limits.

The principal remaining work on the Doppler elements is in sealing the system to obtain a vacuum of about 10^{-7} mm Hg.

2. ZPR-VI

Assembly No. 3, a large (~950-ℓ), flat-pancake-type (L/D ~ 1:3) uranium carbide-fueled core, is being loaded. A number of mechanical and electrical modifications were made and the system was checked.

3. ZPR-IX

The ZPR-IX Assembly No. 4 is a tungsten-diluted core in which each fuel drawer in the assembly contains six $\frac{1}{16}$-in.-thick columns of enriched U^{235} and thirteen uniformly distributed $\frac{1}{8}$-in.-thick columns of tungsten. Aluminum is used for the reflector.

The critical material and physical parameters are shown in Table XI.

Central worth coefficients have been determined for a variety of materials and are presented in Table XII.

The central worths of samples of separated isotopes of tungsten were previously determined in Assembly No. 1, the reference core. Measurements have been repeated for the samples in Assembly No. 4. [illegible]ntal values are reported for both assemblies in Table XIII.

Table XI. Critical Material and Physical Parameters of ZPR-IX Assembly No. 4

Core Material	Atomic Densities ($\times 10^{-24}$)
U^{235}	0.006723
W	0.03422
Al	0.00687
U^{238}	0.000486
Fe	0.00052
Critical Mass (U^{235})	285.2 kg
Core Length	56.2 cm
Critical Radius	24.89 cm
Critical Volume	109.4 ℓ
Central Fuel Worth[a]	120.2 Ih/kg of U^{235}
Edge Worth (Fuel Configuration)	+31.9 Ih/kg of U^{235}
L/D Ratio	1.13

[a]Fuel Worth when diluted with tungsten in the drawer.

Table XII. Central Worth Coefficients

Material	Sample Weight, g	Worth, Ih/kg of U^{235}
Al	166.9	-6.6
Al_2O_3	237.9	-5.3
B^{10}	29.2	-3660
B_4C	59.62	-399
C	103	-22.0
Re	1266.9	-71.7
W	1052.0	-19.6
WO_3	78.37	-12.6
U^{235}	67.94	+270
U^{238}	226.8	-5.5

Table XIII. Central Reactivity Worths of Separated Tungsten Isotope Samples

Sample	% W^{182}	% W^{183}	% W^{184}	% W^{186}	Wt, g	Worth, Ih/kg Assy 1	Worth, Ih/kg Assy 4
No. 0, Normal WO_3	26.4	14.4	30.6	28.4	177.08	-24.3	-13.7
No. 1, W Metal	36.9	17.7	31.5	13.9	257.85	-27.1	-20.2
No. 2, W Metal	24.1	14.7	34.2	26.9	173.74	-21.9	-18.7
No. 3, W Metal	12.5	9.8	30.8	46.8	237.14	-24.2	-17.0
No. 4, W Metal	5.8	5.7	23.3	65.1	211.44	-22.0	-14.7
No. 5, Normal Metal	26.4	14.4	30.6	28.4	224.47	-24.7	-19.3
No. 6, W^{186} Metal	1.6	2.1	11.6	84.7	209.37	-21.0	-13.1
No. 7, $W^{184}O_3$	1.91	1.87	94.3	1.91	163.58	-23.2	-14.6

The lower values of the worths measured in Assembly No. 4 relative to those measured in Assembly No. 1 are a reflection of the harder spectrum in an all-tungsten-diluted system relative to the U^{238}-diluted Assembly No. 1. Central reactivity worths of U^{238} confirm this viewpoint.

A departure from the practice of using only fueled control rods has been made. A control rod loaded with aluminum oxide, located in the reflector at the periphery of the core, was found to have a total integral worth of 35 Ih. The rod is very useful for making accurate measurements of small changes in reactivity.

Measurements of spatially dependent reactivity worths are being made for several materials in the reflector region. Measurements have been completed for aluminum and for carbon (graphite) relative to a void, as a function of radial location. Results are presented in Table XIV.

Table XIV. Material Reactivity Worths Compared to a Void as a Function of Distance from Reactor Centerline

Distance from Reactor Centerline, cm	Aluminum		Carbon	
	Sample Weight, kg	Worth, Ih/kg	Sample Weight, kg	Worth, Ih/kg
26.71	6.26	+9.85	7.19	+15.85
29.46	6.26	+6.40	7.19	+11.40
33.58	22.77	+4.12	14.38	+8.52
39.58	20.87	+1.73	23.96	+5.49
45.69	29.22	+0.87	33.54	+3.83

Extensive studies with a previous ZPR-IX assembly and similar studies with a beryllium-reflected ZPR-III assembly indicate that the conventional Rossi-alpha ($\alpha = \beta/\ell$) is the sum of two components; α_1, having its origin in the long neutron lifetime characteristic of light metal reflectors, and α_2, associated with the relatively short core lifetime. Ithas been the practice in this program to define the "average prompt neutron lifetime" as the ratio of the calculated β_{eff} to the measured α_2 component. Table XV summarizes the kinetic parameters of ZPR-IX Assembly No. 4.

Table XV. Kinetic Parameters of ZPR-IX Assembly No. 4

Calculated β_{eff}	0.00664
α_1	$(1.25 \pm 0.24) \times 10^6$
α_2	$(5.19 \pm 0.28) \times 10^4$
ℓ (measured)	128 nsec
ℓ (calculated)	95 nsec

4. AFSR

First tests of a possible automatic power-level control rod were made, and indications are that it would do an excellent job of maintaining constant reactor power. The rod would be servo-actuated and obtain its control information from the reactor linear operating instrument. The total worth of the rod is 15 Ih, and it would provide reactivity insertion and withdrawal rates of 0.16 Ih/sec^{-1}.

Measurements of the neutron spectrum in AFSR made with the experimental fast neutron spectrometer show agreement with the general features of the calculated spectrum for energies between 40 keV and about 1.5 MeV.

B. General Fast Reactor Fuel Development

1. Metallic Fuels

Uranium-plutonium-base alloys are being investigated for use as fertile-fissile fuel materials in fast breeder reactors because many combinations of the base elements, which are readily available, have good neutron yield and breeding ratios. Alloying additions appear necessary, however, to improve the stability of the uranium-plutonium base in a fast-reactor environment and the compatibility of the fertile-fissile alloy with jacketing materials. Fizzium (Fz), which is a relatively high-zirconium combination of desirable fission-product metals retained in the fuel on reprocessing, has good alloying possibilities. The properties and behavior of uranium-plutonium-fizzium (U-Pu-Fz) alloys, as well as various combinations of the constituent elements, are therefore being investigated.

a. Uranium-Plutonium-Fizzium Alloys.

(i) Creep of U-15 w/o Pu-10 w/o Fz Alloy. The fizzium alloys have been shown to be weak at reactor operating temperatures.[1] Therefore the creep strength of these alloys is being determined. Since in a reactor it may be desirable to load a blanket rod on top of a fuel pin, a load of 11.5 (10^{-3}) kg/mm^2, which is the load exerted by twice the weight of the fuel pin, was used. At about the reactor operating temperature of 640°C, the first stage of creep (decreasing strain rate) of an as-cast U-15 w/o Pu-10 w/o Fz specimen, 0.366 cm in diameter (EBR-II size) and 5 cm long, lasted about 70 hr with a total strain of 0.0005. During 120 hr of the second stage of creep, a constant strain rate of $5(10^{-6})/hr$ (5% in 10^4 hr) was obtained, so that in 1500 hr at this rate the rod is presumed to decrease 0.0075 cm/cm of length. If we assume pessimistically that a 38.1-cm length creeps at this rate, the total decrease in

[1] See Annual Report, Metallurgy Division, 1963, ANL-6868, p. 17.

length will be 0.285 cm. After 1500 hr and 0.5% burnup, restraint by the cladding should prevent further decreases in rod length. At 190 hr the test was terminated.

(ii) Thermal-cycling Behavior of U-10 w/o Pu-10 w/o Fz, U-10 w/o Pu, and U Pins. Thermal cycling tests were made with four pins, one injection-cast uranium pin and three pins cast by tilt pouring into a copper mold, first homogenized for 23 hr at 850°C. The tilt-poured castings consisted of U-10 w/o Pu-10 w/o Fz, U-10 w/o Pu, and uranium, respectively. All four pins were given 100 thermal cycles between 700 and 475°C. In each cycle the specimens were held at 700°C for one hour and at 475°C for 4 hr. The times for heating and cooling each took about 2 hr.

The U-10 w/o Pu-10 w/o Fz alloy suffered no appreciable changes. The tilt-poured uranium pin casting contracted 10%, bowed slightly, and developed an elliptical cross section with a 6% difference in the major and minor axes. The injection-cast uranium pin broke at one end (probably through a blow hole), exhibited 5% growth, and developed a slight elliptical cross section. The U-10 w/o Pu pin increased 20% in length, which is in between the earlier results of 10% and 30%.[2] Apparently there is no simple correlation between growth of this alloy and type of casting or length of transfer time. The chill-cast specimens, which are finer grained, seem to grow less than the injection-cast material.

(iii) Thermal Conductivity of a U-10 w/o Pu Alloy. The thermal conductivity of the U-10 w/o Pu alloy was measured comparatively against an Armco standard, with results as listed in Table XVI. The values, though close to those of uranium, are about 25% lower at 100°C and 10% lower at 700°C.

Table XVI. Thermal Conductivity of U-10 w/o Pu Alloy

Temp (°C)	k, cal sec^{-1} cm^{-1} $°C^{-1}$
100	0.051*
200	0.056
300	0.063
400	0.070
500	0.078
600	0.086
700	0.094
800	0.100

*extrapolated

[2] Ref. 1, pp. 15-17

(iv) Compatibility of U-Pu-Fz Alloys with Potential Cladding Materials. In Figure 5 is plotted the log of the penetration into V-20 w/o Ti cladding by U-10 w/o Pu-10 w/o Fz versus log of the diffusion time for 550, 600, 650, and 700°C. This gives straight lines with a slope of 2. The average or most probable values of the penetration are plotted as circles; the variation in penetration for a given band on one given micrograph is shown as vertical bars. The penetration coefficients may be calculated by use of the standard diffusion expression

$$X^2 = Kt,$$

where X is the penetration into the cladding in centimeters, t the time in seconds and K the penetration coefficient in cm^2/sec.

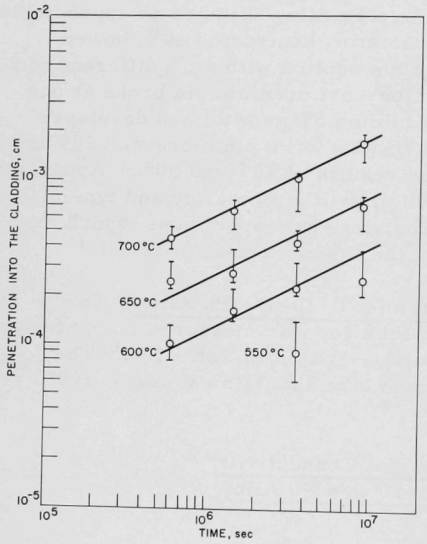

Figure 5

Penetration of V-20 w/o Ti by U-10 w/o Pu-10 w/o Fz at Various Times and Temperatures

Figure 6 shows the variation of log K versus the reciprocal of the temperature. The following equation, describing the variation of K with temperature, was obtained from Figure 5:

$$K = 0.21 \exp(-52{,}800/RT)\ cm^2/sec.$$

Initial results with V-20 w/o Ti versus U-15 w/o Pu-10 w/o Fz indicates behavior similar to U-10 w/o Pu-10 w/o Fz. However, the curves for log X versus log t plot are shifted slightly upward. Apparently V-20 w/o Ti will be an adequate cladding material for U-15 w/o Pu-10 w/o Fz.

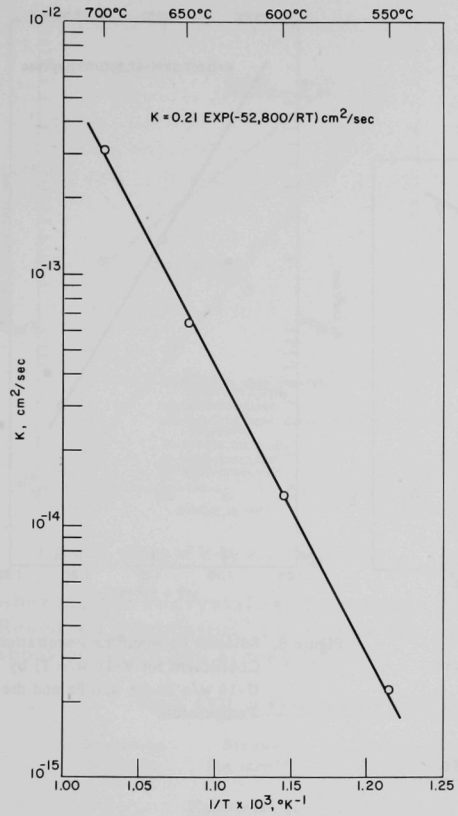

Figure 6

Relationship between the Penetration Coefficient for V-20 w/o Ti by U-10 w/o Pu-10 w/o Fz and the Temperature

Figures 7 and 8 present data for V-10 w/o Ti versus U-10 w/o Pu-10 w/o Fz replotted in the same manner as for V-20 w/o Ti. Again a slope of 2 on the log X versus log t plot adequately describes the data and gives the equation

$$X^2 = Kt.$$

Figure 8, showing the variation of K with temperature, can be described by

$$K = 0.017 \exp(-47,300/RT) \text{ cm}^2/\text{sec}.$$

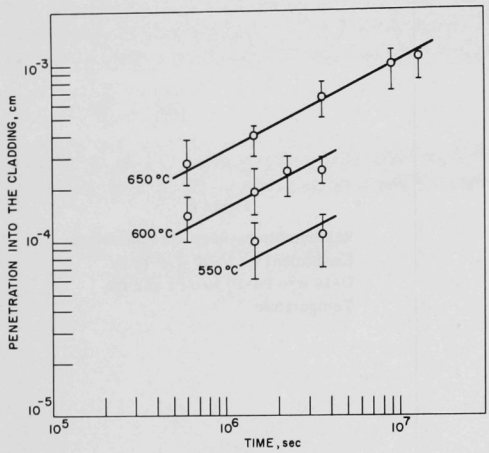

Figure 7. Penetration of V-10 w/o Ti by U-10 w/o Pu-10 w/o Fz at Various Times and Temperatures

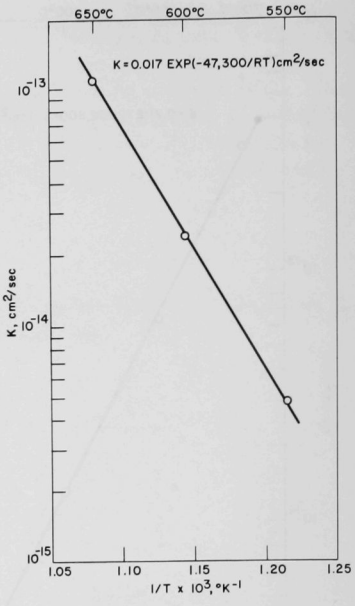

Figure 8. Relation between the Penetration Coefficient for V-10 w/o Ti by U-10 w/o Pu-10 w/o Fz and the Temperature

2. Development of Jacket Materials

a. Vanadium Alloys.

(i) Creep of V-20 w/o Ti. Results of creep testing of V-20 w/o Ti sheet at 650°C are shown in Figure 9 as log minimum strain rate plotted against stress. Minimum creep rates were determined from tests conducted under constant load and tests in which the load was varied, in a vacuum of 2×10^{-5} mm Hg.

Material from two extrusions was used. Extrusion 264 had been solution heat treated at 1300°C for 15 min before a 65% cold reduction in area. Extrusion 281 was not solution heat treated. Specimens from each extrusion were tested in both the stress-relieved and the recrystallized conditions.

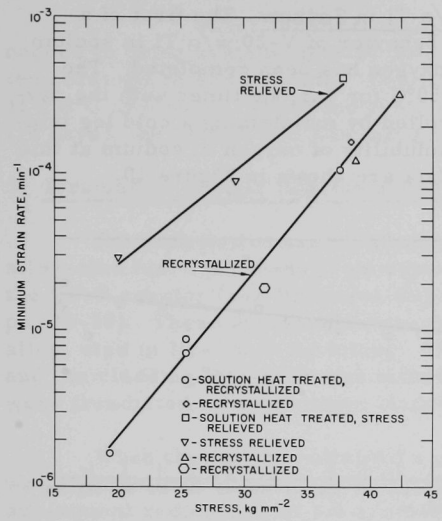

Figure 9. Creep of V-20 w/o Ti at 650°C

As seen in Figure 9 there appears to be no significant difference between the creep rates of specimens that had been solution annealed and those that had been solution annealed prior to the final cold-working operation. There does, however, appear to be an appreciable difference between creep rates of stress-relieved and recrystallized specimens. The stress-relieved material has a higher creep rate for the same stress level in the stress range investigated.

The creep results are presented in greater detail in Table XVII. Two of the tests were conducted at a constant load to permit determination of the rupture time. At stresses around 38 kg mm^{-2} the stress-relieved specimen fractured in 7 hr, whereas the recrystallized specimen fractured in 11 hr. Data by Armour Research Foundation[3] has shown the rupture life of V-20 w/o Ti to be about 50 hr at this stress level.

Table XVII. Creep Results for V-20 w/o Ti Tested at 650°C in Vacuum

Specimen Number	Stress (kg mm^{-2})	Minimum Strain Rate (min^{-1})	Rupture Time (hr)	Condition
	Extrusion 264 - Solution Heat Treated at 1300°C for 15 min			
TV-20-1S	37.8	4.2 x 10^{-4}	7	Stress relieved, 700°C, 1 hr
TV-20-2S	19.3	1.6 x 10^{-6}	*	Recrystallized, 900°C, 1 hr
	25.3	7.2 x 10^{-6}		
	37.7	1.05 x 10^{-4}		
	25.3	8.8 x 10^{-6}		
		Extrusion 281		
TV-20-3S	38.5	1.6 x 10^{-4}	11	Recrystallized, 900°C, 1 hr
TV-20-4S	38.9	1.2 x 10^{-4}	*	Recrystallized, 900°C, 1 hr
	42.3	3.2 x 10^{-4}		
TV-20-6S	31.6	1.9 x 10^{-5}	68	Recrystallized, 900°C, 1 hr
TV-20-7S	29.3	9.0 x 10^{-5}	*	Stress relieved, 700°C, 1 hr
	20.0	2.9 x 10^{-5}		

*Load changed during test.

[3] Development of Vanadium-base Alloys, ARF-2094-1 (Feb 19, 1958).

(ii) Corrosion of V-20 w/o Ti in Sodium. The first of a planned series of experiments on the behavior of V-20 w/o Ti in sodium containing various concentrations of oxygen has been completed. The samples were exposed to sodium at 650°C for various times with the oxygen concentration in the sodium controlled by maintaining a cold leg temperature at 132°C. The equilibrium solubility of oxygen in sodium at this temperature is 6 ppm. Weight-gain data are shown in Figure 10.

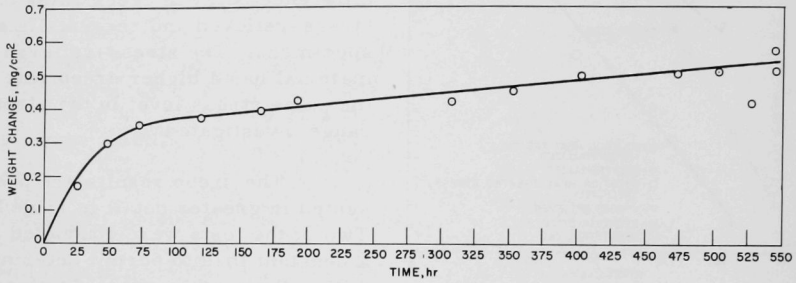

Figure 10. Corrosion of V-20 w/o Ti in Sodium

The depths of oxygen contamination into the underlying metal for two different exposure times are shown in Figure 11, as detected by Knoop Hardness Number (KHN) measurements.

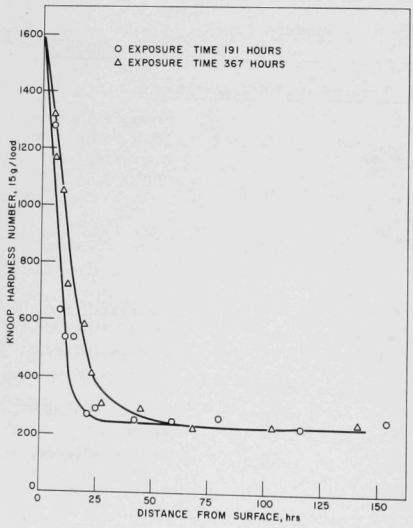

Figure 11

Behavior of V-20 w/o Ti Samples Exposed to 650°C Sodium Containing ~6 ppm Oxygen

After termination of the above test, an excess of Na_2O_2 needed to bring system up to 50 ppm oxygen was added and the cold-trap temperature raised to 232°C. Equilibrium solubility of oxygen in sodium at 232°C is 50 ppm. After the system was believed to be equilibrium (16 days), the second run was initiated.

3. Irradiation of Fast Reactor Fuels

Postirradiation examinations are being made of six refractory-alloy-clad fuel specimens from capsule CP-32 which was irradiated in the CP-5 reactor (see Progress Report for May 1964, ANL-6904, pp. 28-30). These specimens were fueled with U-20 w/o Pu-10 w/o Fz alloy, clad in Nb-1 w/o Zr tubing. The ID of the tubing was 3.96 mm, and the cladding thickness was either 0.38 or 0.64 mm. The specimens were irradiated at a maximum cladding temperature of 615°C.

When the fuel had attained a calculated 3.3 a/o burnup, the capsule was neutron radiographed and all claddings were noted to be intact. The subsequent radiograph at 3.6 a/o burnup revealed a failure of a specimen clad in 0.38-mm-wall tubing. This tubing had been stress relieved. A companion specimen clad in annealed tubing was intact.

When the capsule was opened the failure was found to consist of three longitudinal splits in the cladding at the midsection of the fueled portion of the specimen. The splits did not exceed 1 cm in length, but bowed outward because of internal fuel pressure, so as to produce a bulge at this section of the specimen. Diameter, length, and density measurements made on all intact specimens failed to denote any significant change. Diameter measurements taken adjacent to the bulge on the failed specimen did not show diameter increases. Fuel elongation within the claddings, as measured from the neutron radiographs, averaged 7 percent. A metallographic examination is in progress on the nature of the cladding failure. The intact specimens will be reserved for post-irradiation annealing studies.

Specimens from irradiation capsule CP-36 were also examined. These six specimens were fueled with U-15 w/o Pu-10 w/o Fz and clad in Hastelloy-X tubing lined with 0.05 mm of tungsten to prevent the formation of a eutectic between the fuel and the cladding. The cladding ID was 3.86 mm and the total wall thickness was 0.28 mm. The specimens were irradiated for a calculated 1.2 a/o burnup at a cladding temperature of 550°C. Cladding failure occurred when the cladding temperatures were elevated to about 650°C. Three specimens failed at the midsection of the fueled portion of the rod. Diameter, length, and density measurements on the intact specimens showed no significant change. Fuel elongation within the cladding averaged 10 percent, as determined from neutron radiographs.

Capsule CP-35 contains specimens fueled with U-20 w/o Pu-10 w/o Fs alloy. Two fuel pins have a 3.33-mm diameter instead of the standard 3.66 mm. The other four specimens have the standard 3.66-mm OD but have 1.4-mm-diameter axial holes. The cladding material is Nb-1 w/o Zr alloy tubing with an ID of 3.96 mm and a wall thickness of 0.23 mm. The specimens were irradiated for a calculated 2.5 a/o burnup at maximum cladding temperatures of 650°C. The capsule was removed from the reactor when the temperature indicated the probability of a cladding failure. Neutron radiography has confirmed this supposition. The capsule will be opened and the specimens examined.

4. Development of Fuels for Zero-power Reactors

a. Development and Fabrication of Fuel Elements. Design drawings, product specifications, and a quality assurance plan have been prepared and approved for SEFOR-ZPR-III critical fuel elements. A joint effort by GE-APED,* AEC-SAN,* ANL-Idaho, and ANL-MET* resulted in mutually acceptable requirements defining the desired fuel elements.

Based on supporting engineering development performed by ANL-MET, the SEFOR fuel will consist of U-20 w/o Pu-2.5 w/o Mo precision cast core plates jacketed in Type 304L stainless steel. Jackets will be cold drawn in the shape of a half-can from 0.012-in.-thick material. Two half-can sections will be assembled around each fuel core plate. Matching turned-out flanges on each half-can will be sealed by a peripheral TIG weld. The two ends of each element will have weld-cast bearing shoes that will transmit thermal expansion of the core plate to adjacent fuel elements.

Two 5.1 x 7.6-cm nominal size fuel elements containing 20 w/o Pu-2.5 w/o Mo-U core plates have been fabricated. These elements closely approximate the reference SEFOR design, deviating only in minor dimensions. Inspection of the finished elements revealed the jackets to be leak tight (as observed in a helium mass spectrometer) and free from alpha contamination. Additional plutonium-bearing elements will be fabricated to refine and study the manufacturing procedures. However, the feasibility of producing acceptable elements to the SEFOR-ZPR-III reference design has been demonstrated.

---

*SEFOR = Southwest Experimental Fast Oxide Reactor; GE-APED = General Electric Atomic Power Equipment Division; AEC-SAN = Atomic Energy Commission San Francisco Office; ANL-MET = Argonne National Laboratory, Metallurgy Division.

b. Properties of Fuels for Zero-power Reactors. The U-20 w/o Pu-2.5 w/o Mo alloy has been selected as the fuel for the SEFOR Critical Experiment in ZPR-III. Tentatively, a similar alloy containing 25 w/o Pu appears to satisfy ZPPR* requirements. Titanium also appears to be a promising alloying addition for the ZPPR fuel.

The metallographic structure of a U-22 w/o Pu-2 w/o Mo alloy casting shows what appears to be a thin, continuous-grain-boundary network. Yet this alloy has much better mechanical properties than other alloys that have been studied. At high magnification, and especially in long-time 500°C annealed specimens, this grain-boundary material has been shown to consist of more than one phase. The cast structure proved to be too fine to determine, by electron-beam microprobe analysis, the composition of the phases that make up this network. Its overall average composition is not appreciably different from the composition of the matrix.

The specific heat of a U-20 w/o Pu-2.5 w/o Mo alloy, as determined by drop calorimetry, was found to be 0.37 cal g^{-1} $°C^{-1}$ for the range from 25°C to 501°C and the range from 25°C to 435°C. The accuracy of the heat content data from which the specific heat was calculated was ±3%.

Air corrosion tests have been continued. The U-20 w/o Pu-1.3 w/o Ti alloy specimen (see Progress Report for June 1964, ANL-6912, pp. 28-9) is still sound after 60 days of exposure and has not gained any further weight, but the surface has begun to powder slightly. The U-20 w/o Pu-1.3 w/o V alloy specimen has gained 6.79% in weight after 60 days, and about 80% of it has disintegrated into a very fine powder.

c. Fabrication of Doppler Test Elements. The Reactor Physics Division requires 32 test capsules for studying the relationship between the Doppler effect and plutonia concentration in ZPR-III. Half of the 32 capsules are to be loaded with PuO_2 pellets. The remaining 16 are loaded with pellets of UO_2-12.5 w/o PuO_2. Twelve cored pellets, measuring 1.27 cm in OD by 1.27 cm long, with a 3.6-mm axial hole, are assembled in each capsule over a thermocouple protective tube. The outside of the capsule is covered by a spirally wound brazed-in-place heating element. After loading, the element is pressurized with helium to about 1 kg/cm^2 and sealed. Before acceptance, a helium mass spectrometer is used to leak test each capsule at room temperature and at 1000°C.

Four kilograms of UO_2-12.5 w/o PuO_2 have been processed into granules. Two hundred pellets were pressed, sintered, and loaded into capsules.

---

*Zero Power Plutonium Reactor

Loading the Doppler capsules without contaminating the exterior of the capsules presented difficulties. The oxide pellets tend to form dust and are highly contaminating. The exterior of the capsule is roughened by the spiral heater element and does not present a satisfactory surface for sealing or for decontaminating. Loading was successfully accomplished by attaching the capsule to a tube extending through the hood wall by means of a soft plastic fitting. The plastic was compressed into the heater helices to form a protective seal. The pellets were loaded into the capsules through a 0.1-mm-thick loading funnel that was cemented at the upper edge to the fitting. In spite of these precautions, nearly all of the capsules loaded showed a surface α count of several thousand dpm, but they were cleaned to less than 200 dpm direct count and zero wipe count.

The cap welds were produced by the tungsten-arc inert-gas method. After welding the capsules were again surveyed and decontaminated as required. The final manufacturing operation consisted of evacuating the capsule and backfilling with helium gas. The fill tube was pinched closed and welded. After an additional alpha survey, further decontamination, and rough leak detection, the capsules are heated to 1000°C and leak detected at operating temperature.

All 16 capsules containing UO_2-12.5 w/o PuO_2, have been assembled, welded, and passed rough leak detection. Seven capsules have been leak detected at 1000°C. One was found to leak at operating temperature.

The first batch of PuO_2 for the production of pellets, has been weighed, pressed, and granulated. Approximately 800 g of the granules are ready for firing. Samples have been submitted for spectrochemical analysis and plutonium assay.

5. Development of Carbide Fuels

a. Plutonium and Plutonium-Uranium Carbides. For fast breeder reactors solid-solution uranium-plutonium monocarbide fuels are usable at higher temperatures than solid metallic fuels and have a thermal conductivity which is superior to that of oxide fuels. Methods are being developed for producing vibratory-compacted carbide radiation specimens for EBR-II. Additional development is necessary on both the preparation of the solid-solution carbide fuels and the fabrication of uncontaminated specimens.

The diffusion of plutonium carbide into uranium carbide is being investiaged. Previously reported work showed a large loss of plutonium when -80 mesh (U.S. Standard Sieve Series) powders were mixed and vacuum-fired in the range from 1900°C to 2000°C. Analytical

results from -325 mesh material vacuum-fired in the range from 1800°C to 1850°C for 30 min showed very little loss of plutonium, but a depletion of the carbon from 4.7 w/o in the starting material to 3.9 w/o in the product. The oxygen content of the product was 0.3 w/o. Metallography showed a grain-boundary phase, which supports the hypostoichiometric analytical results. Some reaction occurred at the carbide-tantalum crucible interface. Carbide at the interface contained over 5 w/o tantalum, but the level was less than 100 ppm of the bulk of the material.

Combining all of the data, it appears that the best results will be obtained by pressing pellets from -325 mesh powders and sintering in the range from 1700°C to 1800°C. An atmosphere should be used to retard plutonium volatility, and either molybdenum or tungsten should be used as the crucible material.

b. Vibratory Compaction. The irradiation specimens are to contain a 36-mm column of fuel in a 61-cm-long by 6.53-mm-ID (24-in.-long by 0.257-in.-ID) jacket. This material is being compacted by a Syntron Model V-80 vibrator.

Two methods are being evaluated to produce uncontaminated specimens. The first utilizes a sealed tube holder that screws into the platen of the vibrator. Loading is accomplished through an O-ring-sealed fill tube. The second method utilizes a metallic compression fitting on the open end of the tube. The tube is wrapped with aluminum foil and its base screws on to a stud in the platen. As before, the O-ring sealed fill tube is used.

C. General Fast Reactor Fuel Reprocessing Development

A method of separating plutonium and rare earth elements by extractions between molten metal and halide salt phases is being developed for advanced fast reactor fuels containing plutonium. The procedure would be applicable to fuels of either the metallic or ceramic type.

1. Materials and Equipment Evaluation

A corrosion program is underway to evaluate the performance of various steels in various process systems and environments. Croloy $2\frac{1}{4}$, which has shown promise as a construction material for the containment of Cd-Mg-Zn-U/halide flux systems (see Progress Report for June 1964, ANL-6912, p. 31), has been tested for oxidation resistance in air. Eight samples were exposed to air at 600°C, the probable operating temperature of the High Temperature Extraction Facility.* The samples were examined after 200 hr and after 400 hr. The rate of scale formation

*The High Temperature Extraction Facility will be used to demonstrate the feasibility of separating uranium and plutonium from rare earths in fused salt-molten metal systems and will consist of packed extraction columns and auxiliary equipment.

decreased in the second 200-hr exposure to about 25% of the rate seen in the first 200 hr. Metallographic examination of the samples indicated a scale thickness of about $\frac{1}{32}$ in. in 400 hr. Croloy $2\frac{1}{4}$ is still under consideration for this application, but protection from atmospheric oxidation may be required.

2. Advanced Processes

a. Use of Cd-Zn-Mg Alloys. Use of cadmium-zinc-magnesium alloys instead of zinc-magnesium alloys as liquid metal solvents for the EBR-II Skull Reclamation Process might make it possible to utilize stainless steel instead of tungsten process vessels, thereby decreasing costs and increasing considerably the design flexibility. However, the uranium oxide-reduction step, for which a yield of 95 to 97% is required, might be affected significantly by the change in solvent (because of possible low reduction yields). The rate and extent of U_3O_8 reduction by Cd-Mg-Zn solutions has been studied in two experiments. Charges of 14.15 g U_3O_8 were mixed with 600 g 70 a/o Cd-15 a/o Mg-15 a/o Zn, 300 g 30 m/o NaCl-20 m/o LiCl-50 m/o $MgCl_2$, and 15 g MgF_2 at 600°C under argon for 4 hr. Yields of 87 and 90% were obtained within 30 min, and the extent of reduction remained constant at these levels during the remainder of the tests. These results are sufficiently encouraging to warrant further study of reductions in this solvent.

b. Distribution of Plutonium between 30 m/o NaCl-20 m/o KCl-50 m/o $MgCl_2$ and Zinc-Magnesium Alloys. The distribution coefficient of plutonium between zinc-magnesium alloys of various compositions and 30 m/o NaCl-20 m/o KCl-50 m/o $MgCl_2$ over a temperature range from 600 to 800°C is being studied to aid in the selection of optimum conditions for plutonium-rare earth fission product separations in processes for fast breeder reactor fuels. The results obtained thus far indicate an increasing tendency for the plutonium to distribute to the salt with increasing temperature and a larger temperature dependence at low magnesium concentrations (1-12 w/o) than at high magnesium concentrations (50-90 w/o).

3. Head-end Treatments for Refractory Fuels

a. Decladding. Study of the removal of vanadium-20 w/o titanium (TV-20) cladding from metallic fuels by chlorination in a molten salt has continued. The objective of this study is to find a salt composition, ratio of salt to fuel, temperature, and amount of chlorine addition that will volatilize titanium and vanadium tetrachlorides without significant loss of volatile uranium chlorides. The most promising salt system observed thus far is 40 m/o NaCl-30 m/o KCl-30 m/o $CaCl_2$. In an experiment this salt (containing TV-20 and uranium metal) was sparged at 600°C with chlorine at a ratio of 0.8 liter of chlorine per gram of uranium. More than 99% of the uranium was retained in the salt, and only 0.2% of the vanadium and titanium was retained.

In studies directed at the selection of the appropriate fused salt for the decladding work, two immiscible liquid salt phases were observed in UCl_4-2KCl-$BaCl_2$-$CaCl_2$. The two phases were sampled at a composition in the $CaCl_2$-rich region of the system and were analyzed. The upper phase contained 6.1 m/o UCl_4, 17.6 m/o KCl, 50.5 m/o $CaCl_2$, and 26.8 m/o $BaCl_2$; the lower phase contained 30.8 m/o UCl_4, 53.0 m/o KCl, 6.8 m/o $CaCl_2$, and 9.4 m/o $BaCl_2$. Liquid immiscibility was also observed at one composition of the UCl_4-KCl-NaCl-$CaCl_2$ system.

4. Removal of Nitrogen from Argon

The kinetics of the reaction of nitrogen with titanium sponge is being studied because of a possible future need to remove nitrogen from the argon atmosphere of the Argon Cell of the EBR-II Fuel Cycle Facility. For the first runs, at a nitrogen concentration of 1000 ppm, the apparatus consisted of a series of eight 3-g titanium sponge test beds and a gas-circulating loop. The circulation rate was such that only a very small fraction of the nitrogen in the gas stream reacted with the titanium in a single pass through the beds. Thus, all beds were exposed to gas having approximately the same nitrogen concentration. The nitrogen concentration of the gas was returned to 1000 ppm before each pass. The extent of reaction of the titanium test material was determined at intervals during the run by successively and permanently removing the topmost titanium bed and determining its nitrogen content.

In an earlier run (see Progress Report for August 1963, ANL-6780, p. 24), about 54% of the titanium was converted to titanium nitride at a bed temperature of 900°C and with 1000 ppm nitrogen in the argon stream. Three additional runs at a temperature of 900°C with argon containing approximately 1000 ppm nitrogen have been completed recently. The data indicate that the reaction follows a modified exponential rate law, and that the rate decreases markedly after 50% conversion of the titanium has been obtained.

D. Sodium Coolant Chemistry

1. Analysis for Oxygen

Current efforts to develop a method for the analysis of oxygen in sodium utilize the reaction ^{16}O (n,p)^{16}N. A sodium sample in a container is irradiated by means of a Cockcroft-Walton generator; the sample is then transferred to the counting equipment by means of a pneumatic transfer system.

Previous studies (see Progress Report for May 1964, ANL-6904, p. 43) had indicated that the lower limit of this method would be set by the oxygen content of the container used to protect the sodium from oxidation during irradiation and counting. Tests have been made using 2S aluminum

containers; the oxygen content of this material has been determined to be about 10 ppm. Tests were then made with five replicate samples of reagent-grade sodium in 2S aluminum containers. The sodium was found to contain 103 ± 18 ppm oxygen. Additional studies were made, using a standard oxygen sample, to determine the practical limit of reproducibility and precision of the method. With the Cockcroft-Walton generator presently available, it is estimated that oxygen levels of 50 ppm can be determined to ±20 ppm. Further work on this method is being planned.

2. Solubility of Carbon in Liquid Sodium

As part of the study of the chemistry of carbon transfer via liquid sodium, the solubility of carbon in sodium is being measured. The total carbon concentrations in liquid sodium in contact with graphite were found to be about 73 ppm at 158°C, about 58 ppm at 300°C, and about 110 ppm at 445°C. Whether or not oxygen plays a role in this system is not known, but may be better understood after oxygen concentrations in these samples are measured.

E. EBR-II

1. Reactor Plant

After completion of instrument air and power-failure testing (see Progress Report for June 1964, ANL-6912, p. 36), the temperature of the primary bulk sodium was increased to 700°F, and plant-standby conditions were established. Approval was received to begin the approach to power experiments on July 16, 1964; the reactor was made critical at 2030 hours that day. The reactor has been operated at powers up to 10 MW.

a. Approach-to-power Experiments. With the reactor at 50 to 100 kW, the detectors for nuclear channels 4, 5, 6, and 7 were repositioned to make them effective at power levels up to approximately 80 MW. Voltage plateaus were determined for all installed compensated ion chambers. Transfer function measurements were completed at 50 and 500 kW. The reactor power level was then raised in 1-MW increments to 5 MW. The primary flow was held at 100% and 74% while transfer function data and heat balance data were obtained. The power was then raised incrementally to 10 MW for additional data points.

b. Oscillator Studies. Two independent types of analyzing equipment are being used in oscillator studies: the null device and the cross-correlation integrating device which was used successfully on BORAX V and EBR-I. Comparison of data between the two sets of analyses is better than 1% on amplitude and $\frac{1}{2}°$ on phase. Because the cross-correlation analysis is so much quicker at the lower frequencies, it is being used as the prime data-taking device. Preliminary investigation of the 5-MW data would indicate that the reactor system is producing no unexpected feedback properties.

c. Power and Flow Coefficients. The power coefficient was determined over the small range of 10 MW as -2 Ih/MW by reference to the change in the position of the calibrated control rod. Likewise, the change in control rod position in changing from 100% to 74% flow gives the first indication of the flow coefficient. These results are listed in Table XVIII.

Table XVIII. Power and Flow Coefficients

Power (MW)	Flow (%)	Control Rod No. 3 (in.)	Reactor Temp (°F)	Δk/k (Ih)
0.5	100	9.52	700	0
1.1	100	9.62	700	-1
2.2	100	9.92	700.5	-3.5
3.3	100	10.20	701	-5.5
4.5	100	10.59	701	-9.2
5.6	100	10.89	701.5	-11.2
5.0	100	10.55	699	-10.5
5.0	100	5.31*	699	-10.5
10	100	6.03*	698	-20.5
5.0	100	11.00	700	0
5.0	74	11.31	700	-1.5

*Changed bank rod position.

d. Fuel-handling Maintenance. Under plant-standby conditions, the fuel-unloading-machine gripper was removed, cleaned, inspected, and then reinstalled and adjusted. The fuel-transfer-port hex tube was cleaned because of a tight area about 9 to $9\frac{1}{2}$ ft below the top face of the transfer port.

e. Primary Purification System. During operation at plant-standby conditions, the plugging-valve bellows of the primary sodium-sampling system failed. This bellows was replaced and the sampling system restored to operative condition.

The siphon break system for the sodium-purification line from the reactor is being modified to provide remote opening of the siphon break valve.

f. Fuel Element Rupture Detection (FERD) Loop. The installation of the FERD loop shielding has been completed and sodium flow has been established through the loop. Detection instrumentation is being installed and checked out.

g. Argon-purification System. A filter in the sodium vapor trap No. 1 became partially plugged and was replaced. Plugging was probably due to sodium aerosol and vapor carried into the trap during the purging of nitrogen from the blanket gas last month.

2. Sodium Boiler Plant

Heatup of the primary and secondary systems continued, with 1270 psig steam drum pressure being maintained. When the primary sodium temperature reached 670°F, heat input in the primary and secondary systems was adjusted so that equilibrium conditions were attained with natural convection in the secondary system. At this condition, thermal data were obtained, and flowmeters and temperature indicators were checked. Power was then applied to the secondary pump in the reverse direction to reduce thermal convection flow, and the primary tank temperature was increased to 700°F.

From July 8 to July 24, the primary tank temperature was maintained at 700°F by adjusting secondary flow while low-power physics experiments were conducted with the reactor. Under these conditions, the secondary sodium plugging temperature rose from 250°F to 300°F in approximately 5 days. The temporary cold trap was placed in operation, reducing the plugging temperature to 250°F in about 2 days.

The argon cover gas system was purged twice to reduce the hydrogen, helium, and nitrogen impurity levels. The hydrogen-helium level was reduced from approximately 1700 ppm to approximately 800 ppm. A valve in the sample line between the surge tank and the gas chromatograph was found to be partially plugged and was replaced. It was also found necessary to install a small diaphragm pump in this line to assure an adequate gas sample to the chromatograph.

3. Power Plant

The Power Plant systems remained in operation during the month with steam drum pressure at 1270 psig. During low-power reactor operation, the startup feedwater pump was operated with manual drum level control. To conserve heat, the blowdown system was left in shutdown condition and steam traps were operated manually. On July 25, when the reactor power was increased to 5 MW, the motor-driven boiler feed pump was put into operation, along with the automatic drum level control system. Normal blowdown flow (20,000 lb/hr) was established, and the steam traps were placed in normal operation except for three traps which leaked excessively. Auxiliary steam is used for the air ejector, turbine seals, and the deaerating heater as a convenience in establishing standby plant conditions following reactor scrams.

A temporary blowdown line was installed between the body of the turbine stop valve and the outside of the building. This line will be used to blow debris out of the steam line leading to the turbine just before the turbine is placed in operation.

4. Fuel Cycle Facility

a. Argon Cell. An argon-atmosphere enclosure system is being installed at Argonne, Illinois, in order to test the effect of a dry argon environment on the operation of equipment to be used in the EBR-II Argon Cell. One glovebox and an argon purification system (similar to that in the EBR-II Argon Cell) have been previously installed and placed in operation (see Progress Report for May 1964, ANL-6904, p. 47). The glovebox is being used to test equipment for the last step of the skull-reclamation process. As part of this enclosure system, the construction of a large inert atmosphere enclosure, 24 ft long by 12 ft wide by 14 ft high, was begun. It will be equipped with glove ports and a large roof hatch (12 ft long by $7\frac{1}{2}$ ft wide) for handling large pieces of equipment.

The new enclosure will be used initially for the testing of a prototype (M-2) skull oxide-reclamation furnace whose fabrication is underway. The furnace will be resistance heated and will accommodate a 14-in.-ID pressed-and-sintered tungsten crucible.

b. Development of Remote Controlled Methods and Equipment for Fuel Fabrication

(i) Grapples. Grapple failure can be extremely serious. Two types of grapples were constructed for handling the EBR-II fuel element. A blower-cooled, electrically powered grapple is shown in Figure 12. A second grapple, pneumatically powered and containing no electrical components within the radioactive cell, is shown in Figure 13 and in an exploded view in Figure 14.

(ii) Fuel Element Welding. Remote, arc spot welding is used to complete the final assembly of core and blanket fuel elements in the Fuel Cycle Facility. The hexagonal tube enclosing the upper and lower blanket sections and core sections is attached to the lower adapter by six fusion spot welds. The spot welders are located on a stationary platform in the lower part of the fuel-element assembly machine. Power supply for welding is located in the basement and consists of a Vickers Type 51E30-2 dc arc welder. Mineral-insulated coaxial copper cables conduct the current from the welding power supply approximately 9 m (27 feet) to the assembly machine inside the process cell. The commercial welding supply was equipped for initiation of the arc by a high-voltage radio-frequency current generated by a commercial spark gap oscillator. However, the mineral-insulated cables used in this application attenuated the radio-frequency power so that insufficient ionization was provided at the welding gap. To correct this problem by replacing the mineral-insulated cables with low-impedance cables would be very costly and would not assure that no further problems would be encountered.

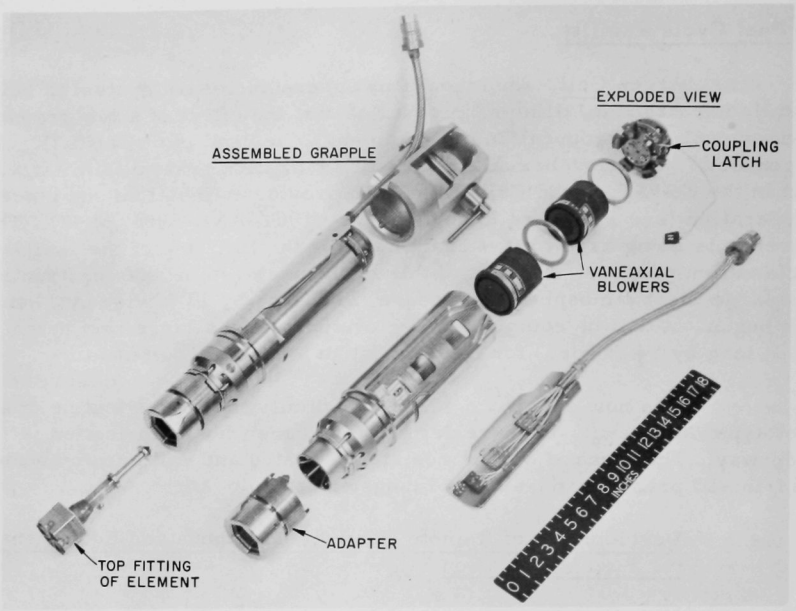

Figure 12. Electrically Powered Grapple for Handling EBR-II Fuel Elements

Figure 13. Pneumatically Powered Grapple for Handling EBR-II Fuel Elements

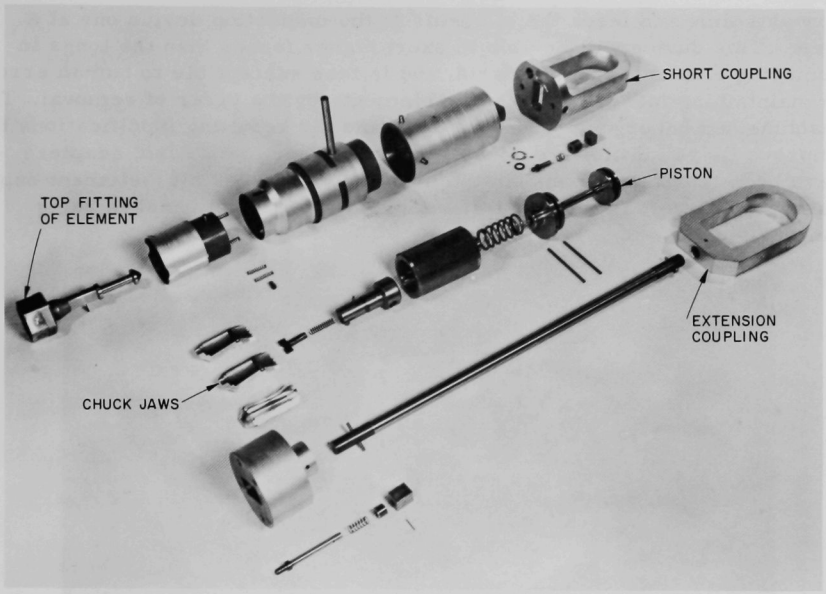

Figure 14. Exploded View of Pneumatically Powered Grapple for Handling EBR-II Fuel Elements

A method was developed to start the arc by means of a dc high-voltage capacitor-discharge circuit isolated from the welder power supply by heavy-duty silicon diodes. The arc starter is shown in Figure 15, and its schematic diagram in Figure 16. In operation, the circuit functions as two power supplies, one providing high voltage to ionize the gap and start the arc, and the other to stabilize the arc by discharge of large capacitors. The circuit is energized when the welder is turned on. This is done by energizing the power relay (R) from a voltage-sensitive relay (R-13). The voltage-sensitive relay also cuts off the arc starter when the weld current is established. Diodes (D-2) isolate the two voltage supplies, and diodes (D-3) isolate the high voltage from the welder. The controls are protected from transient voltage spikes by means of resistor-capacitor networks. Rheostats (R-1 and R-2) adjust the charging rate of capacitor (C-1) to the discharge rate of the arc. The choke stabilizes the arc and insures an even flow of current. Auxiliary controls energize the relay contacts connected to the welding guns, and the entire welding circle is programmed.

(iii) Fuel Element Removal Machine. At the present time the individual fuel elements are removed from the support grid of the fuel subassemblies by special tongs using the Model 8 Master-Slaves. The Fuel Element Removal Machine will perform this operation and will be an addition to the Core Subassembly Dismantler. It removes the elements a

row at a time and feeds the elements to the inspection device one at a time. This device will be able to exert higher forces than the tongs in removing elements from the grid, and is less susceptible to human error in maintaining identification of the elements by the order of removal. The machine has undergone extensive tests and the resulting modifications to improve its reliability are about 90 percent complete. Also, adapters have been fabricated to enable the machine to process a 61-element subassembly as well as the usual 91. A prototype control panel is being built.

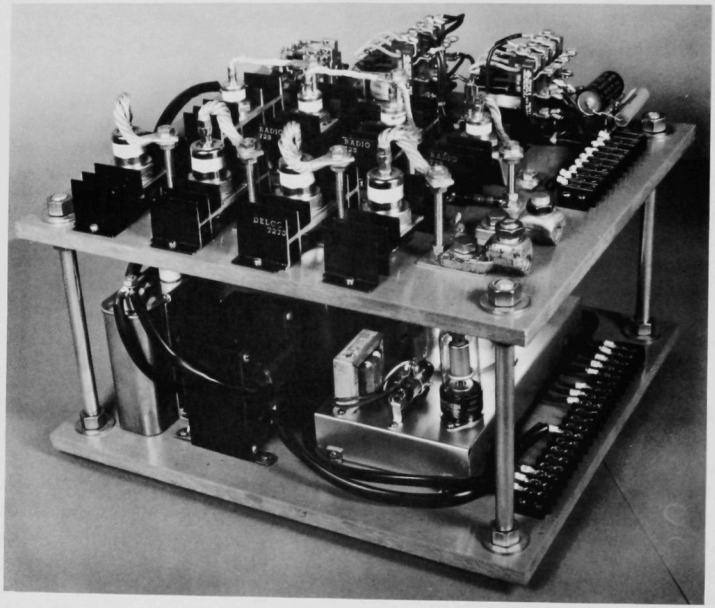

Figure 15. Arc Starter for Remote Spot Welding of EBR-II Fuel Elements

c. Preparations for Operations

(i) Skull Reclamation Process. Mixing tests have been carried out to obtain information for the design of mixing equipment for use in the M-2 furnace. Tests were conducted at 350°C with molten lead (as a stand-in for zinc in the skull reclamation process) in an unbaffled steel crucible into which a stirrer was introduced in a true vertical attitude. Good mixing was obtained at 775 rpm with a four-bladed steel impeller (4 in. in dia by $1\frac{1}{2}$ in. high) with the blades pitched at 45°. For use with zinc, such an impeller (and its shaft) can be fabricated of Mo-30 w/o W. Power requirements for the stirrer motor were modest, $\frac{3}{4}$ hp at a mixing speed of 775 rpm.

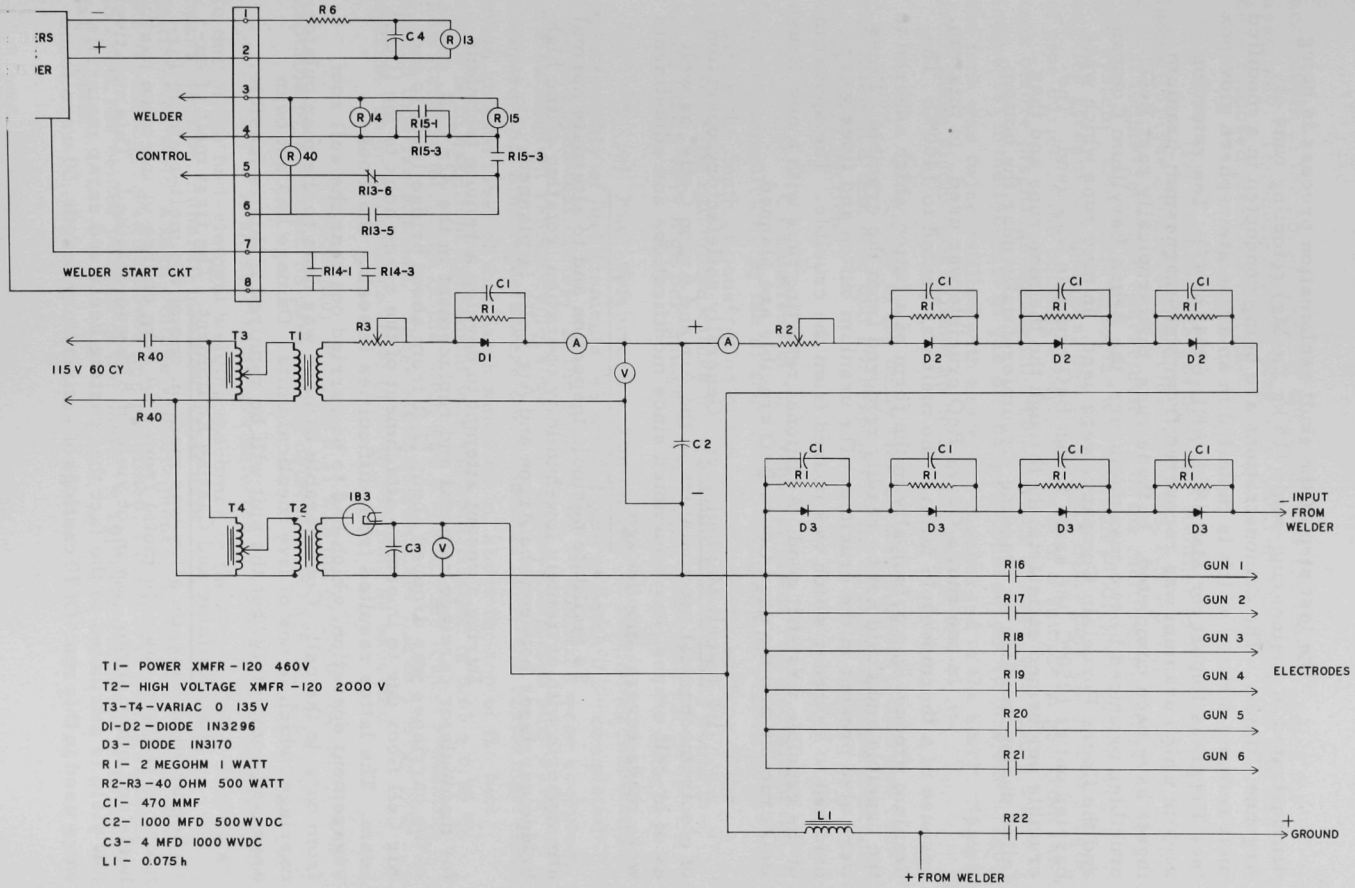

Figure 16. Schematic Diagram for dc High-voltage Capacitor-discharge circuit

The last step of the skull reclamation process is being demonstrated in engineering-scale (15 kg Zn-Mg) retorting runs at Argonne, Illinois. The demonstrations are being conducted in a modified melt refining furnace which is installed in an argon atmosphere glovebox (see Progress Report for May 1964, ANL-6904, p. 47). Ten retorting runs in which uranium was recovered from zinc-magnesium-uranium ingots have been completed. In these runs, thixotropically cast BeO crucibles produced by two manufacturers, the Brush Beryllium Company and the Coors Porcelain Company, were used. In nine runs which were carried out at 1250°C, the same Brush BeO crucible was used. The crucible performed satisfactorily through the the nine runs and then failed during handling by cracking circumferentially near the bottom.

In one run, a Coors BeO crucible was used. In this run, because of a thermocouple failure, the melt was heated to 1400°C. The uranium product was principally in the form of a button which adhered to the crucible and could not be readily removed from the crucible. Fines were also present in the crucible. The uranium button and fines were oxidized to a powder which was poured from the crucible. The appearance of the crucible was still good. Additional retorting runs with a new Brush BeO crucible and the used Coors BeO crucible are planned.

(ii) In-cell Manipulators. Generally satisfactory operation of electromechanical manipulators in the Air and Argon Cells, as well as of in-cell cranes, has been noted since modifications and adjustments were made several months ago.

To facilitate periodic inspection and to alternate normal atmospheric with extremely low-humidity operation, rotating of the high-bridge carriages between the Argon and Air Cells is planned.

During a recent attempt to develop a remote technique for manipulator carriage removal and replacement in the Air Cell, one of the carriages was dropped about 12 ft from about bridge level to the Air Cell floor due to improper attachment of the crane hook to the lifting beam. The latter resulted from difficulties in seeing the hook-engagement operation, which had to be carried out near the cell roof, from outside the cell. Considerable damage was done to the manipulator carriage, which is one of five identical units. Damage has not been assessed completely, but the unit will be repaired if this is feasible.

(iii) Refining and Casting Equipment. The first melt of enriched uranium-fissium alloy was made in one of the melt-refining furnaces to reclaim castable metal from a 10.2-kg charge of injection casting heels and other scrap. An ingot yield of 87% was obtained. This relatively low yield is attributed to the fact that casting heels and scrap materials were used in this run. Of 70 castings of satisfactory length, 50 were found

acceptable in the pin processing operation and are being readied for assembly. The melt-refining slag was oxidized satisfactorily and has been removed from the crucible.

(iv) Process Off-gas System. Another experiment utilizing iodine-131 (see Progress Report for June 1964, ANL-6912, p. 43) was made to test iodine-retention characteristics of the melt-refining furnace off-gas system. One Curie of iodine was volatilized and introduced, with a carrier stream of argon gas, into the off-gas delay tank via a 50-ft length of pipe buried in the building floor. Analysis of a sample of gas from the tank before discharge through the 200-ft stack showed less than 0.2 μC iodine-131 in the 140-cu ft of gas discharged. Subsequent to this discharge, the tank was twice refilled with argon and discharged to the stack. Samples from these discharges showed no detectable iodine.

Survey of the delay tank showed that the iodine was concentrated in a thin disc that corresponds to the upper part of the charcoal in the entry section.

Calculations of the amount of iodine retained within the tank are complicated by the method of surveying and by errors in estimating the depth of penetration of the iodine into the surface of the charcoal. The calculated values (of the order of 0.3-0.5 C) would indicate that a very high percentage of the iodine was retained.

(v) Fuel-refabrication Equipment. In continuing fabrication and assembly of fuel elements, 49 welded pins of batch 0.24 completed bond and bond-test cycles. In the first cycle, 36 elements were accepted; in a subsequent rebond cycle, four of the thirteen rejected pins were accepted. All nine rejects were due to bubbles below the restrainer. The mean sodium level of this batch was 0.65 in. above the top of the fuel, which is in excellent agreement with the specification of 0.65 $\pm$ 0.15 in. The standard deviation of the batch was 0.068 in., the lowest population spread thus far attained. These statistics indicate that in a large production run an acceptance level of 97 to 98% may be expected.

Processing of batch 0.21 was undertaken. Of the 70 acceptable pins welded, 68 passed leak detection and are being bonded.

A short-circuit was detected in an induction feedthrough to one of the fuel-element welding machines in the Argon Cell. This is a heavy-section, mineral-insulated cable with 150 mils of insulation. To initiate the weld, a high-voltage radiofrequency discharge is used. When the feedthrough was removed and examined, a discharge path was found in about the center portion of the cable. A replacement cable is being fabricated.

The tensile and straightness test machine was received and moved into the Air Cell. Installation and check of this machine is under way. The final assembly machine was used to assemble and weld a 61-pin natural uranium dummy assembly. The basic functions of the machine are acceptable with a few minor exceptions. Some of the remote maintenance problems are being corrected.

Progress has continued on the installation of the fuel element assembly machine; the electrical and pneumatic control circuit wiring was completed. The force bridge transducer and readout system, that limits the fuel element assembly forces, was installed and the force limit settings for both compression and tensioning were established. The installation of the hexagonal-tube welding system was completed and successful welds were obtained. This equipment included the new impulse arc-initiation system. The gas-cooled grapple system was installed and successfully operated with the 400-cps power supply.

F. FARET

1. General

The principal activities for the current reporting period continue to be concerned with general Title II engineering at the Laboratory and at the Architect's offices. Bechtel's efforts are at the scheduled peak level. Major attention is continuing to be directed toward finalization of the Piping and Instrumentation Diagrams and plant layout. The amount of development of design criteria is decreasing.

Considerable effort is still being devoted to design problems associated with containment in the immediate vicinity of the reactor vessel. Shielding, containment design, instrument locations, and cooling problems are being studied. Initial comments have been transmitted to Bechtel in connection with their reactor vessel specifications and suggested package drawings.

Recent typical transmittals to Bechtel by the Laboratory have included design information and comments on fuel transfer hoist requirements, radiation zoning, shielding calculations, criteria for electrical operation in argon, equipment list review, flow model data, vault penetration and seal criteria, and reviews of control room and control panel layouts.

An initial review of the plan for procurement and construction activities prepared by United Engineers and Constructors, Inc., has resulted in some minor changes in the Title II design planning. In particular, design Package VII has been revised so that it now covers miscellaneous early procurement items, such as the building bridge crane, heating boilers, and certain process system tanks, originally included in design Package IX.

2. Reactor Vessel

Drawings and specifications for reactor vessel procurement are in the final stage of completion. Sodium flow considerations, steady and transient thermal effects, neutron shield requirements, vessel and core support structure alignment requirements, and vessel support considerations are being resolved. The procurement package will include the double-walled vessel, the vessel conical extension, the vessel cover, and the core support structure. Procurement will be based upon a performance and requirements type of specification. The detailed design of the vessel will be performed by the vessel vendor who will be selected by a Selection Board.

3. Design of Reactor Vessel Cavity

The design of the reactor vessel cavity and associated portions of the containment structure must provide for the absorption of the energy equivalent to 40 lb of TNT released at the center of the core without impairing the integrity of the containment structure liner. The reference Title I design is being modified because of a lack of confidence in liner integrity under the postulated conditions of energy release. Accordingly, a reassessment of the cavity design is in progress. The results of this review indicate the need for some modifications to the reference design.

As presently conceived, the reactor cavity will be surrounded with closely spaced steel bar hoops and vertical bars in the configuration of an open-ended basket. This array form a pseudo-pressure vessel open at the top. The major portion of the incident energy is absorbed by significant elastoplastic deformation of these bars as the "pressure vessel" expands under the influence of the applied forces. Concrete placed inside of the hoops (between the reactor cavity and hoops) serves as a piston system pushing radially outward on the steel bars.

Based on an average elongation of 5 percent, the equivalent of one vertical row of hoops (on a 25-ft diameter) of $1\frac{1}{2}$-in., round, mild steel bars, spaced at about $3\frac{1}{2}$ in. on centers, is required, as well as vertical steel bars. Approximately one-half as much steel is needed in the vertical as in the horizontal direction.

The concrete enclosed by the steel hoops will move radially outward as the steel undergoes plastic deformation. Since this concrete serves as a piston or loading device on the steel bars, the concrete must be able to slide outward. This is accomplished by eliminating any substantial structural ties or continuity between that portion of the concrete which must move to absorb the energy and the rest of the containment structure.

Wherever required, gaps will be provided between the energy-absorption structure and the steel containment liner plate. Also, crushable materials (such as lightweight concrete) will be placed in front of the steel liner at any vulnerable locations. Thus, even though the structure undergoes significant deformation, the liner plate, which forms the ultimate gas-tight barrier, is not subjected to significant loading.

4. In-core Instrumentation

The computer program which analyzes the fuel pin "hot zone" errors (see Monthly Progress Report for November 1963, ANL-6808, p. 29) has been modified to give better representation of the physical properties of the thermocouple materials. The anticipated "hot zone" errors from the prototype thermocouples that will be used to measure the centerline temperature of the tight-fit FARET fuel pins have been calculated (see Table XIX). This thermocouple has a tantalum sheath, thoria insulation, and W-3% Re/W-25% Re wires.

Table XIX. "Hot Zone" Errors* for Tight-fit FARET Fuel Pins

Max Fuel Temp	Immersion Lengths of Thermocouples									
	90 cm		70 cm		50 cm		30 cm		10 cm	
T_{max}, °C	Error	t_a	Error	t_a	Error	t_a	Error	t_a	Error	t_a
2760	+1067.3	1297.4	+125.7	2262.4	-329.2	2735.0	-174.0	2603.9	-2.6	1907.0
2300	+783.6	1101.6	+140.6	1890.3	-118.7	2278.7	-44.8	2176.2	-0.8	1613.7
2000	+486.4	973.8	+82.0	1647.5	-50.1	1981.0	-17.0	1897.3	-0.3	1422.5
1700	+233.2	846.1	+35.9	1404.8	-17.1	1683.4	-5.5	1618.4	-0.1	1231.3
1400	+81.7	718.4	+12.4	1162.1	-4.2	1385.8	-1.3	1339.4	-0.0	1040.1

*$t_m - t_a$ = hot zone error, °C, where t_m is the temperature measured by the thermocouple and t_a the temperature of the thermocouple hot junction.

If this "hot zone" error analysis truly depicts the actual errors, the placement of the thermocouples for measurement of the FARET fuel pin temperatures will have to be carefully planned. If the immersion length is long, careful interpretation of the resulting temperature profile must be made. By means of the results of this analysis, however, corrections can be applied to the measurements to arrive at actual temperature distributions if long immersion lengths become necessary.

5. Fuel Assembly Sodium Flow Test Facility

The dump tank was delivered and set in place on temporary mounts in the deep pit in Building 308. Check revealed that the dump tank did not have the required ASME Code Approval Stamp. Also, further investigation disclosed that none of the flow test facility vessels (pressure and expansion) would bear Code Approval. Since this is an engineering and safety requirement for the loop vessels, action has been initiated to rectify this situation.

The interim pump mounting and stringers for the expansion tank have been welded in position. Welding of the discharge and suction piping to the interim pump and of other pipe components is in progress.

Design and fabrication drawings have been completed for (1) the 19-element core support structure for the pressure vessel, (2) the pressure vessel extension piece and (3) the pressure vessel head that will be used during the test program.

All instrumentation for the loop has been ordered, and some of the available components are being positioned. Prototype core subassemblies which will be used in the test facility have been designed. The initial 19-element test will consist of 12 reflector, 2 buffer, 2 driver, 2 test zone subassemblies, and a control rod. The 12 reflector elements have been ordered.

III. GENERAL REACTOR TECHNOLOGY

A. Experimental Reactor and Nuclear Physics

1. High-conversion Critical Experiment

The thermal disadvantage factor (ζ_{25}) and the U^{238} capture cadmium ratio (C_{28}) were remeasured by direct and thermal activation (substitution) methods in a 1.24-cm pitch square lattice fuel zone with stainless steel-clad fuel. It had previously been noted that the results from the two methods tended to differ as the lattice spacing decreased. However, good agreement between the results were found for the 1.24-cm square lattice.

$$C_{28}^{D} = 1.24 \pm 0.01 \text{ (average of 3 direct measurements)}$$

$$C_{28}^{T.A.} = 1.243 \pm 0.002 \text{ (average of 3 thermal activation measurements)}$$

In each case, the cadmium ratios include corrections for foil self-shielding and for extrapolation to zero mass of cadmium.

In measuring the thermal disadvantage factor, values for the fission-cadmium ratio C_{25} in the fuel and in the moderator, the ratio of fissions in bare foils located in the fuel to those in the moderator, and the ratio of epi-cadmium to subcadmium fissions (ρ_{25}) were also obtained, with the following results:

$$C_{25} \text{ (fuel)} = 4.5 \pm 0.1$$

$$\rho_{25} = (C_{25} - 1)^{-1} = 0.29 \pm 0.01$$

$$C_{25} \text{ (moderator)} = 5.2 \pm 0.2$$

$$\text{Bare-foil fission ratio (moderator/fuel)} = 1.12 \pm 0.01$$

$$\zeta_{25} = 1.16 \pm 0.02.$$

A core in which the central zone has a hydrogen to U^{238} atom ratio of 1:2 was assembled. This zone was housed in an aluminum box in which 388 stainless steel-clad Hi-C fuel pins were packed together without spacers. It is planned to make the standard microparameter measurements in this fuel zone and to determine whether asymptotic spectral conditions have been reached.

2. In-core Fast Neutron Spectroscopy

The techniques for measuring uncollimated neutron spectra in the range from 1 keV to 1 MeV with a recoil-proton proportional counter using pulse-shape discrimination to reject gamma induced events has been investigated.[4] The associated electronic circuitry which must examine each event and decide whether to accept or to reject it is currently optimized to operate

[4] Bennett, E. F., A Study of the 1/E Slowing-down Neutron Spectrum Using 4π Recoil Proportional Counters, ANL-6897 (to be published).

at a total count rate (neutrons plus gammas) of less than 2000 counts/sec. Some preliminary count-rate measurements were made in the core of a zero-power reactor with this type of spectrometer.

A proportional counter was constructed to fit into the standard 5.1 x 5.1-cm matrix fuel drawer used in both the ZPR-VI and ZPR-IX assemblies. The counter had a 0.0025-cm-diameter center wire and a grounded case, 3.5 cm in diameter by 14 cm long. Steel capillary tubing, slipped over the ends of the center wire, defined an active counter length of about 7.6 cm (active volume of about 73 cm^3). The counter was filled with 3 atm of hydrogen, 100 mm Hg of methane (for quenching), and 100 mm Hg of nitrogen (for calibration by means of the n,p reaction).

This detector was placed in one of the halves of the ZPR-VI Assembly No. 2, a 650-liter core. The volume fractions in the core were: 17% stainless steel, 36% sodium, 15% carbon, 5% U^{235}, 21% U^{238}, and 6% voids. The assembly had a depleted uranium blanket. Count rates were taken about 70 hr after the reactor had run for about 40 min at a power level of about 50 W.

With the reactor halves separated and neutron sources removed, the total gamma background count rate in the detector was 2700, 1300, and 500 counts/sec, at the center of the core, at the edge of the core, and in the blanket, respectively.

The reactor sources were then inserted and the halves driven together. Under these conditions with the reactor still subcritical, the detector count rate in the center of the core rose to 6000 counts/sec. Data were taken with a two-dimensional analyzer which sorts events by rise time and pulse height.[4]

For ionization levels (pulse heights) produced by the 5- to 10-keV recoil proton, separation of events based upon rise-time distribution indicated about 30% of the total count were caused by neutron events. The neutron peak was smeared (presumably due to the effect of the excessive count rate) so that there is some uncertainty in analyzing the results. The separation should be better for ionization levels above or below the 5- to 10-keV band chosen here.

Further studies will be made on the possible application of this spectrometer for making in-core measurements. Some new chambers have been fabricated, filled, and calibrated. The chambers have center wires, 0.0025 cm in diameter, but the inside diameter has been reduced to 2.5 cm and the active length to 5.9 cm. One detector has been filled with 3 atm of hydrogen, 100 mm Hg of methane, and 100 mm Hg of nitrogen. The other detector has been filled with 3 atm of methane and 100 mm Hg of nitrogen. The first counter will be used for spectrum measurements in the region from 0.8 to 100 keV, and the second for measurements in the region from 100 keV to 1 MeV.

B. Theoretical Reactor Physics

1. Numerical Analysis

A detailed survey of the expansion of the exponential integral over the range $0 \leq x \leq 4$ in the Fourier-Chebyshev series:

$$E_1(x) + \ln|x| = \sum_{k=0}^{\infty}{}' c_k T_k^* \left[\frac{\beta x}{1 + \{\beta - (1/4)\}x}\right],$$

where the prime on the summation indicates that the first term is to be divided by 2, and $T_k^*(t)$ is the kth shifted Chebyshev polynomial, has been carried out to give more definite information on the dependence of the coefficients c_k on the parameter β. The results for k = 5, 10, 15, and 20 are shown in Figure 17. Sections of the curves where c_k is negative are dashed. The great reduction in magnitude of the higher coefficients as β increases from 0.25 (corresponding to an expansion in Chebyshev polynomials in $x/4$) is apparent. Even between zeros, $|c_{20}|$ at $\beta \approx 0.277$ is almost a million times smaller than at $\beta = 0.250$. The alternation of signs mentioned in the Monthly Report for June, ANL-6912, p. 58, is also well illustrated.

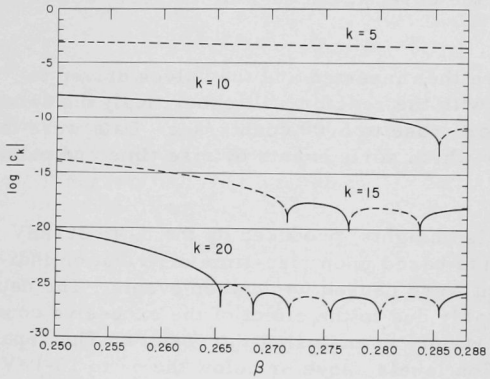

Figure 17

Dependence of c_k on β for $E_1(x) - \ln|x|$

An algorithm has been devised to estimate the integral

$$\int_0^{\infty} e^{-x} f(x)\, dx,$$

where f(x) is given by experimental data at arbitrary points. The method used is to approximate the function f(x) by an interpolating polynomial and then to integrate. Data should be limited to fairly small sets of points and

several sets used to check the estimates of the integral, since the error depends upon the location of the points as well as on the nature of f(x) in an undetermined way.

2. Use of Very Large Fast Breeder Reactors for Desalinization of Water

The advantages of coupling of very large fast power breeder reactors with the desalinization plants are being studied. By going to reactor sizes considerably larger than the 1000-MWe plants now under study for central station power, it is expected that capital costs can be further reduced, enhancing the possibility of economically producing fresh water and power together.

Large (1000-MWe) sodium-cooled fast reactors, using either metallic or ceramic fuel based on the Pu-U^{238} cycle, are subject to both local and/or overall positive sodium void reactivity effects. The role of this effect in the evaluation of reactor safety is still under study.

Calculations have indicated that U^{233}-fueled reactors should be much less subject to undesirably large positive sodium void effects. This is due to the difference in the energy-dependence relationship of the fission and capture cross sections for U^{233}.

A preliminary conceptual study has been undertaken on a 15,000-liter, thorium-U^{233}-fueled, sodium-cooled fast reactor. Early calculations for a "clean" reactor loaded with either metallic or carbide fuel, without considering fission product or higher isotope buildup, predict a large loss in reactivity for uniform loss of core sodium. The Doppler coefficient is predicted to be highly negative. The preliminary calculations indicate that the breeding ratio is only slightly above unity, and some care in design will be required to insure a net breeding gain.

Calculations for an "equilibrium" core are underway.

C. High-temperature Materials Development

1. Ceramics

a. UC-US Systems. Sintered specimens of UC, UC-5 w/o US, UC-20 w/o US, UC-60 w/o US, UC-80 w/o US, and US were crushed to pass a 140 mesh (U. S. Standard) sieve. (The limits of solubility are UC-4 w/o US and UC-60 w/o US.) The powders were mixed with an equal weight of Al_2O_3 and heated in static air at 5°C/min to 1000°C in the differential thermal analysis apparatus.

The curves for UC and UC-5 w/o US were similar; two exotherms occurred, the weaker at 350°C and the stronger at 390-395°C. The first exothermic effect of the UC-5 w/o US specimen was weaker than that of the UC. No other differential heat effects were exhibited up to 1000°C.

Two exothermic heat effects were also exhibited by UC-20 w/o US, the weaker being much reduced in comparison with the two previous specimens; the peaks occurred at 370°C and 415°C. There was also a weak endotherm at 740°C.

The curves for the other three compositions exhibited in common: a large exotherm at 410-430°C, a weak exotherm at 530-560°C, and a weak endotherm at 750°C. In addition the US specimen exhibited a weak exothermic effect at 615°C.

X-ray analyses of specimens heated to a temperature immediately above the largest exotherm and also to 1000°C revealed the presence of only U_3O_8. It is thought that the weak differential effects exhibited by the US-rich specimens at higher temperatures are associated with the retention of sulfur, in the form of higher sulfides, in the oxide lattice. Similar behavior has been observed in other uranium compounds.

b. The Preparation of Uranium Monosulfide. The investigation of the preparation of uranium monosulfide by the fused salt process first reported by Yoshioka[5] was continued. This process involves the reaction of UF_4 with H_2 and H_2S gases in a molten salt bath. One of the major problems appeared to be heavy contamination of the product with UOS due to oxygen or water vapor contamination in the melt.

In order to ascertain the source of contamination, experiments were performed to evaluate the effects of several variables, including salt bath composition, drying procedure, and bubbler-tube material. Table XX summarizes the experimental results. It is evident under "dry" conditions, i.e., when either HCl drying or a fluoride salt bath was used, no product was obtained. On the other hand, under "wet" conditions, a product consisting of a mixture of UO_2 and UOS was obtained.

Allbutt and Junkison recently described attempts to prepare US from a NaCl-KCl bath by this method.[6] With good drying conditions they were able to obtain a product consisting of 95% βUS_2 and 5% UOS. Under no conditions did they obtain US, and they suggested that Yoshioka may have confused UO_2 with US in the interpretation of his X-ray results.

---

[5] Yoshioka, K., U. S. Patent No. 3119653, January 28, 1964.

[6] Allbutt, M., and Junkison, A. R., The Preparation and Properties of Uranium Monosulphide and Uranium Monophosphide. (Preprint of paper presented at Libby-Cockcroft Meeting, Hanford, May 1964.)

Table XX. Results of Attempts to Prepare US by Reaction of UF_4 in Fused Salt Media

Run No.	Salt Charge	Reaction Temperature, °C	Reaction Time, hr	Bubbler-tube Material	Drying Conditions	Results
US-2	90 g LiCl-KCl eutectic; 10 g UF_4	450	2	Alumina	No Drying	Very slight yield. X-ray pattern showed chiefly UO_2.
US-3	90 g LiCl-KCl eutectic; 10 g UF_4	500	3	Alumina	No Drying	Substantial yield - mixture of UO_2 and UOS.
US-4	90 g LiCl-KCl eutectic; 10 g UF_4	530	4	Alumina	65-hr vacuum dry at 400°C. Ice-$CaCl_2$ cold trap.	Good yield - mixture of UO_2 and UOS
US-5	25 g LiF; 25 g NaF; 50 g UF_4	700	2.2	Alumina	16-hr vacuum dry at 300°C. Dry ice-acetone cold trap.	No visible product.
US-7	25 g LiF; 25 g NaF; 50 g UF_4	750	2.5	Alumina	18-hr vacuum dry at 300°C.	No visible product.
US-8	90 g LiCl-KCl eutectic; 10 g UF_4	570	3	Nickel	22-hr vacuum dry at 200°C. 1-hr HCl bubble at 570°C.	No visible product. Nickel tube attacked.
US-9	90 g LiCl-KCl eutectic; 10 g UF_4	570	3	Graphite	36-hr vacuum dry at 400°C. 1-hr HCl bubble at 570°C.	No visible product.
US-10	90 g LiCl-KCl eutectic; 10 g UF_4	570	3	Graphite	No Drying	Good yield of black product.

Although Yoshioka used a NaCl-KCl salt mixture instead of LiCl-KCl, the X-ray patterns of his product were identical with ours except for the presence of some additional lines. The X-ray patterns of UO_2 and US are practically identical, and only differ significantly in the back-reflection region. A careful examination of this region on Yoshioka's and our X-ray photographs showed no lines that could be uniquely associated with US.

In both Yoshioka's and our experiments, attempts were made to evaluate the US content of the product from its solubility in hot 10% H_2SO_4. It has been reported that US is soluble in such a solution whereas UOS and UO_2 are not.[7] This test showed an apparent US content of 49% in Yoshioka's product, and about 25% in ours. However, experiments showed that UO_2 has some solubility in hot H_2SO_4. In addition, βUS_2 is soluble in dilute mineral acids.[7] For these reasons, it seems doubtful that this test can be used as a reliable indication of the presence of US.

In view of the contamination problems involved and uncertainties regarding the product composition, attempts to prepare US by the method will be discontinued. The apparatus is presently being modified for experiments on the preparation of US by electrolysis.

c. Properties of (Th,U) Phosphides. The relative stability of UP and the fact that thorium phosphide exhibits a melting point of about 3000°C arouse interest in the possibility of using actinide phosphides as fuel and/or breeding materials in reactors at very high temperatures. Before the phosphides of uranium and thorium can be evaluated for reactor use a great deal of information on the characteristics of uranium phosphide, thorium phosphide and thorium-uranium phosphide must be obtained. A program has therefore been initiated to supplement the little data now available. The high temperature stability, stoichiometry and fabricability characteristics are among the subjects warranting investigation.

7 Dell, R. M., and Allbutt, M., The Nitrides and Sulphides of Uranium, Thorium and Plutonium, AERE-R 4253 (1963).

The results of research this month show that thorium phosphide (ThP_{1-x}) is slightly more resistant to oxidation than UP, and preliminary results appear to indicate that ThP_{1-x}-UP solid solutions show intermediate oxidation behavior. In addition, densification of UP pellets occurs at a moderate pace with continued heating at 2000°C in vacuum, but grain growth is relatively rapid.

Differential thermal analysis (DTA) studies have been carried out with ThP_{1-x} and ThP_{1-x}-UP solid solutions. These experiments, in which flowing oxygen was used, appear to indicate greater resistance to oxidation for ThP_{1-x} in comparison with UP. The DTA thermogram for ThP_{1-x} is characterized by a small peak at 560°C, a major one at 650°C, and a moderate peak at 740°C. The major peak, which probably represents oxidation of the coarser portions of the powdered sample, is about 100°C higher than the corresponding major peak for oxidation of UP. This is interesting in view of the fact the UP is considerably more resistant to moist air than ThP_{1-x}. A similar situation has been noted in the case of UC, which is more susceptible to attack by moisture than are UN or US, but which under similar conditions, exhibits a DTA exotherm at a somewhat higher temperature than either UN or US.

X-ray diffraction analysis of the DTA residues of ThP_{1-x} only showed ThO_2. No trace of a thorium phosphate compound was observed, in contrast with the situation with UP. The occurrence of an amorphous ThO_2-P_2O_5 phase is suspected in the light of TGA (thermalgravimetric analysis) evidence, which showed little or no loss of P_2O_5 on heating to 900°C. It is unlikely that pure P_2O_5 would survive such heating in flowing oxygen unless it were bonded in some manner to the thorium oxide, which would reduce its volatility.

A sample of 75 ThP_{1-x}-25 UP, fired in the DTA apparatus, showed a moderately strong exothermic peak at 560°C and a major peak at 650°C. The relative strengthening of the peak at 560°C is believed to be due to the contribution of the UP component.

Pellets of UP were fired at 2000°C in vacuum for different times, but all had an identical firing schedule up to that temperature. Densification data are given in Table XXI and show only moderate density changes with increased soaking time at 2000°C. Grain growth, however, was significant. Grain size was about four times larger in the sample fired for 300 min as compared with that fired for 5 min. Considerable coalescence of pores also took place with additional heating.

Table XXI. Effect of Firing Time on the Density of UP Pellets

Time at 2000°C, min	5	20	60	300
Density, % of Theoretical	90.7	93.1	93.6	95.5

d. Anelasticity of Ceramic Compounds. In conjunction with a program for the thorough study of the properties of uranium ceramics, the anelasticity of ceramic compounds is being studied. Uranium dioxide has been selected as the first base material for the investigation. Last month a study was started on the effects of Nb_2O_5 and of TiO_2 on the density and grain size of UO_2, when sintered at a temperature in the range from 1450°C to 1750°C, by minor additions of Nb_2O_5 and of TiO_2, respectively. Work on the parameters mentioned has now been completed. A comparison of Figures 18 and 19 with Figure 20 shows a parallel effect of minor additions on the density and on the grain size.

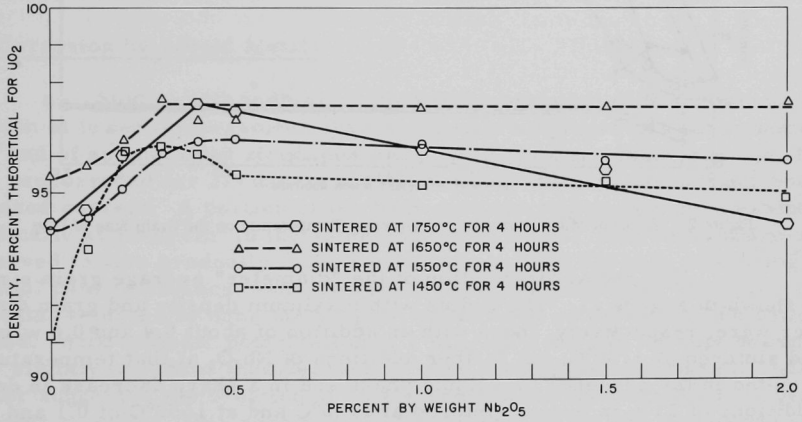

Figure 18. Effect of Nb_2O_5 and Sintering Temperature on the Density of UO_2

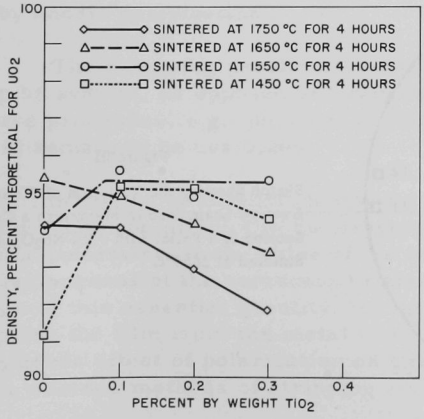

Figure 19

Effect of TiO_2 and Sintering Temperature on the Density of UO_2

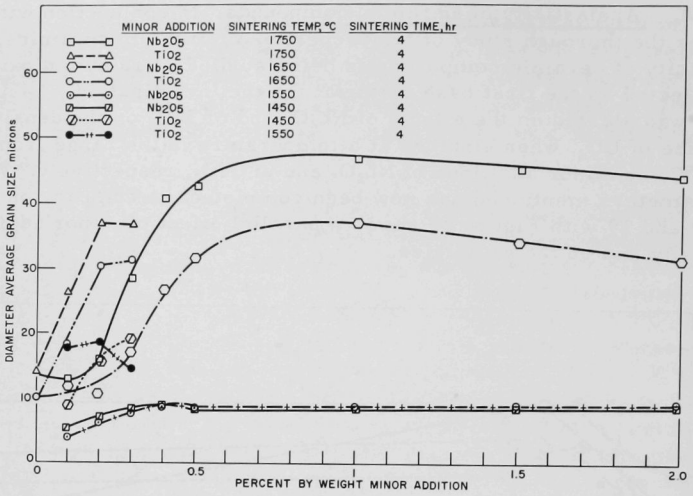

Figure 20. Effect of Minor Additions and Sintering Temperature on the Grain Size of UO_2

The radial distribution of the "diameter" average grain size* is shown in Figure 21. The bodies with maximum density and grain diameter were, respectively, those with an addition of about 0.4 and 0.6 w/o Nb_2O_5 and sintered at 1750°C; but further additions of Nb_2O_5 at that temperature resulted in the presence of a liquid phase and in a sharp decrease in density. Additions of TiO_2 in bodies sintered at 1750°C and at 1650°C of 0.1 and 0.2 w/o produced similar maxima in the density and grain diameter, respectively.

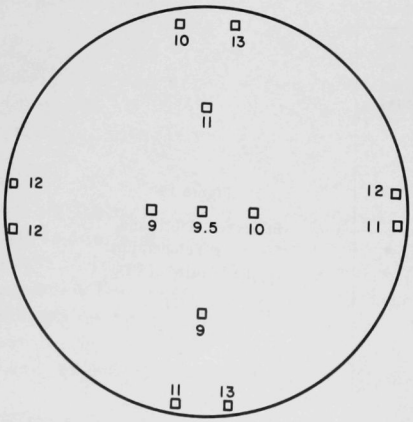

Figure 21

Sketch Showing the Variation of "Diameter" Average Grain Size in Microns in a Cross Section of a Pellet with 0.2% Nb_2O_5 and Sintered at 1650°C

* Hilliard, J. E., Estimating Grain Size by the Intercept Method, Metal Progress 85 (5) 99-101 (1964).

Titanium dioxide, for amounts of 0.3 w/o and less, produced a larger increase in grain size than did Nb_2O_5. Intergranular cracking occurred in most of the TiO_2-bearing samples. Since inclusions, which were observed in several samples, were attributed to nonuniform dispersion of the minor addition, a more elaborate mixing technique was tried. It resulted in a higher density, larger grains, and fewer, more uniformly dispersed inclusions.

Some of the equipment for preparing samples and for measuring the elastic modulus and internal friction is on order, while some is now being assembled and tested.

2. Corrosion by Liquid Metals

a. Studies with Sodium. Polarization behavior of zirconium in liquid sodium at lower temperatures than previously employed has been studied. One end of an unalloyed zirconium rod sample having a hemispherical tip was precorroded for 3.5 days at 540°C in highly oxygenated sodium, without imposed current. A portion of the film-covered region was then polarized anodically at $1 mA/cm^2$ in the same sodium at 300°C. The cell voltage was observed to rise gradually from 8 mV (Sample +) to 900 mV, indicating substantial film resistance, enhanced perhaps by the polarizing current. The potential returned to near the original value when polarization was interrupted. With cathodic polarization at 1 mA/cm^2, the cell voltage became only slightly negative, then decayed to near the unpolarized value. The behavior suggested the creation of an electrical short through the film by cathodic current. This result at 300°C was similar to that obtained in a previous attempt to polarize cathodically at 540°C. The suspected film damage was verified by subsequent resistance measurement with anodic current. Gradual repair of the film resistance was monitored, if not promoted, by anodic polarization.

The foregoing results appear to favor the existence of a reduction step by sodium, as opposed to complexing of ZrO_2 by Na_2O. However, alternative processes, e.g., physical damage due to discharge of impurity hydrogen, remain to be evaluated.

b. Stripping of Zirconium Corrosion Product. Substantial loss of zirconium corrosion product in the oxygenated sodium environment at 650°C introduces uncertainty in the value of the amount of sample metal corroded. Generally, removal of the corrosion product remaining after test permits evaluation of this essential quantity, but no acceptable stripping technique for stripping the film from the metal is known for zirconium. Since determination of the effect of polarization on corrosion rate requires the rate to be known, various methods of stripping are being investigated.

Methods under consideration include i) chemical reduction, ii) cathodic reduction, and iii) metal dissolution.

i) Chemical reduction in sodium vapor at 650°C was attempted. In some instances the texture of the surface was greatly altered, and electrical conduction between surface probes was enhanced after the exposure; but slight weight gains, rather than losses, occurred. Chemical reduction in liquid magnesium or magnesium vapor in the 700°C range resulted in some sample weight loss. However, the rate of stripping was low; and an increased temperature promoted undesirable reaction of magnesium with zirconium metal as well as oxygen dissolution by zirconium.

ii) Cathodic reduction in a mercury-vapor glow discharge is being attempted.

iii) Chemical dissolution of sample metal (leaving the film to be weighed) is a technique that has been developed to a degree by other workers, primarily to study the film. Since a sample is consumed for each datum point, the method is unattractive when the supply of corroded samples is limited. However, if cathodic reduction results are unsatisfactory, the dissolution method will be investigated.

c. Dissolution Kinetics in Liquid Metals. The investigation of the dissolution kinetics of Type 304 stainless steel in Bi-42 w/o Sn eutectic alloy (see Progress Report for April 1964, ANL-6885, p. 44) has continued.

The dissolution data obtained at 450°C and 650°C indicated that the relative concentrations of Fe, Cr, Ni, and Mn in the Bi-Sn eutectic alloy were still changing at times up to 80 hr. In order to obtain equilibrium solubility data, another apparatus was used to equilibrate the 304 SS samples with the eutectic alloy for periods up to 500 hr at 450, 650, and 860°C. The Bi-Sn samples obtained at the end of 500 hr have been submitted for spectrochemical analysis.

The initial data for 650°C also showed that the concentrations of iron, chromium, and nickel in the bath were below the limits of detectability (< 0.003 w/o for iron, and < 0.0005 w/o for chromium and nickel) for the first 6 hr of the dissolution run. Consequently, the investigation of the effect of rotational speed of the disc on the dissolution rate was carried out at 860°C, at which the concentrations of all of the elements could be determined at times greater than 0.5 hr. At the higher temperature, dissolution runs have been made at rotational speeds of 2, 10, 30, 100, and 150 rpm for times up to 150 hr. The range from 2 to 150 rpm defines the region of laminar flow in the vicinity of the disc and covers a range of Reynolds numbers from 1.32×10^3 to 1×10^5. The Reynolds number for the rotating disc geometry is defined as

$$Re = WR^2/Y,$$

where R is the radius of the disc, cm; W is the angular velocity of the disc, radians/sec; and Y is the kinematic viscosity of the Bi-Sn eutectic alloy at 860°C.

A 4.5-fold increase in the dissolution rate was observed when the rotational speed of the disc was increased from 2.0 to 150 rpm. The data obtained from the runs at 10 and 100 rpm indicate that there may be a transition from a liquid diffusion-controlled dissolution process to a surface-controlled process in the vicinity of 30 rpm ($Re = 2.0 \times 10^4$). The spectrochemical analysis data for the run at 30 rpm have not been obtained to confirm this point. Correlation of the data obtained in this study with the convective diffusion model for the dissolution of rotating discs will have to await the completion of the chemical analysis of the solubility samples and an additional dissolution run in the vicinity of 30 rpm.

3. Thorium and Thorium-base Fuels

a. Potential Importance and Problems. Although the use of thorium in high-temperature fuels for fast breeder reactors is in a stage of development that is beset with problems, the solution of these problems may be the key to the production of low-cost nuclear power. When, for example, thorium-232 is used in the core-blanket region of a reactor, a well-known series of nuclear reactions leads to the production of substantial amounts of uranium-233, a fissile material. This valuable nuclear fuel is primarily a beta-decay product of protactinium-233, which is a beta-decay product of thorium-233, which is a product of a neutron-gamma (n,γ) reaction with the original thorium. Although these nuclear reactions compose the principal chain, there are numerous side reactions.[8] These include the (n, γ) conversion of some of the protactinium-233 to protactinium-234, and of some of the thorium-233 to thorium-234 (which in turn forms protactinium-234 by beta decay); and side reactions involving the original thorium-232 include both alpha decay and an (n,2n) reaction. The latter reaction, although of small cross section, leads to the ultimate formation of high-energy gamma emitters that often cannot be ignored.

Although the physics, technology of handling, and metallurgy involved in the development of thorium-base fuel alloys are complicated by the existence of the side reactions, thorium is a material of outstanding promise for use in fuel alloys for power production. Not only is thorium the most abundant potential source of fuel but - quite aside from its breeder potentialities - thorium shows promise of being a useful and economical base for alloying with uranium and plutonium to form a stable, compatible, high-temperature fuel.

---

[8] For example, see Wilkinson, W. D., Uranium Metallurgy, Vol. I, J. Wiley and Sons (1962), pp. 528 and 686.

The study of the ternary thorium-uranium-plutonium alloys was therefore undertaken to determine the usefulness of these alloys as a nuclear reactor fuel from a metallurgical point of view. The study comprises two programs. One is concerned with the structure of these alloys, the phase diagram, transformation kinetics, heat treatment; the other with the engineering properties. A portion of the phase diagram, (see Progress Report for January 1964, ANL-6840, pp. 61-63) casting properties, and density data have been reported. Significant progress has since been made in developing a fabrication method of rolling and swaging an alloy containing 70 w/o Th and 30 w/o Pu, and in measuring its thermal expansion and electrical resistivity.

b. Fabrication of Th-30 w/o Pu. A 40-g arc-melted ingot of Th-30 w/o Pu was cold rolled to an oval of 8.4 x 9.7 mm by a reduction of about 25%, followed by a heat treatment in vacuum for one hour at 700°C. The ingot was then cold swaged to a round rod of 4.2 mm diameter. The total cold reduction by swaging was 78%. A second heat treatment for one hour at 700°C was followed by an additional cold swaging reduction by 49% to a rod of 3-mm diameter.

No difficulties of any kind were encountered during rolling or swaging. The final rods had a good surface. There was no evidence of cracking. Rolling and swaging appeared to be well suited for the fabrication of this alloy.

c. Properties of Thorium-Plutonium Alloys

(i) Dilatometric Behavior. A specimen of 3-mm diameter and 30-mm length was cut from the rolled and swaged rod of 70 w/o Th and 30 w/o Pu alloy, and its thermal expansion characteristics were measured in a vertical vacuum quartz dilatometer. Heating and cooling was at the rate of 1°C/min. A very slight break, possibly due to a precipitation or dissolution of a second phase in the thorium matrix, occurred near 300°C. The mean coefficient of expansion over the temperature ranges from 25 to 300°C and from 25 to 900°C were 11.4×10^{-6} and $12.1 \times 10^{-6}\,°C^{-1}$, respectively. The eutectoid decomposition of the thorium beta phase to alpha thorium and the compound $Pu_{13}Th_6$ or Pu_2Th near 600°C was not reflected in the dilatometric curves. A very strong break, however, was observed in three curves at 932°C on heating, at 937°C on cooling, and at 947°C also on cooling. This break may be attributed to the $Th_\alpha + Th_\beta \rightleftharpoons Th_\beta$ reaction if the beta phase should indeed occur at low temperatures, as was reported in Progress Report for January 1964, ANL-6840, pp. 61-63.

(ii) Electrical Resistivity. The electrical resistivity of the Th-30 w/o Pu alloy as a function of temperature was measured by means of a Kelvin bridge on a specimen 4 cm in length and 0.3 cm in diameter. Here an attempt was made to obtain equilibrium values by making each

measurement after an extended holding time. The results of the resistivity measurements are shown in Figure 22. The curve shows a break at 600°C which is the result of the above-mentioned reaction $Th\alpha + Th\beta \rightleftharpoons Th\alpha + Pu_{13}Th_6$.

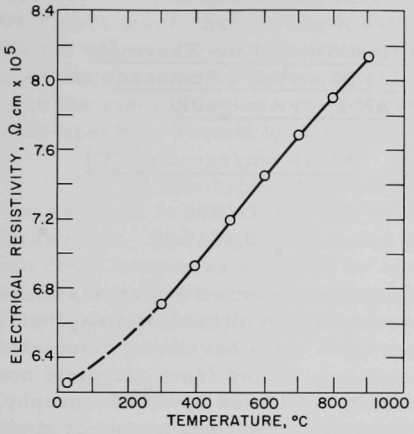

Figure 22. Electrical Resistivity of 70 w/o Th-30 w/o Pu

(iii) Ternary Alloys. Two ternary alloys (80 w/o Th, 10 w/o U and 10 w/o Pu and 70 w/o Th, 20 w/o U and 10 w/o Pu) are being studied by dilatometric and electrical resistance measurements. These alloys were selected on the basis of the preliminary phase diagram and contain no liquid phase at temperatures up to about 900°C. These alloys can be satisfactorily fabricated by rolling and swaging. Their hardness has been determined as a function of fabrication history. The hardness values range from R_B = 20 for the cast alloys to R_B = 60 for the swaged and work-hardened alloys. They are being prepared for irradiation experiments.

D. Other Reactor Fuels and Materials Development

1. Nondestructive Testing

a. Correlation of Heat Transfer and Bond Quality. Following the completion of ultrasonic tests on copper braze-bonded specimens (see Progress Report for June 1964, ANL-6912, p. 68), studies on the correlation of the sound-transmission properties, heat-transfer properties, and bond strength are being extended to rolled bonds. The specimens consist of sections of a BORAX fuel assembly that showed suspect areas when tested with the ultrasonic imaging system; standards were made from areas that indicated a good bond. [The BORAX fuel plate has cladding of Type 304 stainless steel (304 SS) and a core of UO_2 dispersed in 304 SS.]

Tests will be made with both bonded interfaces of the fuel plate. Although it is possible to cut off the cladding and material in the region of the bond on one side of the specimen, this operation would reduce the thickness of the specimen to the point where one of the conditions of the flash method, (i.e., the pulse duration must be short in comparison to the time it takes the heat to travel through the specimen) would probably not be met.

The system has been recalibrated with the use of copper and aluminum (1100) standards, and the amount of heat falling on the front surface of the specimen in one pulse is 0.435 cal/cm^2. Measurements of the thermal diffusivity (α) and conductivity (K) of 304 SS and of a BORAX standard are given in Table XXII.

Table XXII. The Thermal Diffusivity and the Thermal Conductivity of 304 SS and of a Standard Section of a BORAX Fuel Assembly

	α(cm^2/sec)	K(cal-cm/sec-cm^2-°C)
304 SS	0.033	0.0393
BORAX Standard	0.0289	0.0335

b. Ultrasonic Imaging. Metallographic studies of flat, stainless steel-clad fuel specimens subjected to comparison ultrasonic imaging, mechanical-scan-ultrasonic, and radiographic tests have been completed. Defects discovered by both ultrasonic systems varied from complete non-bond areas (blisters), partial bond areas as confirmed by metallography, to suspect areas in which successful metallographic tests were not obtained. The latter are believed to have indicated an ultrasonic response because of large particle concentrations.

c. Infrared Imaging. Response characteristics of the infrared vidicon system have been studied from the threshold object temperature of about 180°C to 450°C. From the slope of the system response (kinescope brightness) versus object temperature curve and a knowledge of the smallest change in kinescope brightness that is visually detectable, the smallest change in object temperature that can be observed with the infrared television system can be calculated at any given temperature. These data show reasonable agreement with experimental observations of ΔT, particularly for object temperatures above 250°C, where the slope of the response curve is probably more reliable. Typical changes in object temperature observable were 10°C at an object temperature of 200°C, 4°C for an object at 300°C, and 3°C or less for objects 350°C or hotter.

d. Electromagnetic Testing with Pulsed Fields. Pulsed electromagnetic test equipment has been used exclusively for about two years for those applications requiring the use of an electromagnetic method. Sufficient experience has been acquired to evaluate the advantages and disadvantages of this equipment as compared with commercial eddy-current equipment, and also with equipment based on the ultrasonic method. At the same time, improvements have been made that have in some measure reduced or have completely eliminated some of the disadvantages as they become evident.

One of the most successful applications of pulsed electromagnetic test equipment has been in the inspection of the 304 SS jacket tubing, 3.96-mm ID x 0.229-mm wall, which is to be used for jacketing the fuel elements produced in the EBR-II Fuel Cycle Facility when it begins operation. Over 18,700 m of this tubing have been inspected with this equipment to a 10% defect level, that is, any localized reduction in wall thickness of over 10% for any reason is cause for rejection. Correlation has been generally excellent considering the variety of defect types encountered, especially since the installation of new pulsed equipment provided with an encircling mask-aperture assembly in mid-1963.

In this application the pulsed electromagnetic test equipment has been as equal in sensitivity and reliability as equipment based on the use of ultrasonics. The inspection speed of 3.7 m/min was considerably higher than could have been obtained by an ultrasonic method of equivalent capability, and this inspection speed could easily have been increased by a factor of 2-4 if the time required for handling and marking the tubes would have justified such an increase.

Pulsed electromagnetic test equipment with point-type mask-aperture assemblies has been used for numerous tubing test applications on a very wide range of materials of up to 0.70-mm wall thickness. With materials of relatively good conductivity, or thicker walls, however, this equipment operates at an increased disadvantage compared with ultrasonic equipment, but has been used successfully to test 304 SS tubing of 0.0508-mm wall thickness and a niobium-tungsten-zirconium alloy (D-43) of 0.483-mm wall thickness. In these applications a 0.0508-mm long, 10% Elox notch on the inner surface served as a standard, and the noise and interference generated by the tube was less than 20% of the standard signal. In some applications, though, interference has been a very serious problem. Zircaloy-2 tubing has been particularly troublesome, usually because of localized concentrations of hydrides. This interference can often be eliminated by longitudinal scanning instead of spiral scanning, but a new interference problem may arise with tubing containing heavy tube reducer marks. The recent development of two-aperture, point-type mask-aperture assemblies has reduced interference problems in general. These devices are provided with two apertures about 1.5 mm apart instead of the single aperture of earlier assemblies. Fields of identical amplitude but opposite polarity issue from each of the apertures so that those conditions that occur under each aperture simultaneously do not appear in the pulse generated across the pickup. Pulse sampling in the time domain is used as with the older mask-aperture assemblies. Other improvements have already suggested themselves.

E. Remote Control Engineering Development

1. Viewing Systems

Electron irradiations at 10 MeV of small samples of shielding window glasses have been continued to determine the effect of changes in glass composition on the susceptibility of the glass to fracture by electrical discharge. The rate of dissipation of injected electrons after irradiation has continued to be a reproducible parameter. The charge remaining in a sample is destructively measured by causing an electrical discharge by impact. The electric charge dissipation rates have been shown to increase for glasses of decreasing resistivity, but not in a directly proportional manner. The exposure of electron-irradiated samples to gamma radiation (10^6 R in 20 hr) did not have a pronounced effect on the charge dissipation rate.

A study has been started to determine the effect of melting time and temperature on the volatilization of PbO from small experimental melts. Three hours at 1500°C reduced the specific gravity of a 3.3-g/cm^3 lead silicate glass by about 4 percent.

2. Electric Master-Slave Manipulator Mark E4

The transistors for the modulator portion of the servo amplifiers were selected for symmetrical limiting and grouped. A sample autotransformer, for use in changing force ratios between the master and slave arms, was received and tested. The four small subassemblies for the servo amplifiers have been assembled and wired. Most of the wiring harnesses for the amplifiers have been completed. Thirty-two gearbox cases are nearing completion in machining - half of these are for the slave arms and half for the master arms.

3. Special Motors for Master-Slave Manipulators

A special design of an aluminum cup-rotor two-phase servo motor was tested under stalled conditions this month. The motor is designed to power a future slave arm which has a maximum load capacity of from 50 to possibly 150 lb. It has special passageways for the flow of cooling air. Class H insulation is used. The motor was tested for three different stalled torques equivalent to manipulator slave arms having 50-, 100-, and 150-lb capacities. Some of the stalled characteristics are given in Table XXIII.

The inertia referred to X, Y, and Z motions was computed on the basis that the extremity of the arm would travel at 3 ft/sec when the motor is running at its synchronous speed of 1800 rpm. The stalled performance of the motor is somewhat better than the original calculations indicated. More recent calculations based on the actual winding distribution instead of the original sine-wave assumptions gave a closer agreement between the calculated performance and the measured performance.

Table XXIII. Stalled Characteristics of Cup-rotor Motor

Manipulator Rating, lb	50	100	150
Inertia of Rotor (lb-in.^{2})	0.12	0.12	0.12
Inertia referred to X, Y, and Z motions (lb)	3.3	3.3	3.3
Torque, lb-in.	9.55	19.1	29.6
Theoretical max angular acceleration (rad/sec^2)	30,000	60,000	90,000
Cooling air			
Head, in. of water	0.4	0.5	0.5
Flow rate, cfm	16.3	17.3	16.5
Temperature rise over inlet air, °C			
Cup	68.5	127	176
Winding	25.5	58	100
Exhaust air	26.5	55	93
Phase voltage, V	111.5	171.3	222.5
Phase current, Amp	1.72	2.55	3.52
Total power input, W	258	560	892
Power factor, percent	67.5	64.0	57.0

Figure 23 shows the idealized torque line, that is, stalled torque x synchronous speed x a constant, and is the inherent minimum rotor loss in a stalled induction motor operating at constant frequency. The winding loss (I^2R) was calculated from the measured phase currents and the measured dc winding resistance at operating temperatures. The stray loss is the difference between the total input power and the sum of the rotor and I^2R losses. Some of the stray losses are caused from nonconstant flux patterns in a revolving field and losses in the iron.

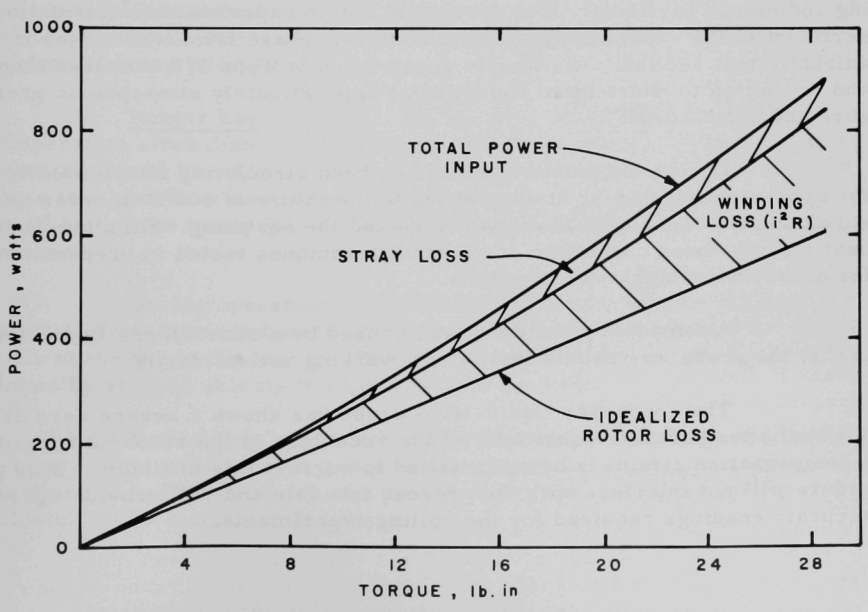

Figure 23. Power vs. Torque under Stall Conditions for Cup-rotor Motor

The motor shows promise of being quite suitable for future master-slave manipulators.

4. Higher-sensitivity Force-feedback Systems for Master-Slave Manipulators

Various methods are being studied for obtaining higher frequencies and more accurate static force fed from the tongs to the operator's handle. A significant amount of improvement can probably be achieved by increasing the stiffness of force-feedback systems similar to those used in the Mod 3 and the Mark-E4 manipulators. The cup-rotor motor mentioned above could help in this direction. Other methods would probably use transducers near the tongs and handles along with others.

Some test apparatus is being designed to measure some of the frequencies and transients that the operator needs for reasonably good manipulation of tools.

F. Heat Engineering

1. Two-phase Flow Studies

a. Void Fraction - Pressure-drop Facility. This experimental facility is designed to investigate the two-phase flow characteristics of boiling sodium; in particular, it is desired to obtain experimental information pertinent to the vapor volume fraction and two-phase frictional losses in an adiabatic test section. The loop is constructed of Type 316 stainless steel and is limited to short-term operation at approximately atmospheric pressure and about 1630°F.

During the month, sodium has been circulating intermittently for approximately 100 hr at an average temperature of 600°F in order to insure complete wetting of the flowmeters and the em pump. Simultaneously, heat loss has been calibrated and control techniques tested in preparation for operation at higher temperature.

A temporary shutdown was caused by a short in one liquid-level probe; the probe was rebuilt and is now working satisfactorily.

The condenser liquid-level probe has shown a severe zero drift due to the temperature sensitivity of the rectifiers in the read-out circuit; a compensation circuit is being installed to correct this difficulty. This procedure will not interfere with the present schedule and will provide the more accurate readings required for the boiling experiments.

2. Boiling Liquid Metal Technology

a. Niobium-1% Zirconium Loop Construction. Reworking of the cooling water lines on the vacuum chamber is continuing. The faulty tubes have been stripped from the bell jar, the surface has been prepared, and attachment of new tubing is approximately 25 percent complete. The operating and maintenance manuals are being prepared, and the chamber is expected to be ready for testing in August.

The additional engineering design required for the installation of electrical service for the vacuum equipment was completed and a cost estimate prepared. The cooling water supply and drain manifolds have also been completed.

A calculated estimate of the rate of consumption of liquid nitrogen indicated that both the anticipated mode of operation of the liquid nitrogen baffle and the present concept for liquid nitrogen storage should be reviewed. Several ideas for reducing the consumption rate were found not to be ineffective or feasible. Consideration will be given to a plan to discontinue use of nitrogen when the loop is inoperative for extended periods and to bake the whole system under vacuum before resuming operation.

Some preliminary design work has been accomplished for the radiating heat exchanger and the shutter controls. A literature review of the operation of bearings in a high-vacuum atmosphere for this and other designs is being pursued.

b. Heater Experiments. The thermal radiation-heated loop has been in operation since June 1, 1964, during which the thermal radiation heater has operated for 50 hr. Liquid metal temperatures ranging up to 900°F and flow rates to 1 gpm have been obtained. Heat fluxes to a conservative 20,000 Btu/hr-ft^2 have been investigated. Data obtained from this experiment are being analyzed.

During operation of the thermal radiation heater, thermal expansion of the inner radiation shield led to shorting out against the power leads at the top of the heater. The inner radiation shields are being replaced by shorter shields to eliminate this problem.

Future loop operation will be concerned with extending the temperature level and heat flux range to determine the ultimate capability of the thermal radiation heater and its feasibility for use in the 2100°F columbium-1% zirconium facility.

3. ANL-AMU Program

Other heat engineering experiments, performed as part of a joint program (not supported by the Division of Reactor Development) between the Laboratory and the Associated Midwest Universities (AMU), are described below:

a. Two-phase Flow Characteristics during the Complete Vaporization of a Fluid. The assembly of the heated test section was completed. Difficulties occurred in sealing the optical windows in the test section. Several windows cracked during the loading of the bolts. A slight misalignment in the inner heated section coupled with small chips in the edge of the glass were believed to be the cause of the failure. The edges of the windows have been reground and two units inserted at bolt pressures lower than calculated.

A pressure check with Freon was attempted. Leakage occurred through the thermocouple lead adaptors. A different type of thermocouple adaptor has been selected, and reassembly of the thermocouple units is in process.

The forced-circulation loop has been completed with the inclusion of a 2-in. pipe in lieu of the heated and unheated test sections. A pressure check of the loop is to be carried out after several valve packings have been replaced. The centrifugal pump will be tested with Freon in the modified loop. Final assembly of the complete loop has been delayed due to a slow delivery of the inlet and outlet sections. In the interim, the heated test section will be incorporated into the loop with a section of 2-in. pipe to check the unit under actual flow and heating conditions.

Two protective devices are to be employed in the test section operation: one is a rate detector for normal burnout operations, and the other a limit detector for the upper level of the wall temperature. The limit detector is to be employed during dry-wall tests in order that elevated wall temperatures may be sustained. Although these temperatures are elevated, they are expected to remain below the tolerance limit of the metal.

b. Propagation of Void Waves in an Air-Water System. During the past year, an experimental project has been undertaken to investigate the propagation of void waves in air-water vertical flow. The system is perturbed with air through use of a controlled solenoid valve. An electrical resistivity probe is being used to determine void fraction.

Two preliminary runs have established the reliability of the experimental procedure and permitted check of the computer program. The results were found to be independent of the playback speed of the probe signals.

c. Power-to-void Transfer Functions. The new thin-walled test section assembly has been installed in the Small Scale Loop, and the power oscillator control unit and enlarged shunt (see Progress Report for June 1964, ANL-6912, p. 75) have been tested to allow continuation of the experimental investigation of power-to-void transfer functions.

In the actual assembly of the test section the back-up plates are bolted directly to the end pieces. This construction minimizes mechanical stresses due to thermal expansion on the $\frac{1}{64}$-in. test section wall, and the tube itself is mounted under tension to further relieve mechanical stresses. This built-in stress was accomplished by electrically heating the test tube to expand it and cooling the back-up plates to allow thin strips of insulation to be positioned and at the same time allow the back-up plates and end pieces to be aligned.

The assembly has been hydrostatically tested at 750 psig, and instrumented for thermocouples and pressure taps. Ten thermocouples were positioned along the test section wall to measure wall temperatures. Seven of these thermocouples are electrically isolated from the test tube wall by a 1-mil mica sheet; the other three are mounted directly on the wall under pressure exerted by the back-up plates. Provision had been made to back up the tube on all four sides by employing a mica mat insulation (GE) which possesses high mechanical strength, as well as good dielectric and low thermal conductivity properties.

The whole assembly has been placed in the Small Scale Loop, void equipment has been realigned, power oscillator has been checked, and a test run made at 250 psig after a 450-psig hydrostatic test. Difficulty was experienced with the powerstat controlling the power supply and the relay in the low-flow power trip, but both of these difficulties have been corrected.

Various values of the experimental parameters (flow rate, power, and pressure) have been substituted in the 704 digital computer program employing the Bankoff model[9] to theoretically find a set of conditions which predict a low-frequency notch in the power-to-void transfer function. The first experimental run will be made with the following loop parameters: 300 psia pressure, 6 gpm flow rate, and 10-kW pressure which has a theoretical notch at approximately 1 cps.

d. Inception of Hydrodynamic Instability in a Natural-circulation Loop. The Armadilla loop was recently incorporated with another test facility for the experimental investigation of void fraction and pressure drop in two-phase flow.

---

[9] Bankoff, S. G., A Variable Density Single Fluid Model for Two-phase Flow with Particular Reference to Steam-Water Flow, J. Heat Transfer, ASME, Series C, 82, 273 (1960).

Some data were obtained at 200 and at 600 psia for a range of inlet subcoolings (5-50°F). The heat balance from these tests indicated that the mass flow rate calculated from the pressure drop across the venturi was far too high, possibly because the manometer connected across the venturi reads mean pressure drop under oscillatory flow conditions, whereas the flow rate is proportional to the square root of the pressure drop. To further ascertain this, two more thermocouples have been installed to measure the exit temperature of the cooling water from condenser and subcooler.

G. Chemical Separations

1. Fluidization and Volatility Separation Processes

a. Recovery of Uranium from Low-enrichment Ceramic Fuels

(i) Decladding of Stainless Steel-clad Fuel. The initial step in the fluid-bed fluoride volatility process, under development for low-enrichment fuels, involves a decladding operation in which the fuel is separated from the metal clad. Two alternative methods are being investigated for decladding stainless steel-clad uranium dioxide fuel: (1) the oxidative decladding by reaction of the UO_2 pellets with oxygen to produce U_3O_8, which forms as a very fine powder and readily separates from the cladding; and (2) the chemical destruction of the stainless steel cladding by high-temperature reaction with oxygen in the presence of hydrogen fluoride. The oxidative decladding method involves prior broaching of the cladding or shearing of the fuel into short lengths. This method has been successfully demonstrated in tests using the two-zone oxidation-fluorination concept (see Progress Report for January 1964, ANL-6840, p. 73).

Experimental work on the destructive oxidation of stainless steel has also been carried out at other AEC laboratories: at Oak Ridge National Laboratory[10] the use of $HF-O_2$ mixtures has been investigated, and at Brookhaven National Laboratory[11] the effect of solid fluoride promoters has been studied. At Argonne the destructive oxidation of stainless steel by hydrogen fluoride-oxygen mixtures involves the oxidation of the cladding in a bed of alumina particles fluidized by a gas stream of oxygen and hydrogen fluoride.

Four tests were made, two in a pilot-plant (3-in. dia) reactor and two in a bench-scale ($1\frac{1}{2}$-in. dia) reactor. A 2-hr decladding test at 550°C was performed in the 3-in.-diameter fluid-bed reactor with use of a reactive gas mixture containing 40 v/o hydrogen fluoride in oxygen. Sintered UO_2 pellets contained within a Type 304 stainless steel tube (0.020-in. wall thickness) were completely disintegrated and no trace of the original tubing was found in the bed material. In addition, oxidation rates of approximately

[10] Oak Ridge National Laboratory, April 6, 1964 (Unpublished).

[11] Reynolds, J. H., (Ed.) Progress Report Nuclear Engineering Department May 1 - August 31, 1963, BNL-823, (Dec 1963).

30 mils/hr were observed for Types 304 and 347 stainless steel specimens which were also inserted within the fluid-bed reactor. In a test at 500°C, the oxidation rates obtained were too low (approximately 1 mil/hr) to be of any practical significance.

In exploratory tests performed in the $1\frac{1}{2}$-in.-dia reactor, the rate of oxidation of a 304 stainless steel rod was markedly higher for the portion of the rod immersed in the fluidized bed than for the section of rod exposed to the gas phase above the bed (see Figure 24). The rate of attack on Type 304 stainless steel rod specimens at 550 and 600°C was approximately 30 mils/hr within the bed.

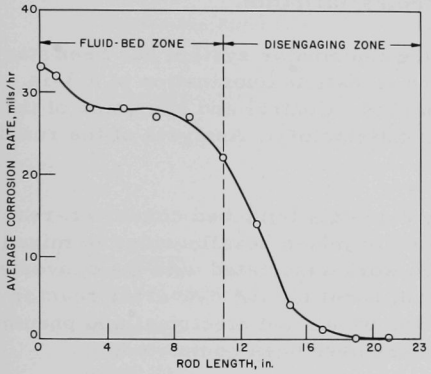

Figure 24

Corrosion Rates at 550°C of Type 304 Stainless Steel Rod Immersed in a Fluid Bed

Initial Dimensions:	1/2-in. dia and 23 in. long
Initial Weight:	583.9 g
Final Weight:	392.4 g
Run Time:	3 hr
Composition of Feed Gas:	40 v/o HF, 40 v/o O_2, 20 v/o N_2
Fluidized-bed Material:	alumina

These results indicate that the chemical decladding technique will be directly applicable to the fluid-bed fluoride volatility process, since both the destructive oxidation of stainless steel and the direct fluorination of uranium dioxide can be conducted in the same vessel. Demonstration of the process is under way in the 3-in.-dia pilot-scale reactor with simulated fuel bundles containing UO_2 pellets in stainless steel tubes.

(ii) Engineering-scale Alpha Facility. An engineering-scale alpha facility is being installed to permit demonstration of the major steps of a fluid-bed fluoride volatility process for the recovery of uranium and plutonium from ceramic oxide fuels (see Progress Report for December 1963, ANL-6810, p. 38). The major processing equipment will be installed in the larger of the two alpha boxes that comprise the facility; the smaller box will contain scrubbers and auxiliaries. Initial studies will investigate the fluorination step for processing batches of uranium dioxide-plutonium dioxide pellets to hexafluorides and the conversion step for the preparation by the reaction with steam and hydrogen of dense mixed uranium-plutonium oxide particles from mixed hexafluorides (see Progress Report for June 1964, ANL-6912, p. 79).

A series of performance tests on the fluorination process scrubber located in the small alpha box has been completed. This scrubber serves two purposes: (1) to scrub both the process off-gas (~1 cfm) and the ventilation air (~600 cfm) coming from the large alpha box, and (2) to humidify this gas mixture to promote hydrolysis of contained hexafluorides (e.g., in the event of an accidental release) to a particulate form that is readily removed by high-efficiency AEC-type filters located downstream of the scrubber. This gas mixture is again scrubbed (in a larger ventilation-air scrubber) and filtered before being discharged to the building stacks. Mechanical operation of the scrubber was satisfactory over the 150-hr test period. Calculated mass-transfer coefficients in the humidifying of the air were in the range from 167 to 245 lb-moles/(hr)(atm).

Shakedown testing of the fluorinator system has been started. The shakedown test involved a two-zone oxidation-fluorination of a 3-in.-deep bed (2.2 kg) of uranium dioxide pellets. Control and operation of the fluorinator reactor during the run was satisfactory. Analysis of the run data is in progress.

The installation of the 2-in.-dia fluid-bed converter-reactor (fabricated of Inconel) for the conversion of mixed hexafluorides to mixed oxides is underway. In-box installation work associated with the converter-reactor is also in progress. The control panel for the converter reactor has been mounted, power brought into the panel, and electrical and pneumatic run-outs from the panel to the alpha boxes have been completed.

b. Recovery of Uranium from Highly Enriched Uranium-Alloy Fuels by Chlorination and Fluorination Steps

(i) Pilot-plant Demonstration Runs. The first two runs with unirradiated uranium-alloy charges have been completed in the pilot-plant facility installed to demonstrate the recovery of uranium from highly enriched uranium-alloy fuels by means of the fluid-bed fluoride volatility process (see Progress Report for April 1964, ANL-6885, pp. 59-60). In Run 7 a uranium-Zircaloy alloy subassembly was processed and in Run 8 a uranium-aluminum alloy subassembly was processed, the hydrochlorination, hydrofluorination, and fluorination steps being carried out. The UF_6 product was collected on two sodium fluoride beds in series. During the hydrochlorination step, the fluid-bed pyrohydrolysis reactor was operated simultaneously for converting the volatile zirconium tetrachloride or aluminum trichloride (each of which represents a waste stream) to their respective solid oxides.

The operating conditions for the two runs are shown in Table XXIV. In both runs, operational performance during the hydrochorination and hydrofluorination steps was highly satisfactory. The fuel charges

were completely reacted in the hydrochlorination times indicated (10.9 and 5.6 hr). The hydrochlorination reaction rates and utilization efficiencies were ~30% lower than those achieved in runs made with subassemblies which did not contain uranium (see ANL-6885, p. 60). The lower, but still very satisfactory, reaction rates and utilization efficiencies may be due to the presence of uranium in the alloy.

Table XXIV. Operating Conditions for Fluid-bed Fluoride Processing of Unirradiated, Uranium-Zircaloy and Uranium-Aluminum Fuel Subassemblies

Inert Bed Material:

Reactor (6-in. dia)	Alcoa T61 granular alumina (28-100 mesh) Runs 7 and 8: 40 kg (48-in. static bed height)
Packed-bed Filter (9-in. dia)	Alcoa T61 granular alumina (14-28 mesh) Run 7: 10 kg (5-in. bed height) Run 8: 15.5 kg (7-in. bed height)
Pyrohydrolyser (6-in. dia)	Run 7: Sand (25-45 mesh) 17.5 kg (24-in. bed height) Run 8: Norton Type 38 alundum (60 mesh) 16.0 kg (24-in. bed height)

	Run Number	
	7	8
I. Run Charge		
Alloy and Subassembly Type	Zircaloy-0.95% U; PWR	Aluminum-4.5% U; ETR
Weight (kg)	19.6	6.06
Number of plates (2.5 in. wide)	14	19
Length (in.)	48	37
Uranium (g)	182 ± 4	273.6
II. Hydrochlorination Step		
Reaction Rate (kg/hr): Avg	1.8	1.1
Max	3.3	1.6
Reaction Time (hr)	10.9	5.6
Utilization Efficiency (%): Max	46	60
Avg	24	40
III. Temperatures (°C)		
A. Hydrochlorination Step		
Reactor bed: Avg	365	370
Max	380	395
Subassembly Channel:[a] Avg	390	380
Max	450	425
Reactor wall	350	350
Packed-bed filter	360	295
Pyrohydrolyser bed	345	315
B. Hydrofluorination Step (2 hr)		
Reactor bed and packed bed filter	350	350
C. Fluorination Step		
Reactor bed and packed-bed filter		
0 to 2.0 hr	250-500	250-500
2.0 to 4.0 hr	500	500[b]

Table XXIV (Contd.)

	Run Number	
	7	8
IV. Reactant Concentrations		
A. HCl (v/o in N_2)	90	78
B. HF (v/o in N_2)	12	8
C. F_2 (v/o in N_2)		
0 to 2.0 hr	6.0	5.5
2.0 to 4.0 hr	45	40
V. Gas Velocity in Fluid-bed Reactor (ft/sec)		
A. Hydrochlorination Step	0.52	0.54
B. Hydrofluorination Step	0.5	0.5
C. Fluorination Step		
0 to 2.0 hr	~0.6	~0.6
2.0 to 4.0 hr	~0.05	~0.05

[a]Channels between plates of the subassemblies charged to the reactor.

[b]After 3-1/2 hr of fluorination, a temperature excursion caused caking at the top surface of the packed-bed filter.

In both runs, the major loss of uranium (~3% of the initial charge) was through the packed-bed filter to the pyrohydrolysis reactor during the hydrochlorination step. Preliminary results of a recent experiment showed that, during hydrochlorination, lower, acceptable uranium losses (<0.4% of the initial charge) were achieved by increasing the bed depth of the packed-bed filter from 5-7 in. to 10.3 in. The efficiency of the NaF beds for collecting the UF_6 product was greater than 99%.

Caking of the filter bed (from top of surface of bed to ~1 in. below the surface) occurred during the fluorination step of the run with the aluminum-uranium alloy subassembly as a result of the sintering of particulate solids that were collected in the filter bed. These solids consisted of alumina fines, nickel and iron fluorides, and nonvolatile uranium fluoride carried over from the reactor. The alumina fines could be derived from both attrition of the fluid-bed material and from the oxide coating on the aluminum alloy fuel. The fluorination reaction of any of these solids might produce local hot spots which could result in caking of the bed. Elimination of the caking problem in the packed-bed filter can probably be achieved by either applying a reverse-flow pulse (blow-back) of nitrogen through the filter in order to remove the foreign particulate materials prior to the fluorination step or operating the filter under fluidized conditions.

2. General Chemistry and Chemical Engineering

a. Preparation of Uranium Monocarbide. The second of two runs to produce uranium monocarbide by the addition of degassed activated

charcoal to a zinc-14 w/o magnesium solution containing enriched uranium was completed. In this run, reaction at 800°C was continued for 19 hr and the settling time was $3\frac{3}{4}$ hr, as compared with 12 and 1 hr, respectively, in the preceding run. A yield of 471 g of UC from a charge which contained 524 g of enriched uranium (93% U^{235}) was obtained. The improvement in yield (85% versus 78% in the preceding run) is attributed to the longer reaction and settling times.

3. Chemical-Metallurgical Process Studies

Thermodynamic functions are being determined for metallic systems that are of importance to pyrometallurgical processes and for systems where knowledge of the thermodynamics will be particularly useful for the testing of theories of metallic solutions. In the systematic study of the thermodynamics of rare earth-cadmium intermetallic systems, it is necessary to know the temperature of the eutectic between MCd and M (M = rare earth metal). The eutectic temperatures experimentally determined for six systems (La-Cd, Ce-Cd, Pr-Cd, Nd-Cd, Sm-Cd, and Gd-Cd) thus far studied have been correlated, by means of the thermodynamic relation derived for an ideal solution system with MCd and M as terminal phases. The atom fraction of M at the eutectic in the six systems was found to be 0.65 ± 0.04.

4. Calorimetry

The combustion of uranium monosulfide in fluorine is being studied in work aimed at determining the heat of formation of US. A fluorine flow reaction vessel (see Progress Report for January 1964, ANL-6840, p. 77) fabricated of Pyrex has been used for preliminary combustions of US in fluorine. Greater than 99.8% combustion of US was achieved without gross melting of the UF_4 intermediate and without detectable attack on the nickel support dish. This reaction will next be studied in a nickel reaction vessel which is now being fabricated.

A series of seven combustions of tantalum diboride in fluorine have been completed. Prior to calculation of the heat of formation of tantalum diboride from these data, additional information is being obtained on the values of the corrections for side reactions.

Work has begun to determine the heat of formation of gadolinium trifluoride. A preliminary combustion series of gadolinium in fluorine has been completed, with combustion yields near 95 percent. Several changes in combustion techniques are planned for the next series in order to improve the combustion yields.

H. Plutonium Recycle Reactor

1. Plutonium Recycle Fuel

Fabrication of the fuel loading for the Plutonium Recycle Experiment (see Progress Report for May 1964, ANL-6904, pp. 91-93) is a joint Argonne-Hanford program.

A total of 90% of all PuO_2-UO_2 oxide fuel required for the Plutonium Recycle loading has been processed through the Nupac step.

A total of 1500 central-type Plutonium Recycle fuel rods acceptable for reactor service have been loaded. An additional 450 rods not acceptable for service are being used in approach to critical and other physics tests at Hanford.

All of the components and hardware needed by United Nuclear Corporation for the enriched and natural fuel-element loadings have been ordered. All of the Zircaloy-2 strip stock has been delivered and accepted. Tooling for forming and welding fuel cans has also been accepted. All of the Zircaloy-2 jacket tubing has been fabricated to size and given a final anneal. Approximately one-half of this tubing has been processed through the final inspection and accepted for loading. Evaluation lots of natural UO_2 pellets, enriched UO_2 pellets containing burnable poison, Zircaloy-2 end plug stock, Zircaloy-2 jacket tubing, finish-machined end plugs, stainless steel retainer springs, stainless steel upper support grids, and stainless steel lower end fittings have been delivered to, inspected, and accepted by ANL. Upper support grids for plutonium fuel rods and stainless steel lower support grids have been rejected as not conforming to specifications and will be replaced. All of the 144 evaluation rods have been fabricated and tested and delivered to ANL for final inspection.

All the natural UO_2 pellets have been fabricated, tested, inspected, and assembled into weighed stack heights ready for loading into fuel jacket tubing.

All 6% enriched UF_6 has been converted to oxide, and all master blends of enriched high-fired UO_2 with the required concentration of rare earth oxides have been prepared. Approximately one-third of the enriched UO_2 containing the correct proportion of master blend UO_2-rare earth oxide has been processed to finished pellets.

2. Plutonium Recycle Control Rods

The boron-stainless steel for the new control rods was fabricated by Carpenter Steel Co. in accordance with ANL specifications. The total boron content analysed 1.92 to 1.94 w/o for strip from Heat No. V-91077 and 1.86 to 1.87 w/o strip from Heat No. V-91084.

All hafnium for the oscillator rod was converted to plate stock by Wah Chang Corporation from material furnished by ANL.

Completed control rods and oscillator rod are being fabricated by Dresser Products, Inc., Great Barrington, Mass., in accordance with ANL specifications.

3. Physics Calculations

As part of the Plutonium Recycle Experiment, it is planned to irradiate foils whose activation will yield information about the slow-neutron spectrum. Besides detecting changes in the spectrum caused by changes in the moderator temperature and density, we want to detect the depressions in the flux caused by absorption in the 0.3-eV resonance of Pu^{239} and the 1.05-eV resonance of Pu^{240}. To help decide which foils should be used, THERMOS problems were run and the ratios of the activities of various nuclides were recorded for either the energy interval from 0 to 0.532 eV or from 0.532 to 1.56 eV. The results of the calculations showed that several activation ratios can detect the hardening of the spectrum with increased moderator temperature and the accompanying decreased moderator density, and also that the activation ratio for Ir^{191}/Ir^{193} changes significantly with Pu^{240} concentration.

The calculations were made for fuel in the plutonium zone at uniform cell temperatures of 68°F, 325°F and 489°F; the density of the water moderator was taken as that of the saturated liquid at the temperature of the moderator. In Tables XXV and XXVI, various activation ratios are given at four positions in the cell: at the center of the fuel, in the fuel near the fuel-cladding interface, in the moderator near the moderator-cladding interface, and in the moderator near the edge of the cell.

Table XXV. Ratios of Foil Activations for the Energy Interval 0-0.532 eV

Radius (cm)	Ratio	68°F 0% BU	325°F 0% BU	489°F 0% BU	68°F 0.6% BU
0	$Pu^{239}_{fiss}/(1/v)$	1.0	1.134	1.253	1.138
0.4295		1.030	1.180	1.319	1.121
0.5534		1.052	1.215	1.368	1.105
0.7281		1.050	1.218	1.377	1.082
0	$Eu^{151}/(1/v)$	1.0	1.190	1.391	1.167
0.4295		0.989	1.184	1.387	1.092
0.5534		0.979	1.179	1.384	1.032
0.7281		0.954	1.155	1.360	0.976
0	$Lu^{176}/(1/v)$	1.0	1.278	1.417	1.085
0.4295		0.985	1.261	1.398	1.047
0.5534		0.972	1.245	1.381	1.015
0.7281		0.955	1.227	1.364	0.984
0	Lu^{176}/Pu^{239}_{fiss}	1.0	1.127	1.131	0.953
0.4295		0.957	1.068	1.068	0.934
0.5534		0.924	1.025	1.010	0.918
0.7281		0.909	1.007	0.991	0.909

Table XXVI. Ratios of Foil Activations for the Energy Interval 0.532-1.56 eV

Radius (cm)	Ratio	68°F 0% BU	325°F 0% BU	489°F 0% BU	68°F 0.6% BU
0	Ir^{191}/Ir^{193}	1.0	0.920	0.810	1.874
0.4295		1.010	0.930	0.819	1.627
0.5534		1.020	0.940	0.830	1.273
0.7281		1.025	0.944	0.817	1.020
0	$Ir^{191}/(1/v)$	1.0	0.966	0.913	1.273
0.4295		1.023	0.987	0.934	1.189
0.5534		1.045	1.010	0.967	1.055
0.7281		1.057	1.020	0.973	0.943
0	$Ir^{193}/(1/v)$	1.0	1.049	1.128	0.679
0.4295		1.012	1.062	1.141	0.730
0.5534		1.024	1.074	1.165	0.829
0.7281		1.031	1.080	1.191	0.925

From Table XXV, for the interval 0-0.532 eV, we see that the activation ratios for $Pu^{239}_{fiss}/(1/v)$, $Eu^{151}/(1/v)$, $Lu^{176}/(1/v)$, and Lu^{176}/Pu^{239}_{fiss} are all strongly dependent upon moderator temperature at all points in the cell. Thus the effect of moderator temperature on spectrum can be detected from the activation of dilute spheres placed in tubes at the edge of a cell. However, effective cross sections for plutonium isotopes cannot be inferred from measurements at the edge of the cell because the depressions in the flux caused by absorption by these isotopes will have died away, as can be seen from Figures 25 and 26. If measurements were to be made near the moderator-cladding interface, it would be possible to detect the increase in concentration of Pu^{240} with burnup from the activation ratio of Ir^{191} to Ir^{193}, as can be seen from Table XXVI.

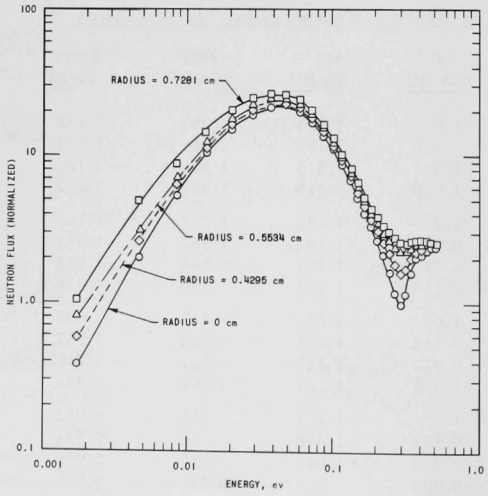

Figure 25

Neutron Flux in the Energy Range 0.001 eV to 0.53 eV; Cell Temperature 68°F; 0 Burnup

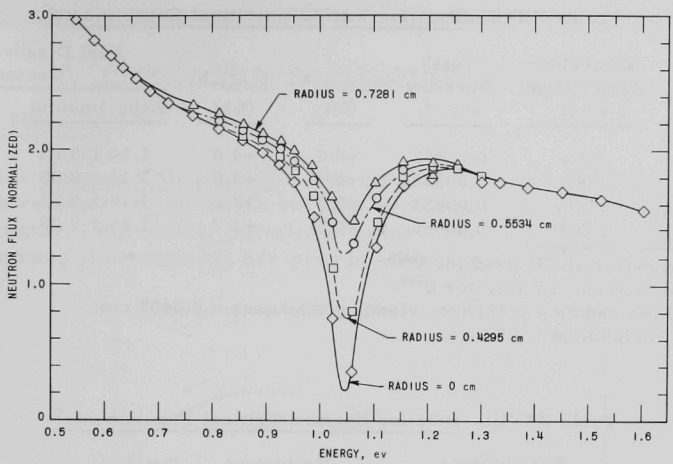

Figure 26. Neutron Flux in the Energy Range 0.55 eV to 1.60 eV; Cell Temperature 68°F; 0 Burnup

The calculational model being used for the physics evaluation of the EBWR Plutonium Recycle Experiment has been tested against data from Hanford's critical experiments with zirconium-clad PuO_2-UO_2 rods and from the YANKEE critical experiments with stainless-steel-clad UO_2 rods. The calculational model is based upon the GAM, SOFOCATE, DSN, and RP-122 codes.

The normal GAM library is used except that materials 132 and 133 (which include resonance parameters) are used for Pu^{240} and U^{235}, respectively, and material 139 is used for U^{238}. The use of material 12 for U^{238} results in calculated reactivities which are from 2% to 4% higher than found by experiment, with the greatest error at small water to metal ratios. The "Kelber" SOFOCATE (with "free gas" scattering) library is used with the following changes:

$$\nu^{49} = 2.91$$

$$\sigma_f^{49} = 1.015 \times \sigma_f^{49} \text{ (SOFOCATE)}$$

$$\sigma_a^{40} = 2.0 \times \sigma_a^{40} \text{ (SOFOCATE)}$$

$$\sigma_a^{41} = 1.43 \times \sigma_f^{41} \text{ (SOFOCATE)}$$

$$\nu^{25} = 2.422$$

The important parameters and the errors in the calculated reactivities are given in Tables XXVII and XXVIII for the YANKEE and Hanford criticals, respectively.

Table XXVII. Data for YANKEE Critical Experiments[c]

H_2O/UO_2 Ratio	Equivalent Bare Height (cm)	Total Buckling (cm^{-2})	Error[a] (%k)	Error[b] (%k)	Fuel Disadvantage Factor	
					Experimental	Calculated
1.05	135.6	0.00407	+0.7	+4.0	1.14 ± 0.03	1.118
1.41	135.1	0.00532	+0.4	+3.0	1.16 ± 0.03	1.129
1.86	135.6	0.00633	+0.3	+2.2	1.17 ± 0.03	1.140
3.38	133.5	0.00656	+0.5	+1.7	1.25 ± 0.08	1.170

[a]GAM material 139 used for U^{238}

[b]GAM material 12 used for U^{238}

[c]Fuel pin radius = 0.381 cm; cladding thickness = 0.0407 cm; U^{235} enrichment = 2.73 a/o.

Table XXVIII. Data for Hanford Critical Experiments[c]

H_2O/UO_2 Ratio	Enrichments				Equivalent Bare Height (cm)	Total Buckling (cm^{-2})	Error[a] (%k)	Error[b] (%k)
	Pu^{239} (a/o)	Pu^{240} (a/o)	Pu^{241} (a/o)	U^{235} (a/o)				
1.10	1.366	0.117	0.011	0.219	137.7	0.00510	-0.5	-0.3
2.71	1.366	0.117	0.011	0.219	137.7	0.00785	-0.7	-0.7
3.79	1.366	0.117	0.011	0.219	137.1	0.00749	-0.4	-0.5
5.14	1.366	0.117	0.011	0.219	139.6	0.00554	+0.2	+0.1

[a]Correction factor on σ_f^{49} (= 1.015) appropriate for the lattice with H_2O/UO_2 = 2.71 was used for all lattices.

[b]Appropriate correction factors (1.021, 1.015, 1.014, 1.013 for H_2O/UO_2 = 1.10, 2.71, 3.79, 5.14 respectively) on σ_f^{49} derived for each lattice.

[c]Fuel pin radius = 0.472 cm; cladding thickness = 0.0685.

IV. ADVANCED SYSTEMS RESEARCH AND DEVELOPMENT

A. Argonne Advanced Research Reactor (AARR)

1. Core Physics

a. Burnup Calculations. The CYCLE 2 code[12] (RP282) is being used to investigate burnup with various burnable poisons, including Sm^{149}, B^{10}, and natural europium, initially present. The resulting graphs of k_{eff} versus burnup time interval are presented in Figure 27.

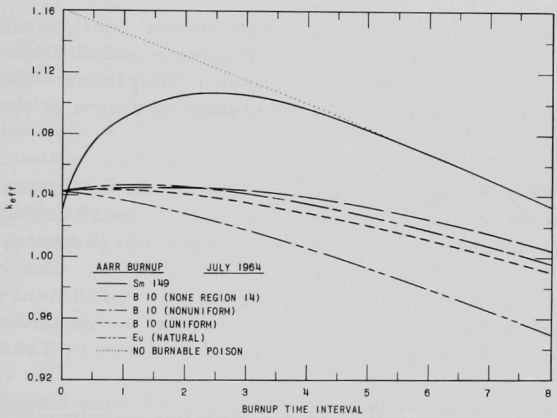

Figure 27. Calculated Burnups in AARR

Sixteen-group cross sections sets have been used in the calculations including cross sections generated for europium isotopes 151-155. It was assumed that 18.2% of the Eu^{151} which absorbed neutrons was transformed into Gd^{152} with an assumed cross section of zero. The remaining Eu^{151} which absorbed neutrons was assumed to advance masswise in the following sequence:

$$Eu^{151} \rightarrow Eu^{152} \rightarrow Eu^{153} \rightarrow Eu^{154} \rightarrow Eu^{155} \rightarrow Eu^{156}.$$

A cross section of zero was assumed for Eu^{156}. Eu^{152} has an appreciable cross section and contributes significantly to neutron absorption.

The initial ratios of poison atoms to U^{235} atoms in the core are as follows:

---

[12] Toppel, B., Avery, R., and Fischer, G., Cycle Cost Codes for Fast Reactor Fuel Cycle Analysis and Related Costs and Evaluation, Am. Nucl. Soc., Vol. 5, No. 1, p. 92.

Material	Atomic Ratio of Poison to U^{235}
Sm^{149}	0.0324
B^{10} (case 1)	0.0295 (uniform)
B^{10} (case 2)	0.0490 (nonuniform regions 1-13, 15-18)[13]
	0.0245 (nonuniform region 14)[13]
B^{10} (case 3)	0.2640 (none in region 14)
Europium	0.0243

Region 14 is the large, interior core region.

Different poison concentrations and configurations are being considered, together with combinations of poisons and the use of thermal neutron-absorbing liners at core-reflector interfaces. These liners are "grey" in that they absorb only a substantial fraction of the incident thermal neutrons.

b. Fine Power Distribution. The power variation within the first eight fuel plates, counting from the internal thermal column-core interface, has been determined by a transport-theory, slab-geometry problem using the previously cited 16-group set of cross sections. The variation within each plate is nearly linear, decreasing in order of distance from the thermal column and departing from linearity somewhat at the inner surface. Inner to outer surface ratios of power generation are given in Table XXIX.

Table XXIX. Ratio of Volumetric Power Generation at Inner Surface to that at Outer Surface of AARR Fuel Plates

Plate # (Counting from ITC-Core Interface)	Ratio	Plate # (Counting from ITC-Core Interface)	Ratio
1	1.10	5	1.15
2	1.11	6	1.14
3	1.13	7	1.12
4	1.14	8	1.09

2. Fuel and Core Design

Work done by Sylcor and Advanced Technology Laboratories, who were requested to make several depleted-uranium, modified-army-reactor-type fuel plates using the basic specification now in use for current army fuel fabrication contracts, but including suggested modifications to the basic

[13] ANL-6904, Reactor Development Program Progress Report, May 1964, p. 95.

processes involved, was completed. Some improvement in homogeneity of dispersion and microscopic distribution of the uranium oxide in the matrix was achieved in certain areas. Fracturing of the spherical oxide particles remains as the largest single factor affecting optimum distribution of oxide in the matrix.

Battelle Memorial Institute has made sample plates with spherical oxide which had less than the desired crushing strength, and has attempted to determine where changes in the manufacturing process normally used for army reactor fuels may be altered to produce low fragmentation of the porous oxides.

Martin Company has succeeded in adapting the fuel-fabrication process developed for the PM-1 core tubular fuel to the flat-plate AARR fuel. Plates having acceptable dimensional tolerances have been obtained by extruding the wet, coated oxide through flat-plate dies, followed by drying, sintering, hydrostatic pressing, annealing, hydrostatic pressing, and hot rolling of the compact in a "picture frame" to form the finished fuel plate. This process requires only a 2:1 to 3:1 reduction in the hot rolling process and results in a very high-quality distribution with very little damage to the oxide.

Pyromet Company has completed a series of vacuum furnace and hydrogen furnace braze metal bond tests in order to assess the net strength and ductility as well as "wetting" action of the first series of braze materials. Most of the materials tested have behaved as expected, in that the higher-temperature brazing alloys provided the best joints. It is hoped that a lower-temperature braze material can ultimately be developed.

3. Beam Tubes for the Experimental Facility

A conceptual mechanical design (see Figure 28) of the beam (blind) tubes has been completed and appears promising. A similar design is contemplated for the through tubes. Basically, the design is characterized by a bolt-breech mechanism for connecting the beam tubes to the reactor vessel nozzle. The bolt-breech fastening, in addition to permitting ease of remote assembly or disassembly of the beam-tube components, is removable, since it is not an integral part of the vessel nozzle, by loosening the bolts until the breech can be rotated sufficiently to be removed. Thus, the bolt and internal threads which are most likely to be damaged are easily replaced. A bolt-breech connection is also used to make the transition to the shield tank nozzle.

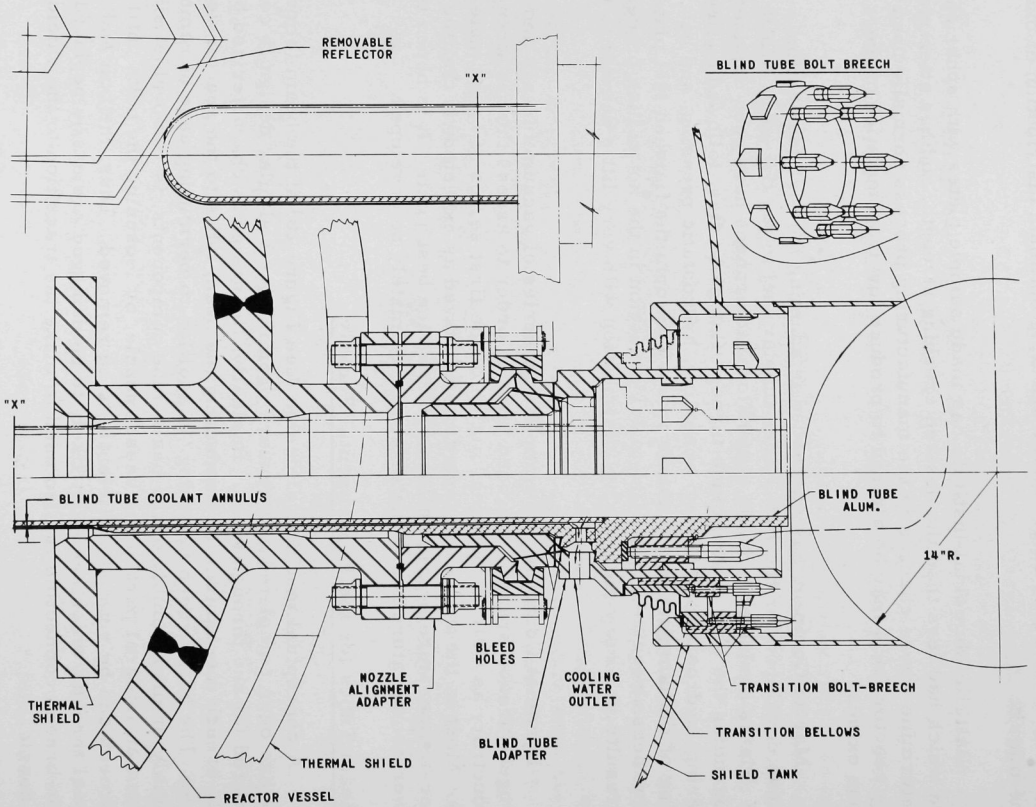

Figure 28. Design of Beam Tube

The beam (blind) tube assembly between the shutter and tube tip consists of six major components: 1) the aluminum beam tube, 2) the stainless steel nozzle alignment adapter, 3) the stainless steel beam tube adapter, 4) the collimator (not shown), 5) the bolt-breech connectors, and 6) the shield tank transition bellows. These components when assembled perform four major functions: 1) seal the beam tube to the reactor vessel nozzle against 800-psig pressure, 2) seal the beam tube adapter to the shield tank nozzle for confining the pool water, 3) provide a flexible bellows between the reactor vessel and shield tank nozzles to account for thermal expansion, misalignment, and movement, and 4) provide the initial collimation of the neutron beam for the experimenter.

4. Critical Experiment

Fuel-foil delivery has dropped below the expected rate, reportedly as a result of uranium corrosion damage encountered because of moisture damage in a storage vault at the supplier's factory. No fuel was delivered during July, but fuel delivery is expected to resume during August. Sufficient fuel to complete the initial loading is expected to arrive during August.

Application of fuel-cladding envelopes to the bare uranium foil is necessary before fuel may be loaded into the critical experiment. Satisfactory samples have been produced by ANL Central Shops.

Fabrication of hafnium control blades for the critical experiment has been delayed. The hafnium is on hand and awaits completion of fabrication in ANL Central Shops.

B. Magnetohydrodynamics (MHD)

1. MHD Studies with Liquid Metals

A comparison of the jet pump and the two-phase nozzle system under identical operating conditions has been made. Neither system has any advantage over the other. A comparison of potassium versus mercury as cycle fluids does not show any advantage of mercury, even if the materials problems are ignored.

Cycle analysis of the condensing ejector liquid metal MHD system have been initiated to determine its feasibility and potential commercial application. A comparison will be made with the extensive cycle analyses of the one- and two-component two-phase cycles. One will then be selected for concentrated study.

A major unknown in the condensing ejector cycles is the efficiency of the ejector itself. The literature has been searched for available data. Where possible, efficiencies based on an isentropic analysis are being compiled to formulate a rough empirical correlation for the ejector efficiency as a function of operating parameters.

C. Regenerative EMF Cells

1. Bimetallic Cells

a. Thermal Regeneration Studies. Additional scouting experiments were performed to determine whether the components of the sodium-bismuth system could be separated thermally under conditions of practical significance to the regeneration of a sodium-bismuth emf cell. In each test, a sample of Na_3Bi was located at one end of a sealed tube (316 stainless steel, 3/4-in. dia by 20 in. long) and was heated to 904-909°C for three days while the other end of the tube was maintained at a lower temperature. The condensation temperatures ranged from 525 to 712°C. At the end of the heating period, each tube was quenched, and the residue at the hot end and the condensate at the cool end were analyzed for sodium and bismuth. The condensate was found to be essentially pure sodium. The concentrations of sodium in the hot-end residues at the several condensation temperatures tested were as follows: 15 a/o at 525°C, 48 a/o at 616°C, 54 a/o at 651°C, and 62 a/o at 712°C. In each test, a small amount of Na_3Bi was found deposited in a zone between the hot and cold ends of the tube. It may be possible to eliminate the solid-vapor equilibrium (and thereby prevent deposition of Na_3Bi) by increasing the pressure of the system. Experiments at higher condensation temperatures have been carried out to test this possibility. The results of these tests are not yet available.

b. Spectrophotometric Studies of Alkali Metal Tellurides in Molten Salts. The spectra of lithium, sodium, potassium, and cesium tellurides in several alkali metal halides have been determined. The following systems were studied: Li_2Te in LiCl, LiCl-LiF, LiCl-KCl, and CsCl; Na_2Te in CsCl and NaCl-NaF; K_2Te in KCl; and Cs_2Te in CsCl. All of the alkali metal tellurides exhibited an intense absorption band. In addition, the spectra of Li_2Te in LiCl and LiCl-LiF exhibited peaks at about 470 mμ, and the spectrum of Na_2Te in CsCl exhibited inflection points at 570 and 500 mμ.

c. Absorption Spectra of Li_3Bi and K_3Bi in Molten Salts. The absorption spectrum of Li_3Bi in LiCl-LiF was reported previously (see Progress Report for February 1964, ANL-6860, p. 95). The spectrum was characterized by a single absorption band whose long wavelength edge was located at 613 mμ. A similar spectrum was obtained for Li_3Bi in LiCl.

The spectrum of K_3Bi was determined in molten LiCl-KCl and in CsCl. The spectrum of K_3Bi in LiCl-KCl at temperatures of 500 to 1000°C exhibited an absorption band similar to the band observed with Li_3Bi and, in addition, exhibited an absorption peak at about 495 mμ. The spectrum of K_3Bi in CsCl at 700°C showed the absorption band, but no other peaks. However, when the solution was heated to 1000°C and then cooled to about 700°C, two peaks were visible: one at about 600 mμ and the other at 390 mμ. To determine whether the two peaks observed after temperature cycling were

the result of the formation of Cs_3Bi at the high temperature, the spectrum of Cs_3Bi in CsCl was determined. No evidence of the two peaks was observed until the solution had been heated to 1000°C and then cooled. On cooling the solution to 650°C, inflection points were observed at 390 and 600 mμ. These findings suggest that the two peaks are not due to Cs_3Bi; additional studies are in progress to determine the nature of the absorbing species.

V. NUCLEAR SAFETY

A. Thermal Reactor Safety Studies

1. Metal-Water Reactions

a. Laser-beam Heating Applications. Additional experiments were carried out to determine the effect of laser energy outputs on the extent of the aluminum-water reaction. In previous experiments (see Progress Report for February 1964, ANL-6860, p. 97), 1 x 1 x 0.025-mm aluminum foils submerged in water were subjected to laser energy outputs that varied from 10.4 to 28.7 Joules. The extent of reaction was found to be about 8%, independent of the laser outputs. In the present experiments, 2 x 2 x 0.025-mm aluminum foils were exposed to laser outputs of up to 50 Joules. No reaction of aluminum with water occurred when the laser outputs were less than 17 Joules. For a laser output of 20 Joules, the extent of reaction was 9%; for an output of 50 Joules the extent of reaction was 15%. The increase in the extent of reaction obtained when the laser output was 50 Joules may be associated with the fact that several metal spheres were formed at the higher output instead of the single sphere that is formed at lower outputs.

Experiments were also performed with 1 x 1 x 0.05-mm foils and with 2 x 2 x 0.05-mm foils. The extent of reaction for these foils was 11% at 33 Joules and 13% at 42 Joules.

These studies suggest that the extent of the aluminum-water reaction is roughly independent of the laser energy outputs for energies sufficiently large to initiate the reaction.

b. Calculation of Pressure History of a Reactor during an Excursion. Calculations of transient heat transfer and pressure buildup occurring during a violent nuclear excursion were continued. Equations describing the SPERT-1 destructive excursion with a plate-type core were programmed for the CDC 3600 digital computer.

In the calculation of the destructive (second) pressure pulse, it was assumed that the pressure pulse resulted from the sudden dispersal of the molten portion (35%) of the SPERT-ID core and that a fresh surface of molten metal was thereby exposed to water. Calculations were made which assumed that the fresh surface area was equal to or was five or ten times greater than the area of the molten portion of the core. For each of the three surface areas, it was also assumed that all of the steam had condensed or that 21, 210, 2100, or 6000* cc of steam (or hydrogen) was present. The set of parameter values that agreed best with the experimental findings (3000 to 4000 psi in a rise time of 150 μsec) was a surface area ten times

*Zivi, S. M., Space Technology Laboratory, Redondo Beach, Calif., private communication.

greater than the area of the molten portion of the core and a near-zero volume of gas (i.e., nearly all of the water vapor in a condensed state) at the beginning of the pulse. The results of these calculations suggest that the second pressure pulse in the SPERT-ID test could have been a steam explosion.

2. Metal Oxidation-ignition Studies

a. Ignition Studies of Irradiated Uranium. Preparations are being made for the study of the ignition behavior of irradiated, 20% enriched uranium. Preliminary experiments have been performed with control samples in both oxygen and in air. The ignition temperatures were found to be 600°C in oxygen and 675°C in air.

Samples from the same batch of uranium were also subjected to 17 thermocycles between 43°C and 260-270°C prior to ignition to determine whether fission product heating might affect the ignition temperatures. The ignition temperatures after thermal cycling were 592 and 598°C in oxygen and 667°C in air, thus indicating that fission product heating will not be an important factor in ignition experiments with irradiated uranium.

b. Thermal Conductivity of Oxide Powders. An equation for the thermal conductivity of oxidized spherical powders has been developed for particles in an orthorhombic arrangement. The mathematical treatment was the same as that for unoxidized metal particles (see Progress Report for May 1964, ANL-6904, p. 109), except that in the new model consideration was given to the effect of a spherical shell of oxide around each particle, the shell having a different thermal conductivity than that of the metal. The theory showed good agreement with experimental results.

c. Aluminum-U_3O_8 Reaction. Additional studies are being made of the aluminum thermite reaction (see Progress Report for June 1964, ANL-6912, p. 95). The present experiments are being carried out with 40 w/o U_3O_8-aluminum specimens. Preliminary results indicate that the reactivity of sintered samples is greater than that of unsintered samples. However, self-heating rates of both sintered and unsintered samples of 40 w/o U_3O_8-aluminum are much lower than those of 85 w/o U_3O_8-aluminum specimens. The results of the tests indicate further that only about two-thirds of the initial reduction reaction (U_3O_8 to UO_2) occurs at a high rate and that the remainder of the reaction occurs at a low, steady rate.

B. Fast Reactor Safety Studies

1. Meltdown in Flowing Sodium

The first Mark-I integral TREAT sodium loop together with the test specimen of seven pins was returned to Argonne, Illinois from Idaho after

the previously reported series of transient irradiations of an EBR-II sample in a flowing sodium environment (see Progress Report for June 1964, ANL-6912, p. 96). The loop was opened, the sodium melted, and the test section removed with the loop-disassembly apparatus, all remotely. The purity of the inert atmosphere was adequate throughout all operations.

In order to check out the apparatus for eventual use with loops containing samples with appreciable burnup, the equipment was set up in a cave mockup facility including remote manipulators and a cave window replica. All work proceeded smoothly and no operations were performed that could not be done in an actual cave.

Inspection of the test section showed that the cladding had not failed but warped appreciably (maximum deviation from a straight cyclinder was ~0.4 mm), around the spiral spacer wire, into a twisted configuration similar to that observed for EBR-II pins exposed in an inert gas atmosphere. Although the steel cladding had not been penetrated, areas of uranium-steel eutectic were found on the surface of the uranium alloy pin after the cladding has been removed. Irregular surface cracks, roughly parallel to the pin axis and about 2 cm in length, were prominent on the pin as well. The cracks were filled with eutectic, with a general appearance suggesting that the surface of the fuel had split open, and molten fuel penetrated to the surface where it reacted with the cladding. The maximum recorded central fuel temperature from the transients was 1280°C, 200°C above the melting range of 1000-1080°C. A large temperature difference, ~300°C, between centerline and fuel-cladding interface was calculated for an intact pin at the time of maximum center temperature during the maximum transient. Samples of pin were taken for radiochemical and metallographic analyses.

2. Photographic Meltdown Experiments with Previously Irradiated Samples

Previous photographic meltdown experiments in TREAT with irradiated specimens have been performed with two EBR-II and two Fermi A pins. Results obtained from these tests appear to be consistent with the earlier data from opaque tests, and have, in addition, added information on the timing of failures and material movements. Preparations for a second series of photographic meltdown experiments in TREAT with previously irradiated samples are in progress and will investigate the following:

1. Transient fuel expansion and motion of a bare EBR-II fuel alloy cylinder during a constant-power reactor excursion.
2. Transient fuel expansion and motion of a bare EBR-II pin segment during a short (~1 sec) excursion.
3. Degree of vigor and modes of failure for a Fermi A pin during a slow (~20 sec) transient.

4. Mode of failure for an EBR-II pin subjected to an axially-shaped power profile by inclusion of tantalum thermal neutron flux absorbers inside the meltdown capsule.

No sample thermocouples will be used with the first two samples. Although a procedure was established for satisfactorily welding chromel and alumel wires directly to the surface of an unirradiated EBR-II fuel alloy specimen, attempts to weld fast-response surface thermocouples to irradiated fuel material inside a cave were unsuccessful.

3. Pressure-pulse Calculations

The general study of the characteristics of a pressure pulse produced during the expulsion of a vaporizing liquid from a coolant channel was continued, by applying the simplified analytic model to the case of an exponentially increasing power source with a constant period, τ. Previously, the model had been used only for a constant power input. Some of the relationships derived for this case, under the "asymptotic" assumption $e^{t/\tau} >> 1$, are as follows:

The time t_i for the liquid to be expelled a distance Z_x is given by

$$t_i = \tau \ln_e\left(\frac{Z_x m_0^2 C}{AS\tau^3}\right),$$

where m_0 is the coolant mass, C is the (averaged) ratio of change in enthalpy divided by change in pressure of the saturated vapor, A is the cross-sectional area of the coolant channel, and S is the initial power level. Evidently t_i is more sensitive to changes in τ than Z_x, and the relationship between Z_x, m_0, C, A, and S is presented directly. Similarly, the maximum pressure ΔP_i developed during the expulsion distance Z_x is

$$\Delta P_i = \frac{m_0 Z_x}{A\tau^2},$$

and a particularly simple form exists for the liquid velocity v_i at t_i:

$$v_i = Z_x/\tau.$$

If the coolant channel is sufficiently long, pressure will rise until the velocity is so large that the rate of increase of the volume filled with vapor is greater than the rate at which coolant can be vaporized to fill the volume without decreasing the pressure. This maximum pressure ΔP_m, is given by

$$\Delta P_m = (Gbc)\left(\frac{m_0}{A\tau}\right)^2,$$

where G is defined as the averaged value of the product of vapor-specific volume and vapor pressure. The velocity v_m at ΔP_m is given by

$$v_m = (Gbc)\, m_0/A\tau,$$

and the distance at which ΔP_m occurs is

$$Z_m = (Gbc)\, m_0/A.$$

From the above, it is seen that v_i is independent of material properties, ΔP depends only on m_0, and t_i is comparatively insensitive to them. If two identical systems have different liquids, are initially at saturation, have the same initial power levels, and have exponentially increasing power at constant (but not necessarily the same) periods, then the differences (within the limits of this simplified model) caused by different liquids can be calculated. Some relationships estimated from material properties gathered from standard sources are as follows:

$$\frac{(\Delta P_i)_{Na}}{(\Delta P_i)_{H_2O}} \doteq 0.9\left(\frac{\tau_{H_2O}}{\tau_{Na}}\right)^2; \qquad \frac{(\Delta P_i)_K}{(\Delta P_i)_{Na}} \doteq 0.9\left(\frac{\tau_{Na}}{\tau_K}\right)^2$$

$$\frac{(\Delta P_m)_{Na}}{(\Delta P_m)_{H_2O}} \doteq 3\left(\frac{\tau_{H_2O}}{\tau_{Na}}\right)^2; \qquad \frac{(\Delta P_m)_K}{(\Delta P_m)_{Na}} \doteq 0.8\left(\frac{\tau_{Na}}{\tau_K}\right)^2$$

$$\frac{(v_m)_{Na}}{(v_m)_{H_2O}} \doteq 3\left(\frac{\tau_{H_2O}}{\tau_{Na}}\right); \qquad \frac{(v_m)_K}{(v_m)_{Na}} \doteq 0.9\left(\frac{\tau_{Na}}{\tau_K}\right)$$

$$\frac{(Z_m)_{Na}}{(Z_m)_{H_2O}} \doteq 3; \qquad \frac{(Z_m)_K}{(Z_m)_{Na}} \doteq 0.9$$

Applications of these equations to generalized scaling estimates for different fluids must be done carefully. If, for example, there are two systems of identical size, initially at atmosphere pressure, with identical power versus time curves, one containing water and the other sodium, and if the water system starts at ~60°C while the sodium system starts at ~300°C, then the values of S when saturation is reached will be different by a factor ~5 and must be included in calculation of the scaling relationships.

Comparisons can be made between results obtained for exponentially increasing power and results obtained for constant-power tests. If the same energy is applied as input to the coolant in two systems, the inputs being identical except that in one case it is applied at constant power and in the other case the power is applied exponentially with constant period τ, then ΔP_i will be the same in both cases. However, in the exponential case, values for the liquid velocity and the distance traveled with both will be less.

4. Reactor Tests with Meltdown Scanning Device

A meltdown scanning system is under development to follow fuel movements during a meltdown experiment by detection of prompt fission neutrons emitted by the fuel specimens (see Progress Report for January 1964, ANL-6840, p. 95).

Both steady-state and transient runs were made at TREAT to test the response of the fast-neutron fuel-meltdown scanning equipment. Steady-state, low-power runs were used to evaluate the detectors, electronic processing equipment, and visual display arrangements. The meltdown transients were made to examine the dynamic response of a single-channel prototype detection, processing, and readout system.

The electronic processing package, including the phototube link, was designed by the Argonne Electronics Division. Faultless operation of the circuitry forecasts a good probability of achieving reliability in a multi-channel system. There are indications that certain precautions against pickup of control rod electrical noise must be incorporated in the design of the final system.

Over one-half dozen photomultiplier tubes (both 10-stage and 6-stage tubes) were tested for relative noise level, gain, and to some extent for transient response. A 10-stage tube, which also happens to be the least expensive, was found to provide the best response under the conditions tested. It is worthwhile to remark at this point that the gamma and neutron background in contrast to the desired fuel pin signal represents an environment which cannot be duplicated away from TREAT either in terms of relative and absolute intensity, or in time dependence. For this reason, a set of 9 Hornyak buttons were tested in an effort to enhance the signal-to-background ratio, if possible. No improvement over the standard arrangement was observed.

Preliminary results obtained from one transient test and recorded by a 1000-fps rotating prism camera, indicated satisfactory performance of the entire camera system. The conversion of images from film density to exposure requires that care be taken to operate over a wide linear film range in order to avoid saturation effects at the peak power level. A suitable single-pulse threshold was not reached in the first transient set; furthermore, the camera was not run fast enough to avoid image saturation. These are all matters apparently within the range of adjustment by selection of operating parameters.

The problem of viewing through steel containment was investigated. Such problems might arise when performing experiments in FARET or elsewhere when the sample is surrounded by steel structure. The results of a steady-state run with various thicknesses of steel interposed between the fuel and the detector indicate a loss in resolution which is roughly equivalent

to an exponential dependence upon thickness, x, times the neutron absorption cross section, Σ, of steel. Results are summarized in Table XXX, which is normalized so that the signal-to-background ratio for zero steel thickness is unity. A 9% enriched EBR-II pin was used in the standard opaque melt-down capsule in the steady-state run.

Table XXX. Relative Signal-to-background Ratios

Steel Thickness, cm	Relative $\left[\frac{\text{Signal}}{\text{Background}}\right]$ Ratio	$e^{-\Sigma x}$
0	1.00 ± 0.06	1.0
0.635	0.69 ± 0.06	0.85
1.27	0.77 ± 0.06	0.72
2.54	0.58 ± 0.06	0.53
5.08	0.32 ± 0.06	0.27
7.62	0.15 ± 0.05	0.15

C. TREAT

1. Large TREAT Loop

The cold trap for the large loop has been completed by Central Shops and the components shipped to Idaho. The fabrication of the cask, cask plug, and drawer have been completed. The lead filling of the cask was completed.

VI. PUBLICATIONS

Papers

PARTITION OF SOLUTES BETWEEN LIQUID METALS. II. THE LEAD-ZINC SYSTEM

F. A. Cafasso, H. M. Feder, and Irving Johnson

J. Phys. Chem. 68, 1944-1948 (July 1964)

THERMOELECTRIC PARAMETER STUDIES ON US, ThS AND US-ThS SOLID SOLUTIONS

Marvin Tetenbaum

A Seminar on Groups V and VI Anions held at Argonne National Laboratory, February 26 and 27, 1964, ed. R. J. Beals, J. H. Handwerk, and J. F. Schumar. ANL-6856 (March 1964). pp. 48-52

FORMATION AND SPECTRA OF URANYL(V) CHLORIDE IN MOLTEN CHLORIDE SOLVENTS

D. A. Wenz, M. D. Adams, and R. K. Steunenberg

Inorg. Chem. 3, 989-992 (July 1964)

AN ANALYSIS OF 23 ZPR-III FAST-REACTOR CRITICAL EXPERIMENTS

W. G. Davey

Nucl. Sci. Eng. 19, 259-273 (1964)

NEUTRON RADIOGRAPHIC INSPECTION OF HEAVY METALS AND HYDROGENOUS MATERIALS

Harold Berger and I. R. Kraska

Materials Evaluation XXII (7), 305-309 (July 1964)

RADIOGRAPHY AS A TOOL OF NONDESTRUCTIVE TESTING

Harold Berger

Forest Products J. XIV (7), 290-292 (July 1964)

PROPERTIES AND PHASE STUDIES OF SOME ACTINIDE MONO-PHOSPHIDE AND MONOSULFIDE COMPOUNDS AND RELATED BINARY SYSTEMS

Y. Baskin

A Seminar on Groups V and VI Anions held at Argonne National Laboratory, February 26 and 27, 1964, ed. R. J. Beals, J. H. Handwerk, and J. F. Schumar. ANL-6856 (March 1964). pp. 27-30

HEAT TRANSFER AND FLUID FLOW - BOILING STABILITY

P. A. Lottes

NASA-AEC Liquid-Metals Corrosion Meeting, Lewis Research Center, Cleveland, Ohio, October 2-3, 1963. Vol. 1, NASA SP-41, pp. 257-271 (June 1964)

NOTE ON THE SIMULATION OF HIGHER-ORDER LINEAR SYSTEMS WITH SINGLE OPERATIONAL AMPLIFIERS

C. E. Cohn

Proc. IEEE 52, 874 (July 1964) Letter

ELASTIC AND INELASTIC SCATTERING OF FAST NEUTRONS FROM Co, Cu AND Zn

A. B. Smith, C. A. Engelbrecht, and Daniel Reitmann

Phys. Rev. 135, B76-B82 (July 13, 1964)

IMPROVED TECHNIQUES FOR LOW FLUX MEASUREMENT OF PROMPT NEUTRON LIFETIME, CONVERSION RATIO AND FAST SPECTRA

R. J. Armani, E. F. Bennett, M. W. Brenner, M. M. Bretscher, C. E. Cohn, R. J. Huber, S. G. Kaufmann, and W. C. Redman

Proc. IAEA Symp. on Exponential and Critical Experiments, Amsterdam, September 2-6, 1963. Intern. Atomic Energy Agency, Vienna, 1964. Vol. 1, pp. 227-259

CHARACTERISTICS OF A THERMAL NEUTRON BEAM FOR NEUTRON RADIOGRAPHY

Harold Berger

Intern. J. Appl. Radiation Isotopes 15, 407-414 (1964)

POWER REACTOR DESIGN AT ZERO POWER

W. C. Redman, K. E. Plumlee, and Q. L. Baird

Proc. IAEA Symp. on Exponential and Critical Experiments, Amsterdam, September 2-6, 1963. Intern. Atomic Energy Agency, Vienna, 1964. Vol. 1, pp. 3-27

REMARK ON ALGORITHM 60 - ROMBERG INTEGRATION [F. L. Bauer, Comm. ACM 4, (June 1961), 255]

H. C. Thacher, Jr.

Comm. ACM 7 (7), 420-421 (July 1964)

CERTIFICATION OF ALGORITHM 128 - SUMMATION OF FOURIER SERIES [M. Wells, Comm. ACM 5 (October 1962)]

H. C. Thacher, Jr.

Comm. ACM 7 (7), 421 (July 1964)

ANL Reports

ANL-6789 THE BREEDING RATIO OF A PLUTONIUM LOADING IN EBR-I
R. R. Smith, R. O. Haroldsen, R. E. Horne, and R. G. Matlock

ANL-6816 INTERDIFFUSION BETWEEN URANIUM-5 w/o FISSIUM ALLOY AND TYPE 304 STAINLESS STEEL
C. M. Walter

ANL-6826 DOSIMETRY FOR RADIATION DAMAGE STUDIES
A. D. Rossin

ANL-6844 CALCULATIONS OF COHERENCE OF FAILURE FOR HYPOTHETICAL MELTDOWN ACCIDENTS IN AN EBR-II-LIKE REACTOR
D. V. Gopinath and C. E. Dickerman

ANL-6851 THE STEADY STATE AND TRANSIENT KINETICS OF EBR-I, MARK-III
J. C. Carter, D. W. Sparks, and J. H. Tessier

ANL-6856 A SEMINAR ON GROUPS V AND VI ANIONS, held at Argonne National Laboratory, February 26 and 27, 1964
R. J. Beals, J. H. Handwerk, and J. F. Schumar, eds.

ANL-6869 APPLICATION OF ELECTRON-BOMBARDMENT HEATING FOR BOILING LIQUID METALS
R. E. Holtz

ANL-6892 CATALOG OF NUCLEAR REACTOR CONCEPTS. Part I. Homogeneous and Quasi-Homogeneous Reactors. Section I. Particulate-Fueled Reactors
Charles E. Teeter, James A. Lecky, and John H. Martens